universität wien

MASTERARBEIT | MASTER'S THESIS

Titel | Title

Characterization of the Hochschwab karst aquifer flow regime using a water stable isotope approach (Austria)

verfasst von | submitted by

Paul Zemann BSc

angestrebter akademischer Grad | in partial fulfilment of the requirements for the degree of

Master of Science (MSc)

Wien | Vienna, 2024

Studienkennzahl lt. Studienblatt | Degree programme code as it appears on the student record sheet:	UA 066 815
Studienrichtung lt. Studienblatt | Degree programme as it appears on the student record sheet:	Masterstudium Erdwissenschaften
Betreut von | Supervisor:	Mag. Dr. Erich Draganits Privatdoz.

Acknowledgement

This work would never have been possible without the active support of many people involved. First and foremost, I would like to thank Lukas Plan (Natural History Museum Vienna) and Eva Kaminsky (BOKU University) for their constant willingness to help and the friendly working environment. Your supervision during this work has not only enabled me to learn an incredible amount, but also to develop a passion for the subject. I would also like to thank Erich Draganits, who accompanied me through my studies for many years and was always on hand with help and advice. Many thanks to Christine Stumpp for her valuable contribution to water stable isotopes and the opportunity to use the laboratory facilities at the BOKU University. I would also like to thank Hatice Türk for her help with the numerical modelling. Thanks go to the Municipal Department 31 of the City of Vienna and especially Hermann Kain for providing data and support with sampling. Michael Nagl carried out the sampling in the Hirschgrubenhöhle with me and took on harsh conditions to make the data collection possible. He deserves just as much thanks for this as for the fact that he, together with Lina Rummler, Barbara Funk and Pauline Oberender, ensured that I had an excellent time at the Natural History Museum Vienna. I would also like to thank Severin Simma and Helene Zauner for not only being great comrades, but also for becoming good friends. Finally, I would like to thank Alexandra, Martin, Tim and Maria, who have always accompanied me with their love and constant support.

I am very grateful for the financial support that was provided by the “Hochschuljubiläumsfonds der Stadt Wien” and the Austrian Speleological Association.

Abstract

Karst aquifers are an important source of drinking water in Austria and worldwide. Due to the high secondary porosity of karst systems and the resulting short residence times of the water, however, karst springs are particularly susceptible to contamination. The transport of water and its storage within karst systems has always posed a challenge to the field of hydrogeology given the high heterogeneity and complex structure of potential flow paths. When modelling flow behaviour, the role of the upper unsaturated zone, which strongly influences the tempo-spatial distribution of infiltrating water in the first few meters, is rarely considered. This is especially true for the up to a few meters thick epikarst, which represents the uppermost part of the unsaturated zone and shows increased porosity and permeability.

The study area includes the largest known karst springs in Austria, the Kläffer springs, and their catchment area, the Hochschwab massif, which is characterized by a pronounced karstified Middle and Upper Triassic plateau. In order to investigate the dynamics of freshly infiltrating water in the epikarst, drip water was analysed for water stable isotopes ($\delta^{18}O$ and $\delta^{2}H$) in the Hirschgrubenhöhle approximately 6.5 m below the surface. This was conducted during a rain event in September 2023, whereby samples were simultaneously taken from the Kläffer springs and from precipitation in addition. Furthermore, water content sensors were installed in the soil within the catchment area of the cave drip water.

The measured isotope values of cave drip water (Hirschgrubenhöhle), spring water (Kläfferquellen) and precipitation were used as conservative tracers for the modelling of water transport in the epikarst, while a clear signal at the Kläffer springs was absent. Within about 18 hours after the onset of rainfall, a significant increase in discharge was observed for cave drip water in the Hirschgrubenhöhle, reaching a maximum of 18 ml/sec. Using a numerical model, the fraction of stored water with different ages in the discharge could be calculated. It was found that on average only one third of the flood water had its origin in the sampled rain event and about two thirds can be attributed to older water. A mass balance also showed that more than 95 % of the rain was still stored in the epikarst or the soil zone when baseflow conditions were reached again. The results of this study suggest that the storage capacity of the epikarst and soil layer is higher than previously assumed for the Hochschwab karst aquifer.

Zusammenfassung

Karstaquifere stellen eine wichtige Ressource von Trinkwasser in Österreich und weltweit dar. Wegen der hohen sekundären Porosität des Karsts und den daraus resultierenden kurzen Verweilzeiten des Wassers sind Karstquellen allerdings besonders anfällig für Kontaminationen. Der Transport von Wasser, bzw. dessen Speicherung innerhalb von Karstsystemen stellt die Hydrogeologie wegen der hohen Heterogenität und dem komplexen Aufbau von potenziellen Fließwegen seit jeher vor eine Herausforderung. Bei der Modellierung des Fließverhaltens wird allerdings selten auf die Rolle der obersten ungesättigten Zone eingegangen, welche die räumlich-zeitliche Verteilung von infiltrierendem Wasser in den ersten Metern stark beeinflusst. Dies trifft vor allem auf den bis einige Meter mächtigen Epikarst zu, welcher den obersten Teil der ungesättigten Zone darstellt und eine erhöhte Porosität und Permeabilität vorweist.

Das Untersuchungsgebiet beinhaltet die größten bekannten Karstquellen Österreichs, die Kläfferquellen, und deren Einzugsgebiet, das Hochschwabmassiv, welches durch ein verkarstetes Plateau aus mittel- und obertriassischen Gesteinen charakterisiert ist. Um die Dynamik von frisch infiltrierendem Wasser im Epikarst zu erfassen, wurde Tropfwasser in der Hirschgrubenhöhle ca. 6.5 m unter der Oberfläche auf stabile Wasserisotope ($\delta^{18}O$ und $\delta^{2}H$) untersucht. Dies geschah während eines Regenevents im September 2023, wobei zeitgleich auch Proben von den Kläfferquellen und vom Niederschlag genommen wurden. Im Einzugsgebiet des Tropfwassers wurden außerdem Sensoren zum Messen des Wassergehalts im Boden installiert.

Die gemessenen Isotopenwerte von Tropfwasser (Hirschgrubenhöhle), Quellwasser (Kläfferquellen) und Niederschlag wurden als konservative Tracer für die Modellierung von Wassertransport im Epikarst eingesetzt, während ein deutliches Signal an den Kläfferquellen ausgeblieben ist. Etwa 18 Stunden nach Einsetzten des Regens konnte ein deutlicher Anstieg der Schüttung des Tropfwassers in der Hirschgrubenhöhle beobachtet werden, welche ein Maximum von 18 ml/sec erreichte. Mittels eines nummerischen Modells konnte der Anteil von gespeichertem Wasser unterschiedlichen Alters in der Schüttung berechnet werden. Die Ergebnisse zeigen, dass im Schnitt nur ein Drittel der angestiegenen Schüttung ihren Ursprung im beprobten Regenevent hatte und etwa zwei Drittel auf älteres Wasser zurückzuführen ist. Eine Massenbilanz ergibt außerdem, dass mehr als 95 % des Regens noch im Epikarst oder der Bodenzone gespeichert war, als der Basisabfluss wieder erreicht wurde. Die Ergebnisse dieser Studie legen nahe, dass die Speicherkapazität des Epikarst und des Bodens höher ist, als bisher für den Hochschwab-Karstaquifer angenommen wurde.

Abbreviations

ANIP	Austrian Network of Isotopes in Precipitation and Surface Waters
atm	standard atmosphere
CDF	cumulative density function
CET	Central European Time (corresponds to UTC+1) used for all time information in this study
CRDS	Cavity Ring-Down spectroscopy/spectrometer
EC	electrical conductivity [µS/cm @ 25°C]
ET	evapotranspiration [mm]
Few	fraction of event water
GMWL	Global Meteoric Water Line
HG	Hirschgrubenhöhle
KQ	Kläffer springs
LMWL	Local Meteoric Water Line
m_{ASL}	meters above sea level
MS	meterological station
NSE	Nash-Sutcliffe efficiency
OLSR	ordinary least square regression
P	precipitation [mm]
P_{CO2}	partial pressure of CO_2
PWLSR	precipitation least square regression
pdf	probability density function
Q	discharge/flow rate (different units)
SAS	StorAge Selection
TTD	transit time distribution
VSMOW	Vienna Standard Mean Ocean Water

Table of Content

Acknowledgement .... **I**

Abstract .... **II**

Zusammenfassung .... **III**

Abbreviations .... **IV**

1 Introduction **1**

2 Basic concepts **4**

2.1 Definitions 4

2.2 Karst formation 4

2.3 Karst Hydrogeology 7

2.4 Water stable isotopes 9

3 State of the art and recent developments **12**

3.1 Hydrogeology research at the Hochschwab 12

3.2 Development of hydrograph separation and water transit time approaches using stable isotopes 14

4 Study Area **16**

4.1 Geographical and climatic overview 16

4.2 Geological overview 19

5 Methods **22**

5.1 Timeframe and data collection 22

5.2 Meteorological data 23

5.3 Physiochemical parameters of karst water 24

5.4 Volumetric soil water content 27

5.5 Isotope data 29

5.5.1 Long-term ^{18}O and ^{2}H in precipitation 29

5.5.2 Water stable isotopes (^{18}O and ^{2}H) event sampling 30

5.6 End-member mixing 33

5.7 Numerical modelling 36

6 Results and interpretation 40

6.1 Meteorological data 40

6.2 Physicochemical parameters of karst water 41

6.3 Volumetric soil water content 45

6.4 Isotope data 46

6.4.1 Long-term ^{18}O and ^{2}H in precipitation 46

6.4.2 Water stable isotopes (^{18}O and ^{2}H) event sampling 47

7 Results and interpretation from mixing models 52

7.1 End-member mixing 52

7.2 Numerical modelling 58

8 Discussion 69

9 Conclusion 73

10 Further work 76

11 List of figures 77

12 List of tables 82

13 References 83

14 Appendix 14-A

14.1 Soil profiles 14-A

14.2 Water stable isotope samples 14-B

"I declare that I have written this thesis independently and have only used the resources indicated. This work has neither been submitted elsewhere (e.g. for other courses) nor submitted by other persons (e.g. work by other persons from the Internet)."

„Ich erkläre, dass ich die vorliegende Arbeit selbstständig verfasst habe und nur die ausgewiesenen Hilfsmittel verwendet habe. Diese Arbeit wurde weder an einer anderen Stelle eingereicht (z.B. für andere Lehrveranstaltungen) noch von anderen Personen (z.B. Arbeiten von anderen Personen aus dem Internet) vorgelegt.“

1 Introduction

Worldwide around 678 million people depend on drinking water from karst aquifers (Stevanović, 2019). With increasing demand for fresh water and warming of the global climate (IPCC, 2023), the protection of karst springs and their catchment areas are a key task to enable well-being and resilience of our societies in the future. About half of the population of Austria is dependent on water from karstic areas, which cover approximately 22 % of the surface of Austria (Kralik, 2001) and provide high quality drinking water in large amounts. A privilege that not only cities like Vienna, Linz, Salzburg, or Graz benefit from, but the whole country of Austria. Karst springs in the Northern Calcareous Alps, such as the Kläffer springs at the base of the Hochschwab massif are important suppliers of this water. Located in Styria, 100 km southwest of Vienna, these springs are one of the biggest in central Europe and with an average discharge of around 5.2 m^3/s (Plan et al., 2010) essential to secure the daily transport of up to 217 000 m^3 of fresh water on the Second Vienna Water Main for the population in Vienna (City of Vienna, 2024). Most of the drinking water (more than 95 %) for the city of Vienna originates from karst springs and more than 57 % is obtained from the Hochschwab massif alone (Plan et al., 2010).

Due to a well-developed secondary porosity in karst systems, reactions of springs to precipitation are usually quick and therefore discharge may vary strongly (Ford & Williams, 2007). Fast water transport in conduits and large fractures is one of the main reasons for the high vulnerability of karst springs to contamination (Kačaroğlu, 1999). Since this is also the case for the Hochschwab massif and the Kläffer springs, most of the Hochschwab area is within a water protection zone to secure drinking water (City of Vienna, 2024). Natural purification and availability of water sources are strongly influenced by mixing processes, storage behaviour and transit times of the water in the aquifer, but unfortunately these factors are often difficult to assess (Hrachowitz et al., 2016). A profound understanding of the various natural processes and conditions of this karst aquifer are therefore crucial, and many studies have been dedicated to investigating the hydrology of the Hochschwab massif (e.g. Plan et al., 2010; Exel et al., 2016; Kaminsky et al., 2021) as well as karst aquifer flow regimes in general (e.g. Ford & Williams, 2007; De Waele & Gutiérrez, 2022).

While recharge and discharge are often studied for the entire aquifer at its outlets (i.e. springs), caves provide an opportunity to study the flow regime directly in the unsaturated zone of the karst system (Poulain et al., 2018), which is also called vadose zone. Since the distribution of water within the karst system, as well as mixing of fresh water from precipitation and stored water is strongly influenced by flow and storage behaviour in the uppermost vadose zone (Klimchouk, 2004; Williams, 2008), a more elaborate knowledge of this process is of great importance for our understanding of the complex hydrological characteristics. In recent decades, the use of water stable isotopes as natural tracers for modelling water transport within aquifers, including karst aquifers (Zhang et al., 2021) and even recharge processes in caves (Perrin et al., 2003), has gained relevance and has led to new insights (Klaus & McDonnell, 2013). Nevertheless, the application of isotope sampling in caves poses great logistical efforts and has therefore rarely been applied. Mixing ratios are also poorly described for the Hochschwab karst aquifer but would be beneficial information to enable better water management. A drip water bearing cave, the Hirschgrubenhöhle, located at 1896 m above sea level (m_{ASL}) within the catchment area of the Kläffer springs, as well as the springs as such were chosen as a suitable study site at the Hochschwab karst plateau. Both are equipped with in-situ measurements providing long-term water parameters of discharge, temperature, and electrical conductivity and the near-surface parts of the Hirschgrubenhöhle allow direct measurement of recharge processes within the karst aquifer.

The goal of this study is to characterize water mixing processes and storage behaviour in the uppermost vadose zone and at the springs of the karst aquifer using water stable isotopes. Three major questions can be derived:

- To what extent is the isotopic signal of water dampened in the vadose zone of the aquifer (Hirschgrubenhöhle) compared to the whole system (Kläffer springs)?
- How do water storage and transit times in the upper vadose zone relate to each other during a particular precipitation event?
- Which method is suitable for drawing conclusions about intra-event processes of water storage and transit in a karst catchment using water stable isotopes as tracers?

For this study, water samples from the drip water in the Hirschgrubenhöhle and water of the Kläffer springs, as well as from precipitation are collected in high frequency during a particular rain event for water stable isotope analysis. To get a better understanding of the overall flow regime, discharge, electrical conductivity, and water temperature of the cave drip water and at the Kläffer springs, as well as punctual volumetric soil water content and precipitation intensity are measured. In order to find answers to the above stated questions two different modelling approaches were tested out to calculate mixing ratios.

2 Basic concepts

2.1 Definitions

Some terms in karst water hydrology are subject to different definitions in the literature, which is why a selection of frequently used concepts is explained here.

- Flood event: temporally limited distinct increase of flow rate at a certain point in the (karst) aquifer (Perrin, 2003, p. 5)
- Flow: movement of water through an (karst) aquifer (Ford & Williams, 2007, p. 109)
- Flow rate: volume of water flowing through a certain point within one second (De Waele & Gutiérrez, 2022, p. 268-271)
- Discharge: released water from a certain point in the (karst) aquifer, usually given as flow rate (De Waele & Gutiérrez, 2022, p. 268-271)
- Storage: water that is flowing at rates that are too low to transit out of a defined part of the aquifer within the observed time frame (Hrachowitz et al., 2016)

2.2 Karst formation

The term “karst” lacks a standardized definition in the literature but is described by Ford & Williams (2007, p. 1) as “a special style of landscape containing caves and extensive underground water systems that is developed on especially soluble rocks such as limestone, marble, and gypsum”. The formation and development of karst systems is controlled by various factors, such as lithology, topography, stratigraphy, climate, precipitation and its chemical composition, as well as chemical composition and base level of water in the karst system (De Waele & Gutiérrez, 2022; Fig. 1).

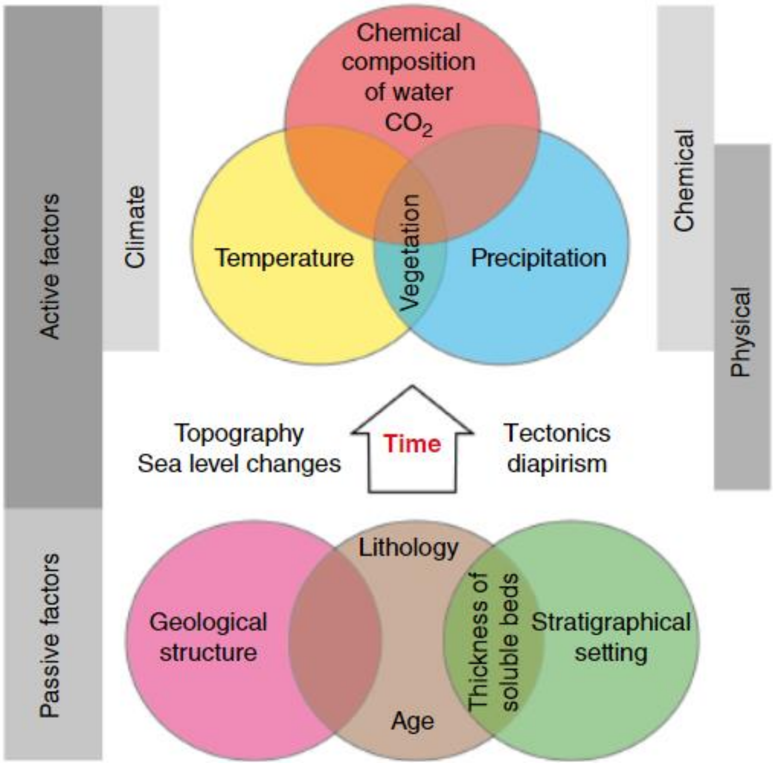

Fig. 1: Factors controlling the formation of karst systems (from De Waele & Gutiérrez, 2022).

From a process-based perspective dissolution of rocks is the main driver for the formation of karst features (Palmer, 1984; Ford & Williams, 2007; De Waele & Gutiérrez, 2022). Therefore, minerals, that are soluble in water form karst structures when exposed to it in sufficient quantities. These include for example gypsum, halite or quartz, but the most prominent ones are calcite and dolomite (Ford & Williams, 2007). For the latter two, the solubility by dissociation in pure water, however, is extremely low, whereas it is much higher if free H^+ are involved in the reaction (Ford & Williams, 2007). Water in the atmosphere reacts with surrounding CO_2 or CO_2 from soil while infiltrating into the subsurface and forms carbonic acid H_2CO_3, which then dissolves to H^+ and CO_3^- (Palmer, 1984). Dissolution of calcite thus proceeds according to the following three reactions (Fig. 2):

$$CO_2 + H_2O \leftrightarrow H_2CO_3$$

$$H_2CO_3 \leftrightarrow H^+ + HCO_3^-$$

$$CaCO_3 + H^+ \leftrightarrow Ca^+ + HCO_3^-$$

Which can be summarized as,

$$CaCO_3 + \ CO_2 + H_2O \leftrightarrow \ Ca^+ + 2HCO_3^-. \tag{Eq. 1}$$

This applies analogously for the dissolution of dolomite $CaMg(CO_3)_2$. While other factors might impact solubility further (e.g. temperature, grain size, impurities, etc.), the here described reaction is the most dominant one (Freeze & Cherry, 1979). Consequently, besides the amount of precipitation the availability of CO_2 plays a key role. The partial pressure is the common unit in which the concentration of a gas is measured and is P_{CO2} = 0.00038 atm for CO_2 in the atmosphere at sea level, whereas in the soil it usually is between 0.01 and 0.1 atm (Palmer, 2007).

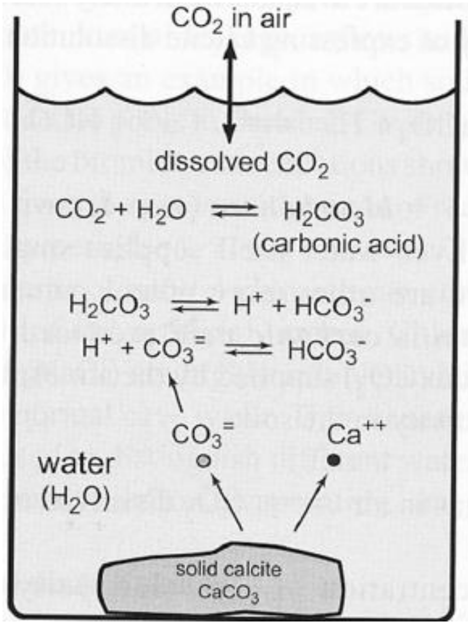

Fig. 2: Figure showing calcite dissolution through the described reactions (from Palmer, 2007).

At 25 °C and 1 atm pressure, the solubility of calcite ranges from 60 mg/l at P_{CO2} of 0.001 atm to 400 mg/l at P_{CO2} of 0.1 atm and to solubilities of 50 and 300 mg/l for dolomite respectively (Freeze & Cherry, 1979). While water is becoming more saturated with dissolved ions, the rate of dissolution drops lower. In the case of calcite, dissolution occurs at a rate of around 0.1 mg/l/sec at 0 % saturation and decreases in a linear way to around 0.01 mg/l/sec at a saturation of 70-80 % (Ford & Williams, 2007; Palmer, 2007). From this point onwards the rate of dissolution no longer follows the linear trend and slows down to around 0.001 mg/l/sec at 90 % saturation, whereas full saturation is hardly ever reached.

The concepts of dissolution and karst formation explained here are only a brief summary and can be found in more detail in the literature cited above. Nevertheless, the described processes are responsible for the shaping of the typical surface and subsurface structures that can be found in karst systems. Along already existing zones of mechanical weakness (e.g. faults or bedding surfaces), as well as along conduits and fractures water can flow faster and in higher quantities leading to increased dissolution (Palmer, 1984). However, dissolution is highest within the first meters where the linearly increasing dissolution rate is still present, water is not as saturated and there is still plenty of free H^+ from carbonic acid available

(Palmer, 2007). High CO_2 concentrations in the soil lead to acidification of percolating water and further enhance dissolution in the uppermost subsurface. The range of resulting structures under different environments is large, but often can be depicted in a more or less similar pattern as shown in Fig. 3 and Fig. 4 (Ford & Williams, 2007).

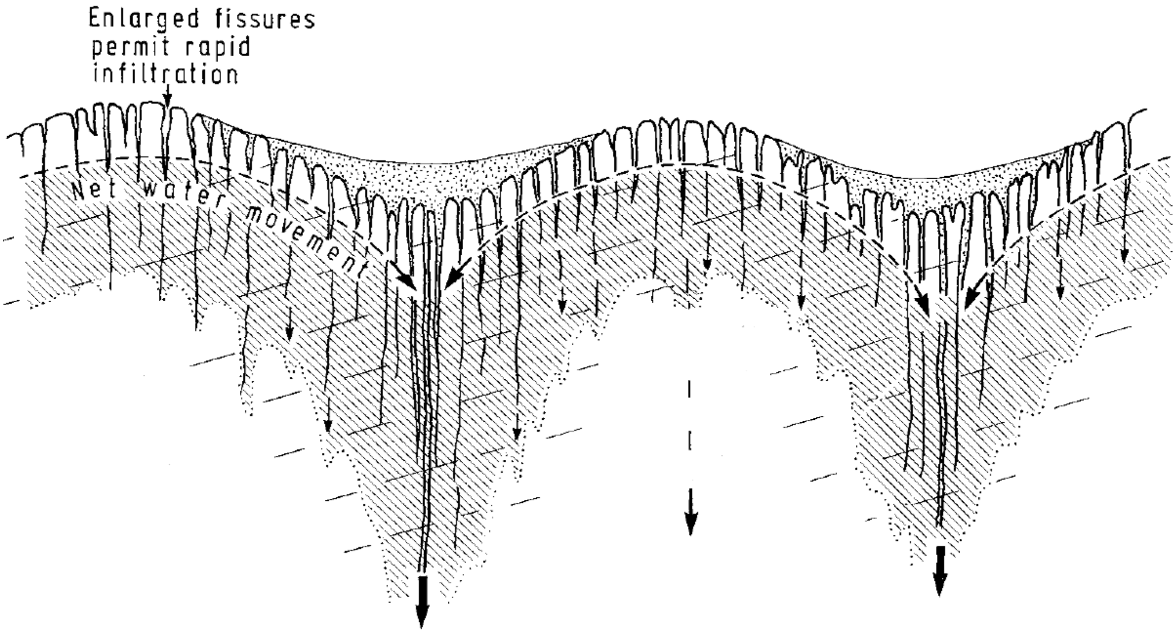

Fig. 3: Schematic profile of the first meters below surface in a typical karst setting with a highly porous zone at the top and prominent sub-vertical conduits (from Williams, 1983).

2.3 Karst Hydrogeology

A karst aquifer can be divided into different zones on the basis of hydrogeological properties, as can be seen in Fig. 4 (Ford & Williams, 2007). The phreatic zone is the aquifer below the lowest possible water table, permanently filled with water and can reach dimensions of up to several hundred meters depth. Zones that are only filled temporarily with water are called epiphreatic and expand from the highest to the lowest possible water table. The vadose zone is the upper part of the aquifer, where there are no large, connected, stagnant water bodies. It is overlain by the relatively thin epikarst layer (if present) and a soil cover on top (if present). Sometimes these are considered part of the vadose zone, whereas the actual vadose zone would be called transmission zone.

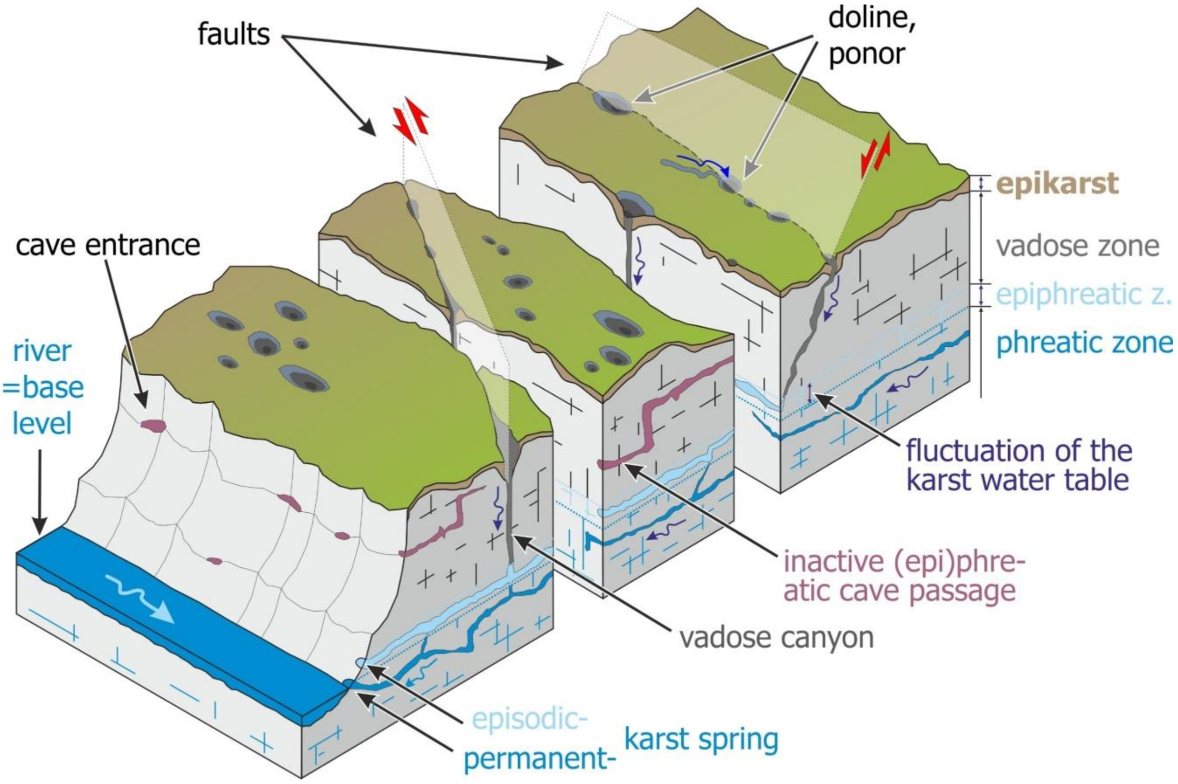

Fig. 4: Figure showing the different hydrogeological zones and features in a typical karst aquifer. Infiltrating water enters the karst aquifer preferentially through surface structures such as dolines or ponors. After percolating through the soil, the epikarst, and the vadose zone the water reaches the (epi)phreatic zone, from where it leaves the system through permanent or episodic springs (from Plan, L.).

The epikarst layer plays an important role in distributing infiltrating water into the underlying vadose zone due to its increased secondary porosity of 10-30 % (see above) and characteristic storage behaviour (Williams, 2008). It may be overlain by a soil cover, consists of a dense network of fissures and is estimated to reach up to 15 m in thickness (Klimchouk, 2004). With permeabilities of 10-20 cm/sec and enlarged fissures, the epikarst contrasts strongly in terms of hydrologic functioning from the underlying bedrock, which usually shows a permeability around 1 cm/sec and a porosity of a few percent (De Waele & Gutiérrez, 2022). As can be seen in Fig. 3 and Fig. 5, flow in the vadose zone occurs preferentially along large conduits, where most of the porosity is concentrated (Klimchouk, 2004). Together with the sharp contrast in permeability this can lead to temporal water backflow at the bottom of the epikarst layer during high inflow rates, creating some kind of “bottleneck” (Klimchouk, 2004; Williams, 2008). Epikarst layers, therefore, do not only regulate infiltrating water flow, but also constitute an important water storage in karst systems (Klimchouk, 2004; Ford & Williams, 2007; Palmer, 2007; Williams, 2008).

Perrin (2003) even suggests that in some special cases, storage in the epikarst could be even more significant than in the phreatic zone. However, an epikarst layer is not always present due to removal by glacial erosion or because it could never develop in limestone with high primary porosity (Williams, 2008).

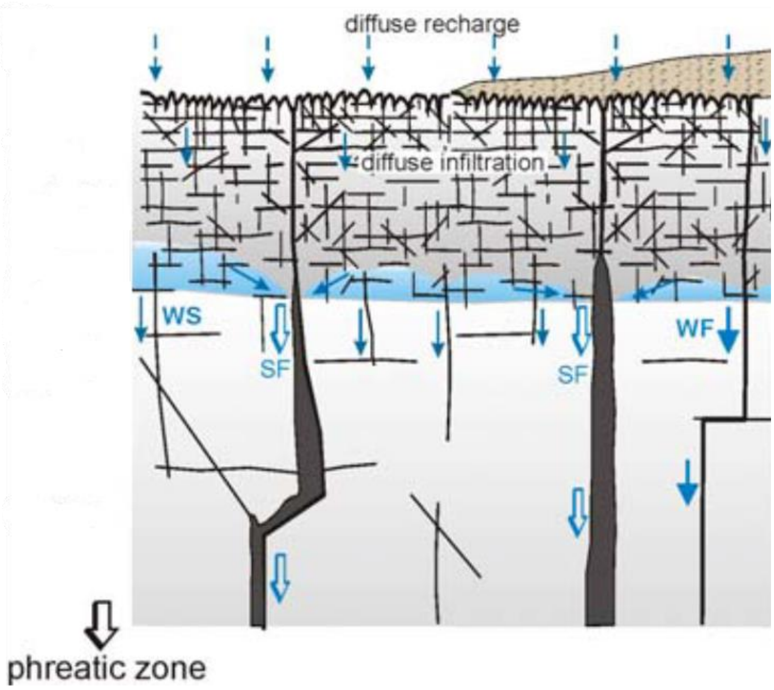

Fig. 5: Hydrologic functioning of the epikarst layer in relation to the underlying vadose zone. The figure shows the development of a temporal aquifer at the base of the epikarst due to increased recharge and preferential flow along larger shafts in the vadose zone (SF = shaft flow), that is accompanied by little flow along smaller fissures (WF = vadose flow) and even smaller rates through the matrix (WS = vadose seepage). From Klimchouk (2004).

2.4 Water stable isotopes

Natural occurring isotopes of water are ^{1}H, ^{2}H, and ^{3}H for elemental hydrogen and ^{16}O, ^{17}O and ^{18}O for elemental oxygen. Except ^{3}H (tritium) all of these are stable isotopes, meaning that they do not decay into daughter isotopes. ^{1}H (protium) and ^{16}O are by far the most abundant isotopes of water on earth, while ^{2}H (deuterium), ^{17}O and ^{18}O occur with a concentration of around 150 ppm, 400 ppm, and 2000 ppm, respectively (Goldscheider & Drew, 2007). In other words, ^{1}H accounts for 99.985 % of the hydrogen isotopes in the global average and ^{16}O for 99.76 % of the oxygen isotopes. Since the isotopes differ in number of neutrons, they also differ in terms of mass. While ^{1}H consists of one proton and zero neutrons, ^{2}H contains one proton and one neutron, having a mass number twice as large as ^{1}H (Fig. 6).

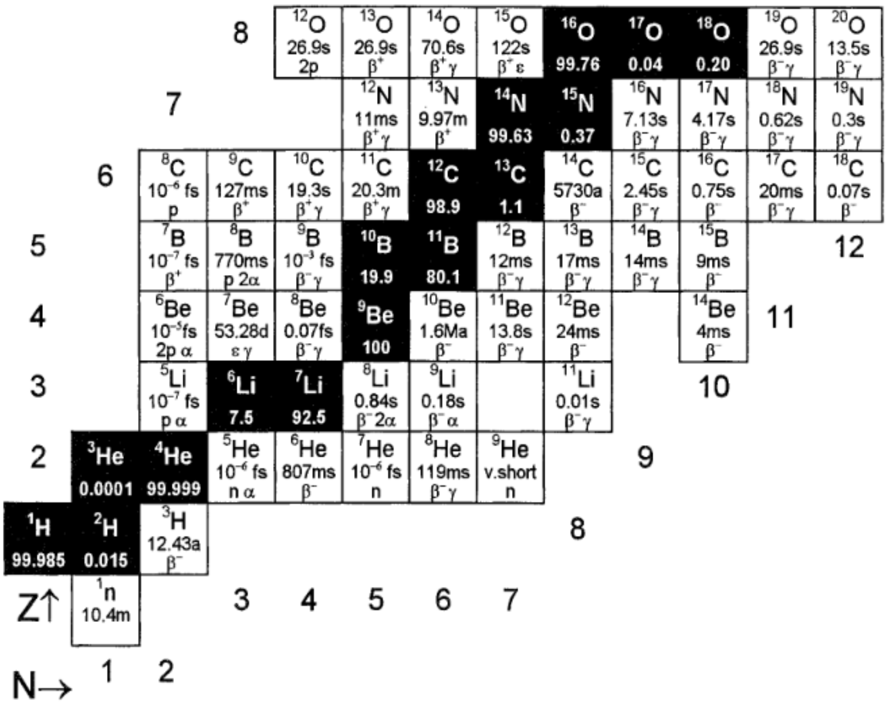

Fig. 6: Light element isotopes and the abundances of stable isotopes (black), as well as half-lives of radioisotopes (white). Number of protons (Z) is shown vertically and number of neutrons (N) horizontally. From Clark & Fritz (1997).

Usually, isotopes are not given in absolute values, but as the ratio of the heavier isotope to the lightest (and most abundant) one, expressed as R = $^2H/^1H$ in the case of hydrogen and R = $^{18}O/^{16}O$ for oxygen (Diamond, 2022). Widely used for the denotation of stable isotope is the delta-notation, whereas the isotope ratios of a sample are given relative to the Vienna Standard Mean Ocean Water (VSMOW):

$$\delta = \left(\frac{R_X}{R_{VSMOW}} - 1\right) * 1000$$

(Eq. 2)

where R_X is the isotope ratio of the sample, and R_{VSMOW} that of the VSMOW reference isotope ratio. The result is given as per mil (Clark & Fritz, 1997; Goldscheider & Drew, 2007).

Fractionation of environmental isotopes (e.g. hydrogen and oxygen) is the reason for changes in isotope ratios and therefore crucial for understanding and tracing hydrological processes (Clark & Fritz, 1997). If the isotope ratio R is getting higher, then it is commonly referred to an enrichment, whereas vice versa it is called depletion (Diamond, 2022). These thermodynamic processes, changing the relative amount of different weighted isotopes, can be separated into equilibrium fractionation or kinetic fractionation (Clark & Fritz, 1997; Goldscheider & Drew, 2007; Diamond, 2022). For example, as the bond strength ^{18}O–H is stronger than ^{16}O–H, evaporating water will show a higher initial transfer of lighter water molecules to vapour than of heavier water molecules. Therefore, the liquid phase is enriched (in heavy isotopes) and the gas phase depleted (Clark & Fritz, 1997).

Craig (1961) was able to establish a global correlation of δ^2H and $\delta^{18}O$ from freshwater samples that is known as the Global Meteoric Water Line (GMWL):

$$\delta^2 H = 8\,\delta^{18} O + 10 \qquad \text{(Eq. 3)}$$

However, spatial differences in this relationship can be significant, thus Local Meteoric Water Lines (LMWL) are often established to analyse long-term data from different regions. In order to trace the hydrological cycle, it is important to understand that not only spatial, but also temporal variations occur. Both are affected by factors such as temperature and the preferential rain out of heavier isotopes, leading to characteristic isotope ratios from different sources, sometimes referred to as isotopic fingerprint (Clark & Fritz, 1997). This holds true for large and small scales, making water stable isotopes effective tracers for water transport processes. Since water stable isotopes are not altered by chemical reactions and can be used as tracers for water flow, they can also provide information about water mixing.

3 State of the art and recent developments

3.1 Hydrogeology research at the Hochschwab

To the author's best knowledge, Stadler and Strobl carried out the first isotope sampling on the Hochschwab in 1971, investigating ^{3}H from different catchments and springs in the Hochschwab mountain range (Stadler & Strobl, 1997). From 1986 on they additionally sampled ^{18}O and from 1994 onwards ^{13}C (Stadler & Strobl, 2006). It was attempted to use $\delta^{18}O$ values for the calculation of average catchment elevations by establishing a gradient of -0.235 ‰ per 100 m (Stadler & Strobl, 1997). For the Kläffer springs the average elevation of the catchment was modelled to be 1718 m_{ASL} (Stadler & Strobl, 2006). Furthermore, $\delta^{18}O$ values from springs and precipitation were used to estimate mean transit times as a function of amplitude dampening of spring $\delta^{18}O$ ratios. Another method used for calculating mean transit times was the radioactive decay of ^{3}H, also called exponential model. Mean transit times calculated for the Kläffer springs are 0.5-0.8 years based on $\delta^{18}O$ measurements and 0.8-1.5 years based on $\delta^{3}H$ (Stadler & Strobl, 1997). However, these approaches of calculating mean transit times have been critically examined by recent publications (Kirchner, 2016).

Apart from this, a large number of hydrogeological research studies have been conducted in this area for many decades, due to its large springs and their importance for the supply of drinking water. As mentioned above, the largest of these springs are the Kläffer springs at the northern foot of the Hochschwab. Plan et al. (2010) gave an overview of the hydrological characteristics of the Kläffer springs as well as the geological setting, important karst features and the overall importance for the water supply of Vienna. The authors presented the results of discharge measurement of the several outlets of the Kläffer springs that were made from 1995 until 2006. The data shows the seasonal rhythm of the discharge that is mainly driven by snowmelt processes starting at the end of February and leading to a peak of discharge in May. Temporary but heavy rain events in August and September interrupt the decrease of discharge towards February. The mean discharge during this period was 5.2 m^3/s, with a maximum discharge of 45 m^3/s in August 2006 and a minimum of 0.39 m^3/s in December 1999. The opposite behaviour is observed for electrical conductivity and water temperatures, both reaching their lowest values at the end of May. Based on the geology of the Hochschwab and a water balance, a catchment area for the Kläffer springs of 60-70 km² was suggested.

In recent years, monitoring of the springs and precipitation at the Hochschwab mountain range has been supplemented by research of hydrological properties and functioning of the vadose zone. In the well karstified rocks of the Wettersteinkalk, flow and storage behaviour in the uppermost part have been investigated by various authors. Exel (2014) studied the water flow regime of the upper vadose zone and the epikarst in the Hirschgrubenhöhle with the installation of a weir. Together with measurement of electrical conductivity, temperature, and discharge, two precipitation events in 2013 were used for sampling water stable isotopes in the cave drip water. Conditions of low air temperatures between 1-11 °C for the first event and 1-7 °C for the second event were measured at a nearby meteorological station. During the first event temporary snowfall occurred. Reaction time of discharge to the precipitation was 4-5 h for these two events, whereas during the first event a sum of 73 mm of precipitation and 55 mm for the second event was measured. An epikarst overlay of 6 m thickness was estimated and the idea that epikarst holds significant potential for water storage is emphasized and supported by isotope data showing a mixing of newly infiltrated and old stored water within the epikarst. However, a quantification of the storage potential was not possible and seems to pose a great challenge.

Kaminsky (2020) investigated the water flow regime of the Furtowischacht. A master recession curve and a rainfall-runoff model were established on the basis of geological mapping, precipitation data and discharge measurements at a depth of 100 m within the vadose zone of the Hochschwab karst aquifer. In contrast to the Hirschgrubenhöhle major storage capacities in the epikarst could not be suggested for the investigated catchment area of the cave stream. Recession coefficients for quick flow of 4 1/d, intermediate flow of 1.4 1/d and baseflow of 0.4 1/d were calculated, alongside with volume proportions of 10 %, 40 % and 50 % respectively.

Recession analysis was also conducted for the cave drip water in the Hirschgrubenhöhle by Rabl (2023), which is situated within the catchment of the Kläffer springs. The catchment of the cave drip water is therefore a sub-catchment of the Kläffer springs and is estimated to be approximately 60 m² large. Based on a dataset from 17 month of continuous discharge measurements Rabl furthermore calculated a mean of 4.1 ml/sec and a mean delay of 84 min after precipitation events. By conducting a recession analysis, a minimum storage volume of 2 m³ was estimated.

3.2 Development of hydrograph separation and water transit time approaches using stable isotopes

The use of water stable isotopes as tracers has led to important breakthroughs in the evaluation of hydrogeological processes at catchment scale in the past (Klaus & McDonnell, 2013). For example, early hydrograph separations using $\delta^{18}O$ and $\delta^{2}H$ changed existing concepts of runoff generation and demonstrated the high proportion of stored water in springs reacting to preceding storm events (e.g. Mook et al., 1974). Perrin et al. (2003) were able to identify a significant mixing reservoir in the vadose zone of a karst aquifer in the Swiss Jura using water stable isotopes, precipitation data, and physiochemical measurements of the discharge. Furthermore, they quantified the fraction of fresh water on storm hydrographs by means of isotope event sampling and demonstrated the importance of soil and epikarst storage in karst aquifers.

In recent years water stable isotopes were also used to model water ages at catchment outlets, i.e. water transit times, based on mass conservation over age and time (Benettin et al., 2022). The time that is needed for one parcel of water to travel through the aquifer from its input to output location is called transit time (Rinaldo & Marani, 1987; Hrachowitz et al., 2016). In other words, the transit time is the age of the water parcel when it leaves the system as runoff (e.g. spring water) or is sampled as percolating water (e.g. cave drip water), whereas the age is per definition equal to zero when it reaches the catchment area and infiltrates into the subsurface. With this information it is possible to differentiate between water of different ages that contributes to the discharge generation (Hrachowitz et al., 2016). The concept of transit time distribution (TTDs) was developed to describe stored, mixed, and released water and solutes in a catchment (e.g. Kirchner et al., 2000; McDonnell & Beven, 2014).

In order to account for changing TTDs over time, a mathematical approach including the temporal evolution of the age of water entering the system was established by Botter et al. (2011), called master equation. The foundation was laid for the development of so called “StorAge Selection” (SAS) functions, which were successfully applied on different settings by various authors (e.g. Harman, 2015). These SAS functions quantify how volumes of stored water, differentiated by their age, contribute to runoff fluxes (Benettin & Bertuzzo, 2018), whereas preferential release from relatively younger or older stored water are distinguished (Benettin et al., 2022). From the resulting TTDs the fraction of water below or above a certain threshold age can be calculated in the discharge and insights about mixing from different temporal sources can be gained (Kirchner, 2016). Numerical models based on the solution of the master equation using SAS functions were developed and some are even available as open-source software, such as the *tran*-SAS model by Benettin & Bertuzzo (2018). SAS functions constitute a “state of the art”-tool to investigate flow path and water age distributions in karst aquifers (e.g. Zhang et al., 2021), but have not yet been applied to cave drip water, nor been applied in any form on the Hochschwab karst aquifer to the authors best knowledge.

4 Study Area

4.1 Geographical and climatic overview

The study area is located in northern Styria 100 km southwest of Vienna in the Hochschwab massif, which emerges south of the Salza River (Fig. 7). With an extend of 650 km², the mountain range is one of the largest karst massifs in the Northern Calcareous Alps, whereas the main plateau is covering an area of approximately 85 km² (Plan et al., 2010). Steep valleys with elevations from 550 to 900 m_{ASL} surround the plateau that ranges from 1400 m_{ASL} to the Hochschwab summit at 2277 m_{ASL}. The tree line is situated at approximately 1600 m_{ASL}, whereas up until around 1900 m_{ASL} extensive accumulations of *Pinus mugo* (known as mountain pine) can be found (Plan, 2016).

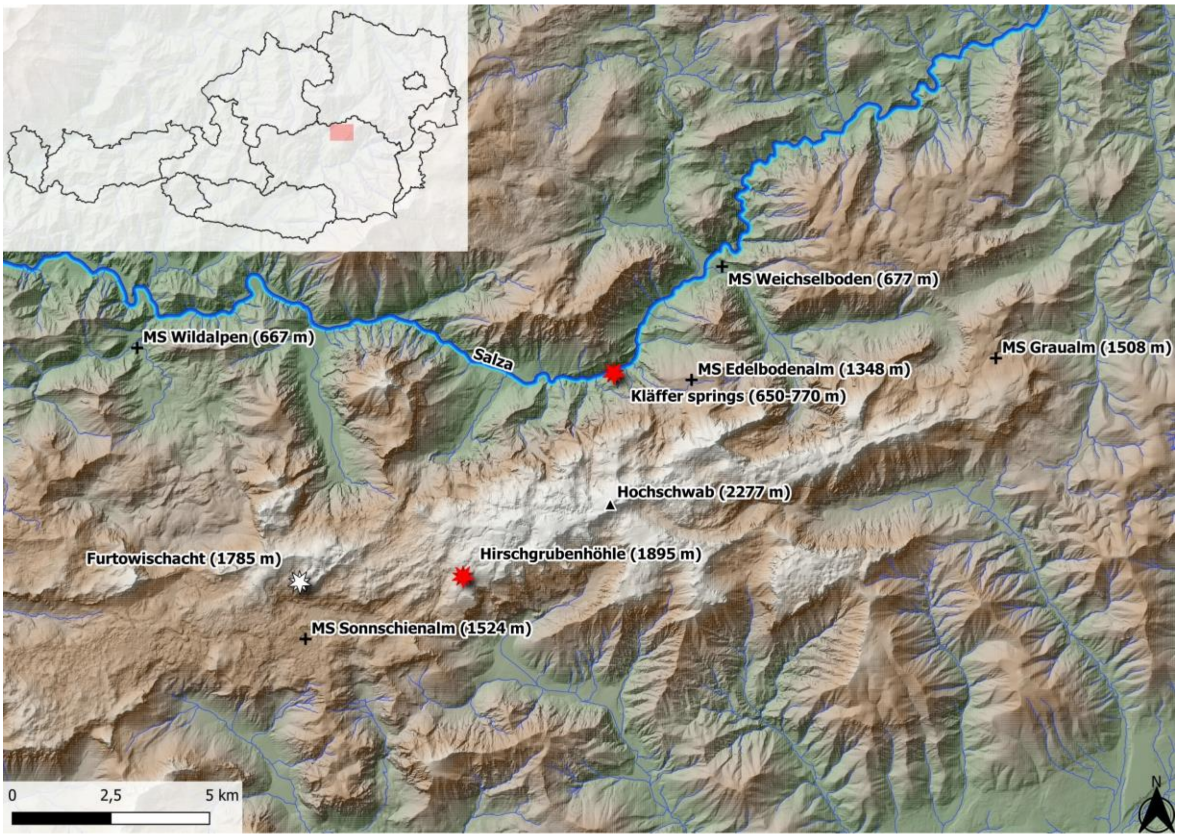

Fig. 7: The study area, the Hochschwab massif, with its characteristic karstic plateau in the Northen Calcareous Alps, south of the Salza river in northern Styria. The locations of the meteorological stations used in this study are indicated with crosses and the cave entrance of the Furtowischacht with a white star, whereas the Kläffer springs and cave entrance of the Hirschgrubenhöhle where water samples are taken are shown as red stars. Background: coloured digital terrain model, resolution 10 m, UTM 33N (data and layers from https://www.landesentwicklung.steiermark.at/cms/).

More than 900 caves with a cumulative length of ~ 90 km have been documented in this area, with a history of exploration dating back to the 17th century (Plan, 2016). The Hirschgrubenhöhle (Fig. 8), with a length of 5.6 km, is the second longest known cave within the Hochschwab massif. It was chosen for this study due to intensive hydrogeological research in the past and data availability from an already installed weir in the cave (Exel, 2014; Exel et al., 2016). The proximity to the surface of the phreatic parts of the cave and its spatial intersection with the eroded surface and vadose structures were another reason. The cave entrance, a collapse doline, is situated at 1896 m_{ASL} north of the Zinken summit (1926 m_{ASL}). Cave drip water is captured after an overlay of approximately 6.5 m, whereas soil cover represents a few tens of centimetres and epikarst ~ 6 m.

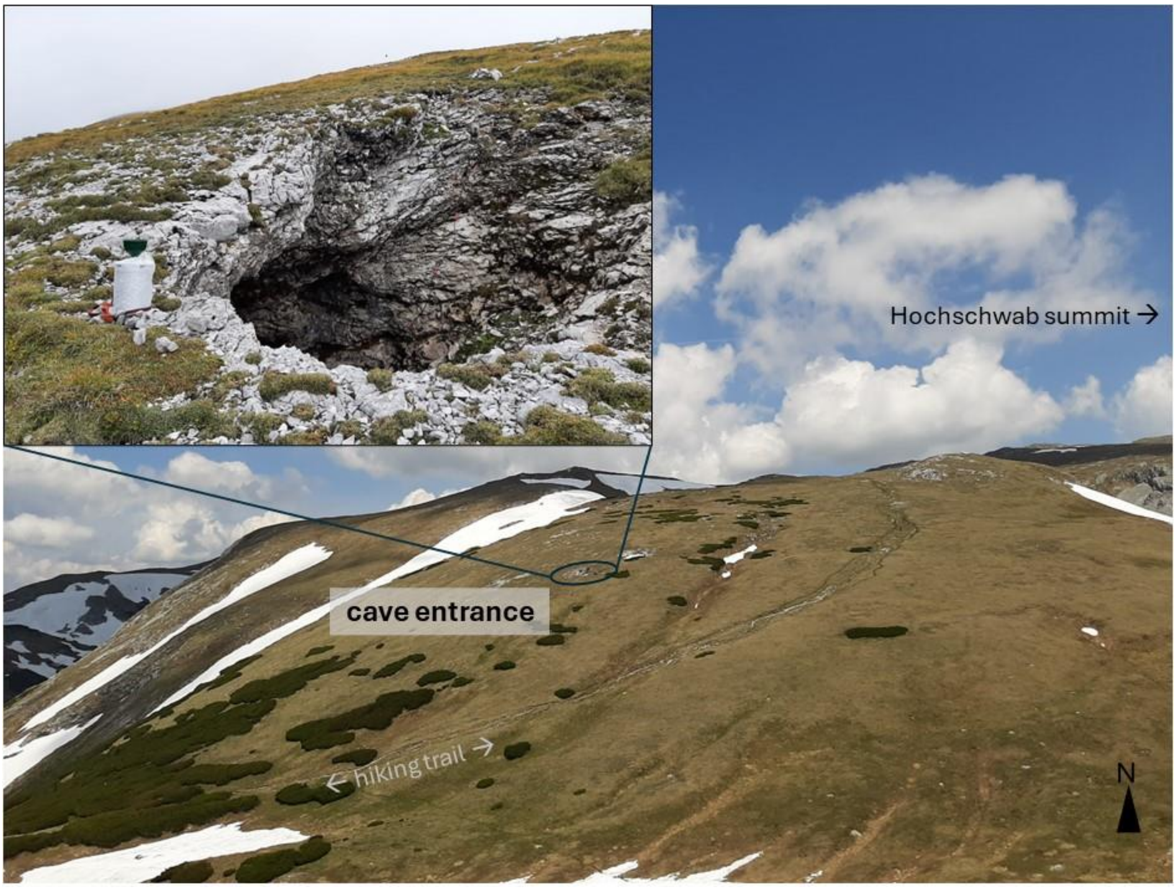

Fig. 8: Entrance of the cave Hirschgrubenhöhle at 1896 m_{ASL} (lower) on a SW dipping slope on the Hochschwab plateau. Direction of view is North. A rain sampler with a total height of ~ 0.5 m can be seen in front of the entrance.

The Kläffer springs (Fig. 9) have been developed for the Second Vienna Water Main in 1910 due to their high discharge of high-quality drinking water. At 650 m_{ASL} the permanent spring "Große Kläffer" is tapped for the water supply, whereas intermittent springs are located above from 650 to 770 m_{ASL} on a steep slope (Plan et al., 2010).

Fig. 9: The Kläffer springs draining into the Salza river during high flow conditions of ~ 14 m^3/sec (photograph taken on 9th May 2017 during snowmelt conditions). Direction of view is South (picture from Plan, L.).

The region of the Hochschwab massif has an Alpine climate, which is reflected by the wet and relatively cold conditions for Austrian standards. Mean annual temperatures are between 6-8 °C in the valley and slightly below 0 °C at the Hochschwab summit (2277 m_{ASL}). Precipitation is 1600-1800 mm per year in the valleys and over 2500 mm per year on the Hochschwab massif above 2100 m_{ASL}. The mean duration of dry periods above 1500 m_{ASL} is 2.9 days. Thunderstorms occur on the Hochschwab about 20 days a year. The climatic data was taken from Prettenthaler et al. (2010), which is based on a dataset from 1971 to 2000 and is made available at *https://www.umwelt.steiermark.at/cms/ziel/16178332/DE/*.

4.2 Geological overview

The Hochschwab massif is situated within the southernmost reaches of the Northern Calcareous Alps and is part of the Juvavic Mürzalpen Nappe, that was thrusted over the Tirolic Nappe system during the Upper Jurassic, as described in Bryda et al. (2013). In the study area, the stratigraphic sequence is mainly composed of limestone and dolomite up to 2000 m thick, which were deposited during the Middle and Upper Triassic (Fig. 10). Most dominant at the Hochschwab massif are the Steinalm and Wetterstein Formation, compromising an approximately 1500 m thick platform of limestone and dolomite in lagoonal and reef facies together with a few hundred meters thick slope and basinal limestones in the southern parts (Bryda et al., 2013). The evaporites (gypsum, anhydrite, halite, etc.), which originally formed the Permian base of the Mürzalpen Nappe, were mostly sheared off during thrusting onto the Tirolic Nappe system during the Jurassic. The overlying Werfener Unit comprises sandstones and shales of the Lower Triassic, which are superimposed by carbonates of the Gutenstein Formation, followed by the Steinalm and Wetterstein Formations. In the most elevated parts of the Hochschwab massif these are overlain by the Upper Triassic limestones of the Dachstein Formation (Bryda et al., 2013).

Three major fault sets are developed on the Hochschwab massif (Plan & Decker, 2006). A NW-striking set of dextral faults was formed during the folding and thrusting of the Northern Calcareous Alps in the Alpine orogeny with lateral extensions below 4 km. The most dominant tectonic structures are ENE-striking sinistral strike-slip faults from the Oligocene to Miocene, extending up to several tens of kilometres. This set is part of the shear zone of the SEMP (Salzachtal-Ennstal-Mariazell-Puchberg) Fault System delineating the boundary of the Mürzalpen Nappe to the Tirolic Nappe system in the north and shows signs of neotectonic movements in the Hochschwab area. The associated faults are forming permeable cataclasites, which are major pathways for water flow (Bauer, 2010). The third set compromises N-striking normal faults from the Miocene crosscutting older structures and length below 2 km.

The karst plateau of the Hochschwab massif was partially overprinted by glacial processes during Pleistocene glaciations, shaping the morphology and separating the plateau into glacial and paleosurface landforms (Van Husen, 2000; Plan & Decker, 2006). The former is characterized by large cirques that cut into the plateau and surrounding u-shaped valleys. At different elevations occurrences of paleosurfaces and epikarst can be found (e.g. the area around the Hirschgrubenhöhle), which is missing glacial overprint. The numerous and distinctive karst forms of the Hochschwab massif, as well as discharge behaviour are controlled (among other factors) by the different karstification properties of the various lithologies. Most karst features are developed in the limestones of the Steinalm and Wetterstein Formation, as well as the Dachstein limestones (Bryda et al., 2013). Karren fields and dolines are therefore most pronounced in limestones, reaching scales up to 100 m in diameter on paleosurfaces, where the rock was not glacially eroded. Of minor importance for the formation of karstic structures are the dolomites from the Steinalm, Wetterstein, and Dachstein Formation. In terms of storage capacity, however, these dolomites show a high potential. Sandstones and conglomerates from the Gosau Group and Prebichl Formation only carry small amounts of water in fractures and pores, whereas the finer grained sediments from the Werfener Unit are basically impermeable, compromising an aquiclude.

The uppermost parts of the Hirschgrubenhöhle are developed in the limestones of the Dachstein Formation, while the cave reaches down into the underlying dolomites of the Wetterstein Formation at a depth of approximately 80 m depth (Plan, 2004; Plan et al., 2019). Elliptical cave profiles, large scallops and karren structures in the ceiling clearly indicate phreatic conditions during cave development. Vadose structures cut through the initial cave system and are relatively younger. The entrance is situated within a paleosurface area on an approximately 20° SW-dipping slope. Exel et al. (2016) documented the presence of epikarst in the area of the Hirschgrubenhöhle, which is estimated to 6 m thickness.

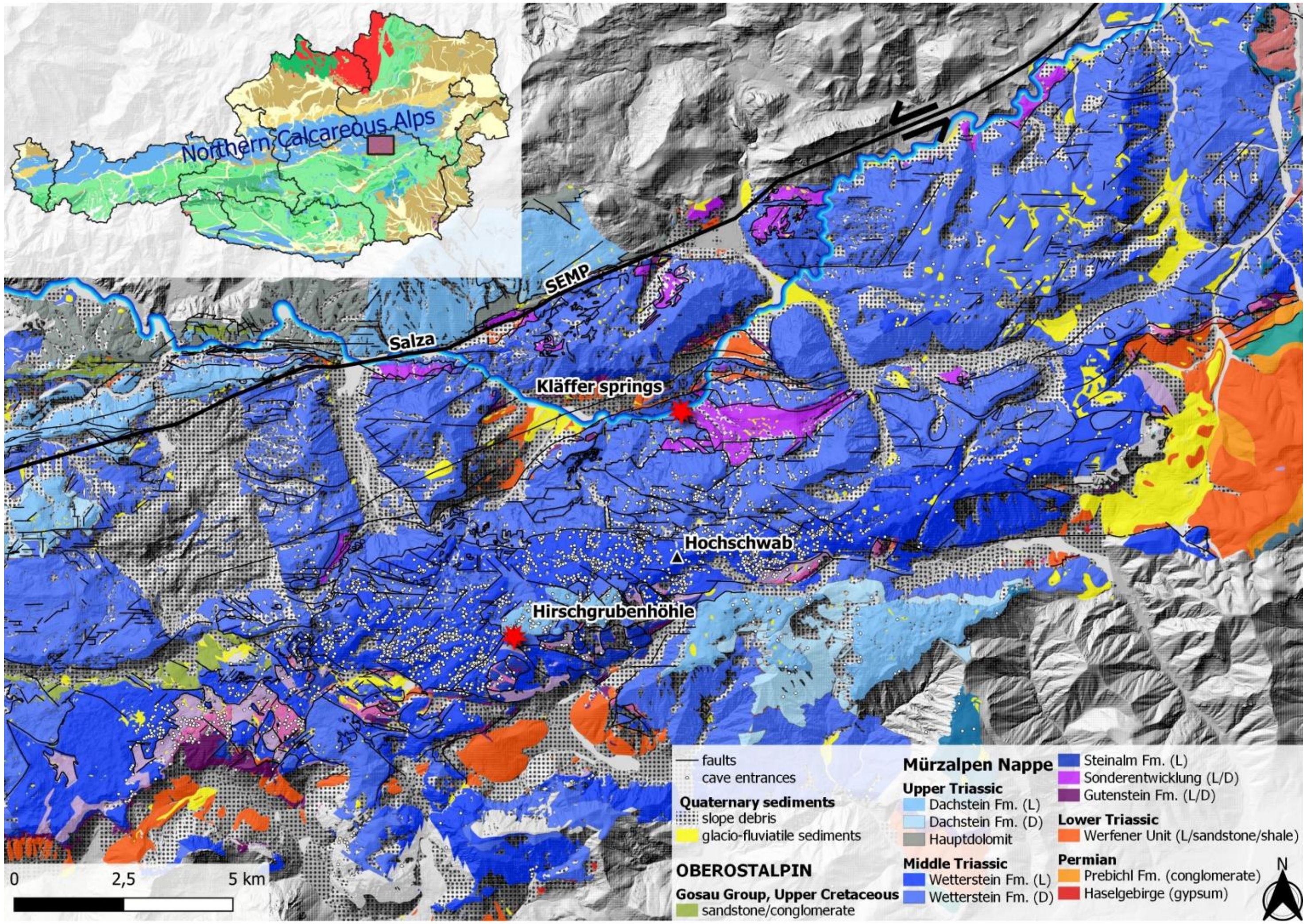

Fig. 10: Geological map of the Hochschwab massif after Mandl (2002). Cave entrances are courtesy of Plan, L. (Natural History Museum Vienna) and faults of Decker, K. (University of Vienna). Background: digital terrain model, resolution 10 m, UTM 33N (data and layers from https://www.landesentwicklung.steiermark.at/cms/). L: limestone; D: dolomite; Fm.: formation.

5 Methods

5.1 Timeframe and data collection

Between June and December 2023, seven one- to three-day field trips were undertaken in the Hochschwab mountain range (Fig. 11), as well as one day spent at the laboratory facility to prepare the water samples for stable isotope analysis using Cavity Ring-Down Spectroscopy (CRDS). Over a time period of approximately 3 months different modelling approaches for mixing ratios were conducted.

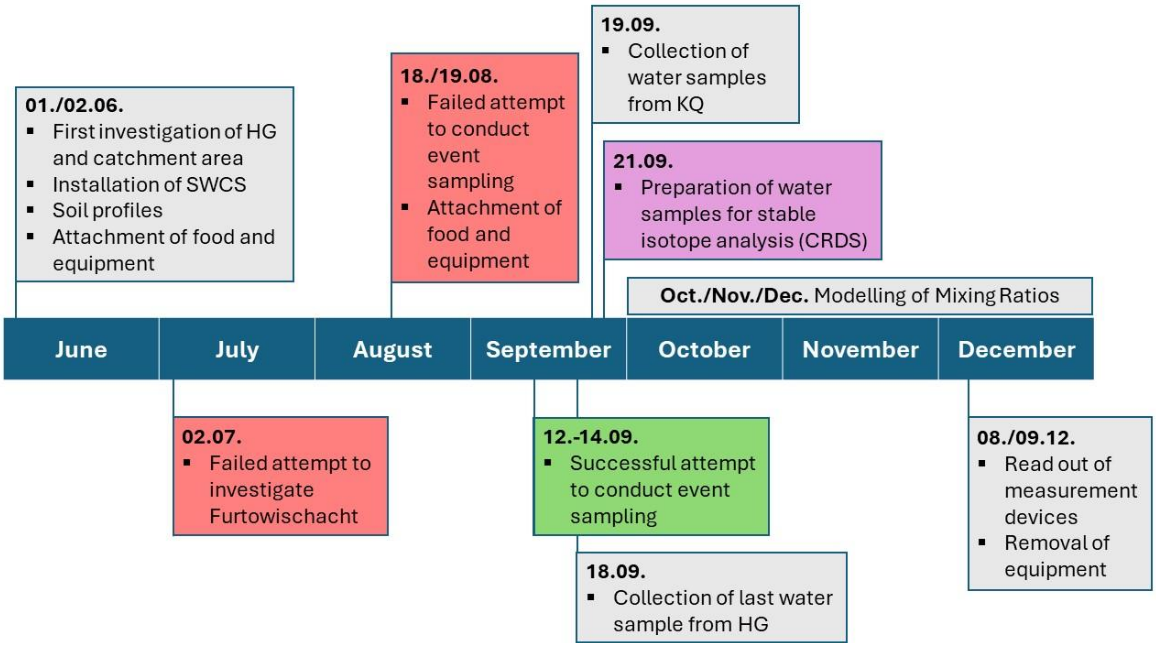

Fig. 11: Timetable for maintenance/installation of measurement devices and logistics as well as in-field preparation regarding the event sampling on 12-14th Sep 2023, as well as preparation of water samples in the laboratory facilities. SWCS: soil water content sensors; HG: Hirschgrubenhöhle; KQ: Kläffer springs.

During the first field trip on 1st and 2nd June 2023 preparations and investigations for the event sampling were conducted in the area of the Hirschgrubenhöhle, including installation of soil water content sensors and taking three different soil profiles. Event water sampling was carried out on 13th and 14th Sep 2023, whereas samples were taken from discharge in the Hirschgrubenhöhle and the Kläffer springs, as well as from precipitation at high frequency for subsequent stable isotope analysis. Continuous measurements were read out during further field trips or provided including meteorological data from different sites, physiochemical parameters of the cave drip water in the Hirschgrubenhöhle and the Kläffer springs outflow, the volumetric soil water content in the catchment area of the cave drip water and continuous isotope data ($\delta^{18}O$ and $\delta^{2}H$) from precipitation at two sites close to the Hochschwab mountain range. An overview of the different sites and their locations is given in Tab. 1 and Fig. 7.

Tab. 1: Overview of different measurement stations and their locations. MS: meteorological station; VSWC: volumetric soil water content; Q: discharge rate; T: temperature; EC: electrical conductivity; HG: Hirschgrubenhöhle; KQ: Kläffer springs.

	Type	Elevation [m_{ASL}]	Distance to HG* horizontal [km] vertical [m]	Distance to KQ horizontal [km] vertical [m]	Coordinates [UTM 33N]
Edelbodenalm	MS	1350	7.6 -546	2.0 +700	512723 E 5277014 N
Graualm	MS	1510	14.5 -386	9.6 +860	520502 E 5277503 N
Sonnschienalm	MS	1525	4.3 -371	10.4 +875	502993 E 5270422 N
Weichselboden	MS + isotopes	680	10.2 -1216	3.8 +30	513542 E 5279906 N
Wildalpen	isotopes	610	10.1 -1286	12.1 -40	498738 E 5277778 N
Hirschgrubenhöhle	rain gauge	1920	0.06 +24	6.4 +1270	506979 E 5272084 N
Hirschgrubenhöhle	VSWC	1915	0.05 +19	6.4 +1265	507008 E 5272064 N
Hirschgrubenhöhle	Q, T, EC	1890	0.04 -6	6.4 +1230	507005 E 5272059 N
Kläffer springs	Q, T, EC	650	6.4 -1246	0 0	510756 E 5277200 N

* Refers to the entrance of the Hirschgrubenhöhle at 1896 m_{ASL} (UTM 33N: 506986 E | 5272020 N).

5.2 Meteorological data

Data from four different meteorological stations (MS; Fig. 12) in the area of the Hochschwab was collected and provided by the "Municipal Department 31 – Vienna Water". The measured parameters include air temperature, global radiation, snow height, and precipitation intensity. For the purpose of this study only the intensity and amount of precipitation (in mm) and air temperatures (in °C) were used in 10 min intervals. Precipitation measurements were also taken nearby the entrance of the Hirschgrubenhöhle with a bucket type rain gauge at a frequency of 5 min.

Fig. 12: Meteorological station Sonnschienalm.

5.3 Physiochemical parameters of karst water

Discharge rate, water temperature and electrical conductivity are measured continuously for the cave drip water in the Hirschgrubenhöhle and the outflow at the Kläffer springs. Cave drip water around 6.5 m below surface is measured with an acrylic glass weir and tarps that channel the water (Fig. 13). A data logger and a *KELLER™ 36XW-CTD* multiparameter pressure rod were installed to measure water level, water temperature and electrical conductivity at 5 min time intervals. This monitoring system was set up in 2013 by Exel (2014) originally and rearranged to the current status, so that the minimum water column between overflow and logger is 7.7 cm (Fig. 14).

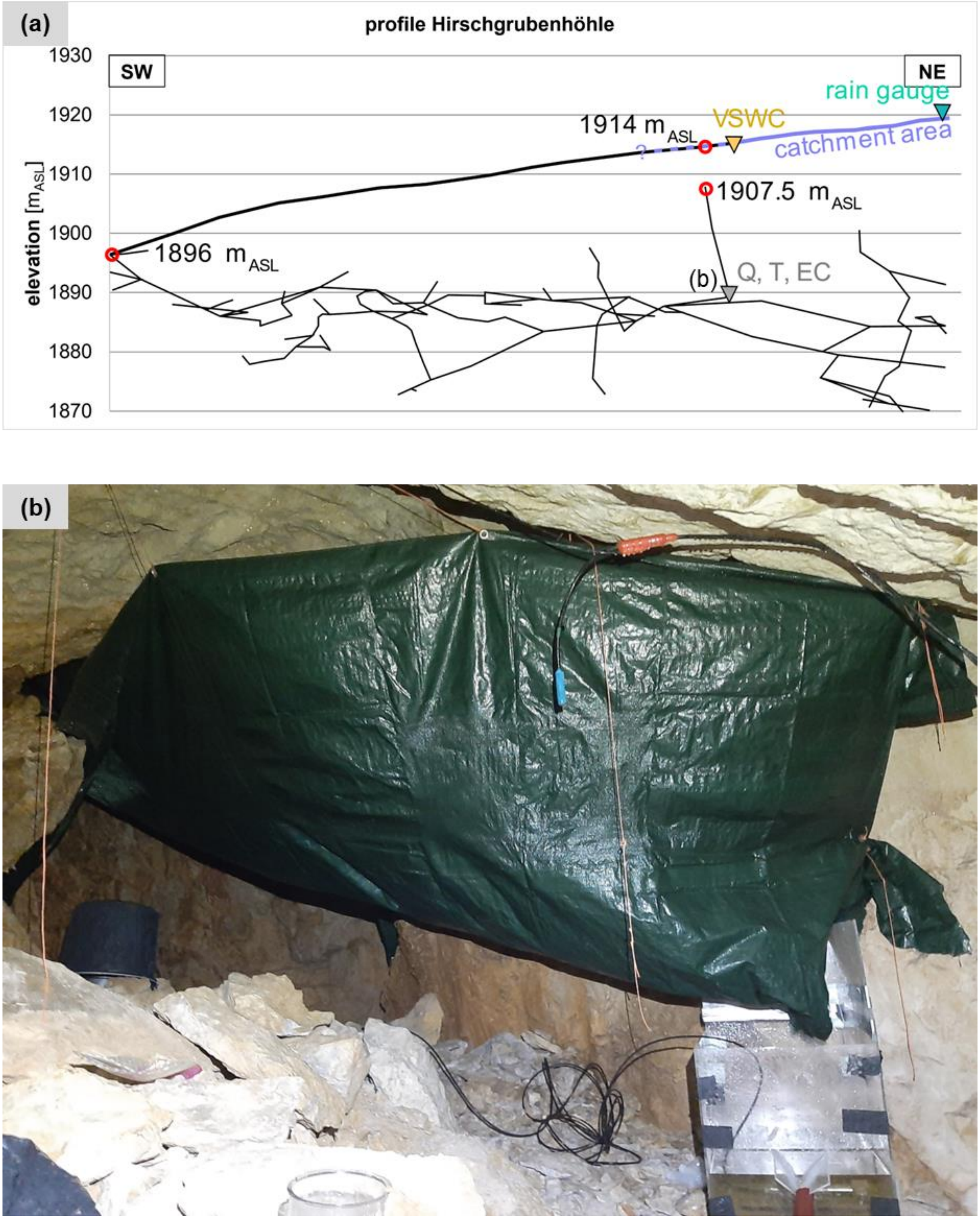

Fig. 13: (a) Cross section of the uppermost parts of the Hirschgrubenhöhle with height of the entrance and source of the cave drip water, as well as locations of volumetric soil water content (VSWC) sensors and rain gauge indicated (modified from Exel, 2014). (b) Setup to measure discharge (Q), temperature (T) and electrical conductivity (EC) consisting of tarps channelling the water into an acrylic glass weir with an overflow and a pressure rod.

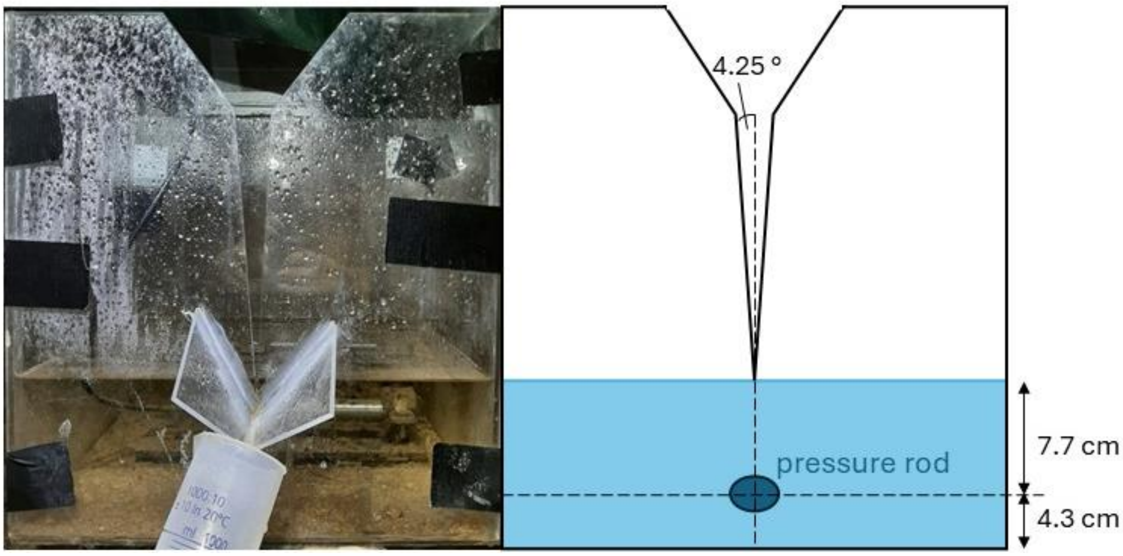

Fig. 14: Acrylic glass weir with overflow and a sketch of the minimum water level.

The following rating curve was used to convert from the measured water level (WL) in cm into discharge (Q) in ml/sec. It is based on 28 manual hand measurements conducted with a simple measuring vessel during the event sampling, which are fitted with a non-linear damped least-square approach (Fig. 15):

$$Q = 0.2303 * WL^3 - 3.2608 * WL^2 + 11.3395 * WL \quad \text{(Eq. 4)}$$

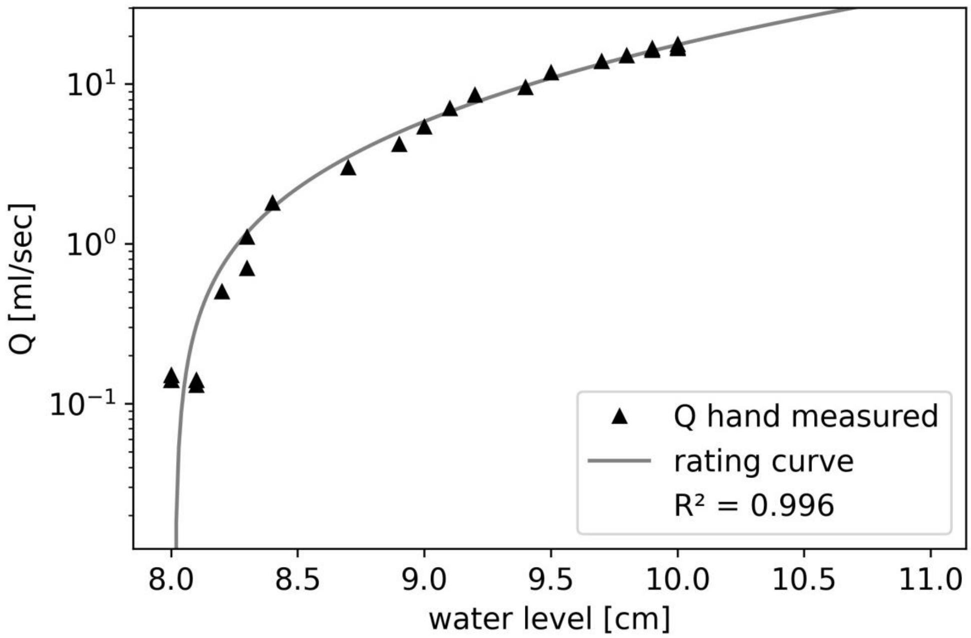

Fig. 15: Rating curve based on 28 discharge measurements conducted with a simple measuring vessel for very low flow conditions.

The Kläffer springs have been monitored in a complex setup by the city of Vienna since 1995 (Plan et al., 2010). As there are several surface springs, as well as springs that drain directly into the artificial water gallery, total discharge is calculated by the summation of two differential measurements. Water temperature and electrical conductivity are measured at three outlets (i.e. Large Kläffer, Small Kläffer and Kläffer tapping). The data for the Kläffer springs was provided by the "Municipal Department 31 – Vienna Water" with a resolution of 10 min.

5.4 Volumetric soil water content

The used data logger is a *METER*^{TM} *ZL6* with an integrated solar charging panel (Fig. 16). The soil water content sensors include five *METER*^{TM} *Teros 10* and one *Teros 12* which record the volumetric soil water content every 5 min and additionally soil temperature in the case of the *Teros 12*. The sensors use a dielectric measurement technique referred to as capacitance technology by the manufacturer (METER Group Inc., 2024), whereby a frequency of 70 MHz is applied to form an electromagnetic field between the two electrodes. The volumetric water content is therefore measured indirectly as a function of the apparent dielectric permittivity of the soil. Since the *Teros* sensors have not been calibrated according to the specific soil characteristics at the study site, deviations from the measured values of volumetric water content are possible, but relative changes are seen as reliable.

Fig. 16: Left: *ZL6* data logger with an integrated solar charging panel, stabilized with rocks; Right: *Teros 12* sensor for measuring volumetric water content.

An illustration of the measurement setup is given in Fig. 17. All six sensors were installed in various depths at three different locations with the help of a conventional soil auger. Soil profiles were taken down to the rock with the depth up to 50 cm and show humus at the top, and more sandy soil at the bottom. For a more detailed description of the soil in that area the reader is referred to the appendix (chapter 14.1) and Exel (2014). Boreholes were refilled with the soil matrix taken out once the sensors were placed with the electrodes parallel to the surface. Since the *Teros 10* sensors are 5 cm in length and the *Teros 12* sensors even 8 cm, the actual depth shown in Fig. 17 is to be understood as the given value ±2.5 cm (and ±4 cm for the Teros 12 respectively). The sensors are placed at a horizontal distance between approximately 3 and 4 m to it. Different sensors are referred to as “Port” 1 to 6, which relates to the different ports they are connected to in the *ZL6* logger. This setup was installed ~ 50 m uphill north of the entrance of the Hirschgrubenhöhle at an elevation of approximately 1915 m_{ASL} and is therefore situated in the expected catchment area of the cave drip water.

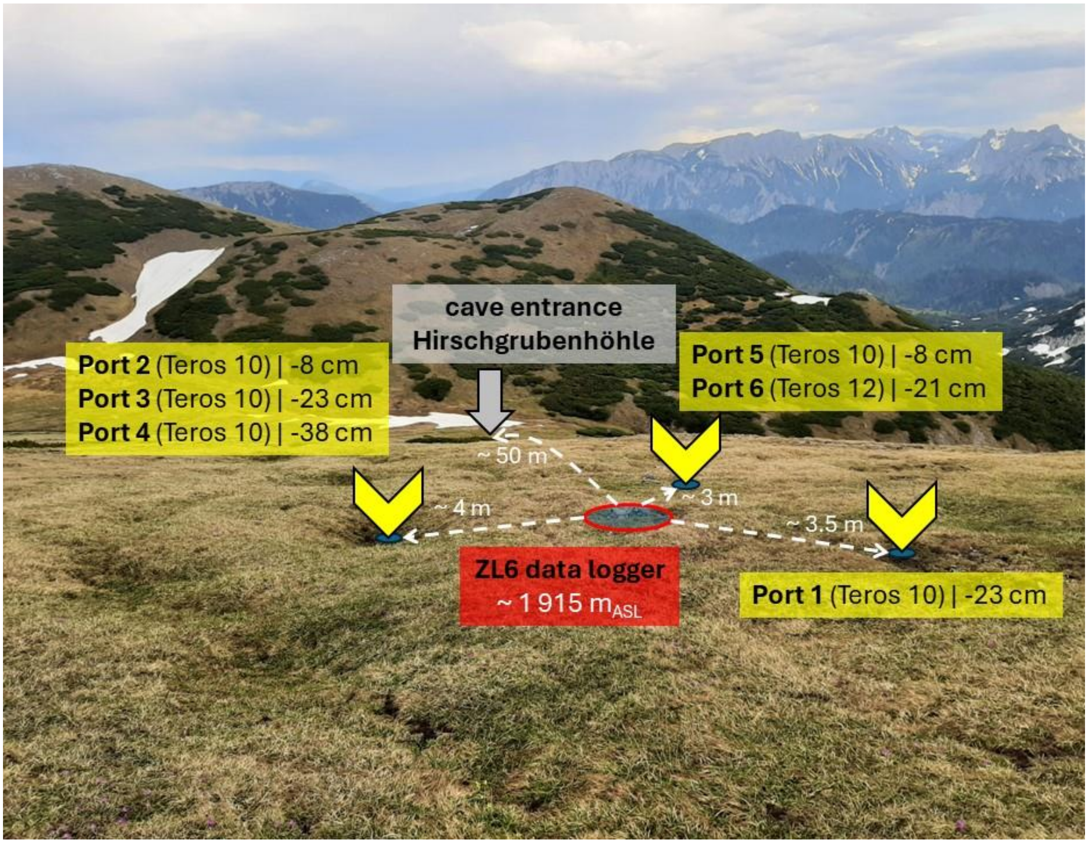

Fig. 17: Overview of the setup for measuring volumetric soil water content in the supposed catchment area of the cave drip water. Yellow arrows indicate locations of sensors, differentiated with associated values of depth below the surface. The *ZL6* logger (red) is located at approximately 1915 m_{ASL} and 50 m from the cave entrance. Direction of view is roughly South.

5.5 Isotope data

5.5.1 Long-term ^{18}O and ^{2}H in precipitation

Two precipitation measuring stations from the Austrian Network of Isotopes in Precipitation and Surface Waters (ANIP) were used to gather data about long term average isotopic composition of precipitation in the study area. The first station is the station IN60000080 located in Wildalpen at 610 m_{ASL} and provided continuous monthly $\delta^{18}O$ and $\delta^{2}H$ values from Jan 2007 to Mar 2023. The second one, at 680 m_{ASL}, is the station IN60000081, which is situated in Weichselboden and had continuous monthly $\delta^{18}O$ and $\delta^{2}H$ values available from Jan 2015 to Mar 2023. It should be noted that the ANIP precipitation measuring station in Weichselboden is integrated into the meteorological station, which is also used for precipitation intensity data in this study. An overview of the locations is given in Fig. 7, as well as in Tab. 1 and data is available under https://wasser.umweltbundesamt.at/wisa-datenabfrage/#/.

Precipitation samples are collected by the ANIP every last day of the month and therefore represent a mixture of the entire precipitation since the last collection. Data is made available in the Water Information System Austria (Federal Ministry, 2023). This data was subsequently used to calculate a LMWL and compare it to the GMWL. Therefore, $\delta^{18}O$ and $\delta^{2}H$ values were plotted against each other and both ordinary least square regression (OLSR) and precipitation weighted least square regression (PWLSR) trend lines were generated (Hughes & Crawford, 2012) in the form of $\delta^2 H = a * \delta^{18} O + b$, whereas x corresponds to $\delta^{18}O$, y to $\delta^{2}H$, and p to the respective amount of precipitation associated with each isotopic value.

	OLSR	**PWLSR**
a	$\dfrac{\sum xy - \frac{\sum x \sum y}{n}}{\sum x^2 - \frac{(\sum x)^2}{n}}$ (Eq. 5)	$\dfrac{\sum_{i=1}^{n} p_i y_i x_i - \frac{\sum_{i=1}^{n} p_i x_i \sum_{i=1}^{n} p_i y_i}{\sum p_i}}{\sum_{i=1}^{n} p_i x_i^2 - \frac{(\sum_{i=1}^{n} p_i x_i)^2}{\sum p_i}}$ (Eq. 6)
b	$\dfrac{\sum y - a \sum x}{n}$ (Eq. 7)	$\dfrac{\sum_{i=1}^{n} p_i y_i - a \sum_{i=1}^{n} p_i x_i}{\sum p_i}$ (Eq. 8)

5.5.2 Water stable isotopes (^{18}O and ^{2}H) event sampling

On the 13th and 14th Sep 2023, sampling was conducted at all sites during a storm event. A total of 85 water samples were taken from (a) precipitation, (b) cave drip water and (c) Kläffer springs outflow between 12th and 18th Sep 2023 (Tab. 2). Water was collected in airtight plastic bottles, protected from sunlight and cooled during transportation to the laboratory facilities.

Tab. 2: Amount of water samples taken from different locations.

	Hirschgrubenhöhle	Kläffer springs	MS Sonnschienalm
precipitation	6	-	1
karst water	30	48	-

Precipitation

Precipitation was sampled directly within the catchment area of the cave drip water in the Hirschgrubenhöhle and additionally one sample was taken at the MS Sonnschienalm, which is a bulk sample representing the rainfall from the whole rainfall event. Since both sites are located within the catchment of the Kläffer springs, no additional samples from precipitation were taken.

Fig. 18: Rain sampler at the entrance of the Hirschgrubenhöhle.

Precipitation samples were taken for logistical reasons at the entrance of the Hirschgrubenhöhle with the help of a *Palmex^{TM} Rain Sampler 1B* (Fig. 18). Different bulk samples have been taken by transferring water from the rain sampler into smaller glass and plastic bottles with a volume of 2-20 ml (Fig. 19). An effort was made to ensure airtight sealing and to avoid any air bubbles. Six samples at this location have been taken, whereas every sample represents a bulk of rainfall that was falling between the time of transfer into the sampling bottle and the last sample taken.

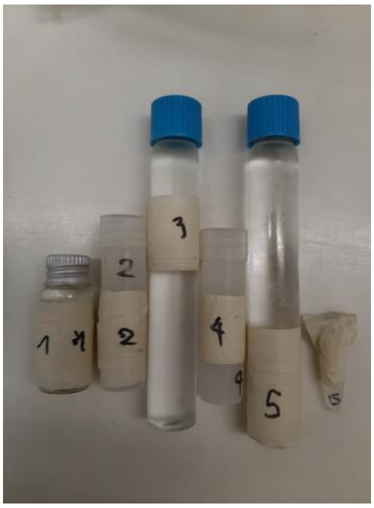

Fig. 19: Precipitation samples from the rainfall event on 13th and 14th Sep 2023.

Samples were taken every 48-520 min preferentially at times with low to zero rainfall to ensure that bulks for every sub-event could be measured (Fig. 20). For this purpose, the rain sampler at the cave entrance was checked at irregular intervals, depending on the weather conditions and the availability of those carrying out the operations. On the 14th Sep 2023, 20:30 CET* another sample was taken at the MS Sonnschienalm, representing a bulk of the entire event precipitation.

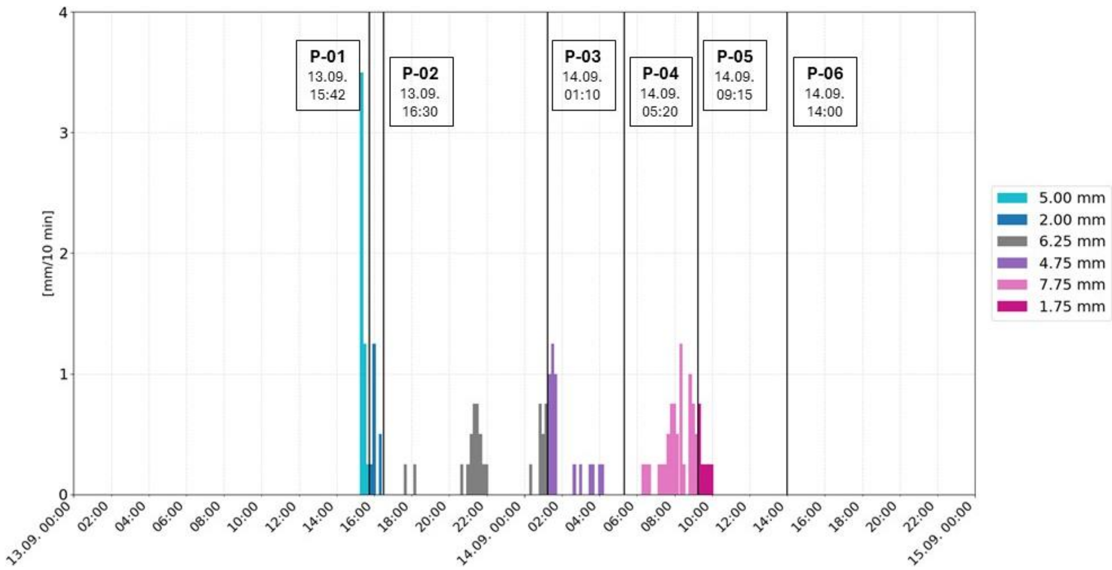

Fig. 20: Timing of precipitation sampling at the entrance of the Hirschgrubenhöhle in relation to rainfall intensity.

(All time information is given as CET in this work.)*

Cave drip water

Samples from the cave drip water were taken during the rain event on 13th and 14th Sep 2023 and during pre-event and post-even conditions to be able to compare isotopic ratios. Karst water in the cave Hirschgrubenhöhle was sampled at around 25 m below the surface, where an already existing weir for measurement of discharge, temperature and electrical conductivity is located (chapter 5.3). Water samples have been taken directly from the stream before entering the weir to avoid mixture with older water or fractionation processes. Plastic bottles by *Kautex™* with a volume of 50 ml and screw caps have been filled entirely with water and an effort was made to avoid air bubbles in the closed bottles, which was done successfully for most of the samples. At low discharge rates the sampling interval was between 60 to 340 min, while this was increased to up to 8 min during high rates of discharge. Two samples (HG-01 and HG-02) have been taken on 12th Sep, 11:15 and 13th Sep, 10:50 before rainfall started, to be able to measure stable isotope ratios of pre-event conditions. The two last samples have been taken on 14th Sep, 17:48 and 18th Sep, 12:30, which was a few hours before the next storm event started (chapter 5.2).

Kläffer springs outflow

Water samples have been taken simultaneously from the outflow at the Kläffer springs with a *Lange™ Bühler 2000* autosampler provided by the "Municipal Department 31 – Vienna Water". Bottles with a volume of 125 ml have been used for sampling at every hour from 13th Sep, 09:00 to 14th Sep, 08:00 (KQ-01 to KQ-24) and every two hours from 14th Sep, 10:00 to 16th Sep, 08:00 (KQ-25 to KQ-48). It should be noted that the bottles were filled up to approximately 1 cm below the rim but have been stored protected from sunlight and in a cooled place.

Cavity Ring-Down spectroscopy

The istopic ratios of $\delta^{18}O$ and $\delta^{2}H$ have been meassured for all precipitation and karst water samples taken between the 12th and 18th Sep 2023 using a *Picarro™ L2140-i* isotopic water analyzer (Fig. 21), which is equiped with a CRDS. Samples were prepared in the laboratory facilities on the 21st Sep 2023 for subsequent CRDS, whereas meassurment of all 85 samples was completed over a time period of five days until 26th Sep 2023. Samples were vaporized and injected into the spectrometer with the help of a vaporizer and a autosampler, respectively. Each sample was measured 7 times and the mean of the last three measurements used due to the memory effect, if the standard deviation was less than 0.1 ‰ for $\delta^{18}O$ and 1.0 ‰ for $\delta^{2}H$. Otherwise the measurement was repeated. All meassurments were subsequently plotted together with the GMWL as well as LMWL and OLSR and PWLSR trend lines were calculated (chapter 5.5.1; Eq. 5-8).

Fig. 21: *Picarro^{TM} L2140-i* isotopic water analyzer with CRDS technology.

5.6 End-member mixing

As described in chapter 2.4, water stable isotopes can be used as tracers for water flow. For the end-member mixing model both $\delta^{18}O$ and $\delta^{2}H$ values have been applied on the cave drip water in the Hirschgrubenhöhle and the outflow at the Kläffer springs. One way to look at the composition of the discharge at a certain sampling point is that it is derived by simple mixing of water that entered the aquifer as precipitation during the most recent rain- or snowfall and of water that was stored in the system from previous precipitation events. Under the assumption that discharge is such a mixture of two components the following equation describes this process (Fritz et al., 1975; Lakey & Krothe, 1996):

$$Q_T(t)C_T(t) = Q_P(t)C_P(t) + Q_E(t)C_E(t)$$

(Eq. 9)

where Q is the flow rate, C the δ values of the water and the subscript characters T, P and E stand for “total”, “pre-event” and “event”. In this equation “event” water refers to freshly infiltrated water from rainwater, while “pre-event” water represents the part of the water volume that was stored within the aquifer before the “event” water entered the system. The summation of both end-members results in the “total” amount of discharge. This equation can also be rewritten to eliminate Q_E and according to the only non-measurable parameter left Q_P:

$$Q_P(t) = \frac{Q_T(t)C_T(t) - Q_T(t)C_E(t)}{C_P(t) - C_E(t)}$$

(Eq. 10)

under the assumption that $Q_T = Q_P + Q_E$. It should be noted that the application of this approach was used mostly on watershed-scale in the past and underlies four different assumptions, as stated by Buttle (1994) and modified by Klaus & McDonnell (2013):

1. The isotopic content of the event and the pre-event water are significantly different.
2. The event and pre-event water maintains a constant isotopic signature in space and time, or any variations can be accounted for.
3. Contributions from the vadose zone must be negligible, or the isotopic signature of the soil water must be similar to that of groundwater.
4. Surface storage contributes minimally to the streamflow.

Especially assumption 2 is generally difficult to assess, since quantifying the influence of changing end-member isotopic ratios on discharge composition poses a great challenge (Kirchner, 2019). This is especially true for karst aquifers due to their complex and extremely heterogeneous hydrologic functioning (Zhang et al., 2019). Thus, in this study, high resolution sampling of water stable isotopes in precipitation and karst water flow was applied (chapter 5.5.2) before, during and after the rainfall event on 13th and 14th Sep 2023 to minimize the amount of interpretation needed. Nevertheless, it is clear that the choice of end-members influences the resulting mixing ratios strongly (Liu et al., 2004). Therefore, different choices of end-members (C_P and C_E) were modelled, to find the most plausible approach. Especially for the isotope ratios of the event water (C_E) several approaches were tested out:

C_{E-min}	This value assumes that 100 % of the event water in the discharge is derived only from precipitation with the <u>lowest</u> measured $\delta^{18}O$ (or δ^2H) ratios.
C_{E-max}	This value assumes that 100 % of the event water in the discharge is derived only from precipitation with the <u>highest</u> measured $\delta^{18}O$ (or δ^2H) ratios.
C_{E-med}	This value assumes that 100 % of the event water in the discharge is derived from precipitation with a $\delta^{18}O$ (or δ^2H) ratios of $\frac{C_{E-min}+C_{E-max}}{2}$.
$C_{E-shift}$	In this approach it is assumed that the variations in $\delta^{18}O$ (or δ^2H) values of precipitation during the event are reflected in the same order, but with a time shift equal to the time difference between start of the event and reaction of discharge.
$C_{E-weighted}$	In this approach it is assumed that 100 % of the event water in the discharge is derived from precipitation with an average $\delta^{18}O$ (or δ^2H) ratio weighted by rainfall intensity (Fig. 20).

For the pre-event water (C_P) it was assumed that it equals the isotope ratio of the total discharge (C_T) until discharge rates react to the rainfall event, meaning that pre-event water represents 100 % of the total discharge until then. From this point onwards C_P is decoupled from C_T and considered a constant value. This approach, however, is already limited strongly by the preconditions that are necessary to obtain results from Eq. 10, which are the following: $C_E \geq C_T \geq C_P$ or $C_P \geq C_T \geq C_E$

Otherwise, results will include end-member fractions of above 100 % or below 0 %. For this reason, the approach $C_{E-shift}$ was only applied in the parts, where preconditions were not violated. This was not necessary for the other C_E approaches, since they are fixed values (and are excluded in the further course of this study anyways if requirements are not met). As described here, the end-member model is subject to a number of assumptions that cannot always be fulfilled (Kirchner, 2019). Apart from this, some more advanced models for calculating water mixing have been developed in recent years (Klaus & McDonnell, 2013). One of these is the *tran*-SAS model by Benettin & Bertuzzo (2018), which was further applied to the collected data and is described below.

5.7 Numerical modelling

SAS functions are a more complex tool to calculate the proportion of stored water and fresh water using water stable isotopes. To be more precise, numerical modelling using a SAS functions framework can be used to calculate TTDs of water entering the karst aquifer as rainfall and leaving it as runoff (Benettin & Bertuzzo, 2018; Kaandorp et al., 2018; Benettin et al., 2022). To my best knowledge this approach has not been applied to percolating water in an aquifer yet, making this the first time to be tested on cave drip water. This method was only applied to the data from the Hirschgrubenhöhle during the rainfall event on 13th and 14th Sep 2023, as results from the isotope event sampling and end-member mixing model for the Kläffer springs show no clear signal of event water mixing (chapters 6.4.2 and 7.1). As common in tracer hydrology, only $\delta^{18}O$ isotopic ratios were used (e.g. Perrin, 2003; Weiler et al., 2003; Liu et al., 2004) as tracer input for this approach, since $\delta^{2}H$ should yield the same output (Stumpp et al., 2014). Similar results are expected for $\delta^{2}H$ values since they show the same patterns (chapter 6.4) and give similar results for end-member mixing (chapter 7.1).

In order to solve the age master equation numerically with SAS functions the *tran*-SAS model by Benettin & Bertuzzo (2018) has been used. This package is compatible with *MATLAB* and the theoretical basis is briefly outlined in chapter 3.2. The possible SAS functions that can be used are power law, beta and step functions. These can be selected separately for discharge and evapotranspiration fluxes, whereby the latter has been neglected (see below). Not all functions are explained here, but the best results for discharge fluxes were obtained using a time-variant power law function, which is defined as follows (in terms of a cumulative distribution function):

$$\Omega(S_T, t) = \left[\frac{S_T(T,t)}{S_0 + V(t)}\right]^k$$
(Eq. 11)

whereas S_T represents the storage volume younger than an age T at a given time t and S_0 the initial storage. V is the volume of water that has been added or removed from storage at a given time t and is obtained from the hydrologic balance equation $dV/dt = P - ET - Q$. Values of k [0, 1[imply preferential release of young water and k]1, +∞] for old water from the storage, whereas k = 1 represents no preference. If k is a fixed value this is called an invariant power law (invpl) age distribution. A time-variant power law (pltv) SAS function is obtained when defining $k(t) = kmin\_Q + [1 - wi(t)](kmax\_Q - kmin\_Q)$, with kmin_Q correlating to the wettest (wi = 1) conditions and kmax_Q to the driest (wi = 0) conditions. Wi is the wetness index and is one of the input parameters (see below), meaning that affinity for relatively younger water is established under wet conditions and vice versa.

The *tran*-SAS package was downloaded from GitHub and subsequently modified using *MATLAB R2023a* (The MathWorks Inc., 2024). The preparation workflow to use this model can be separated into two different steps: (a) creating a dataset that can be read by the model, and (b) changing the code according to the specific requirements of the measurements of the event sampling. For the model to solve the hydrologic balance equation dV / dt = P – ET – Q (deep losses neglected), the input dataset must include precipitation (P), evapotranspiration (ET) and discharge rate (Q) in the units of mm per time interval and the tracer input of precipitation (C_E) and discharge (C_T). To account for time-variant conditions an index is needed to control the affinity to younger or older water contributing to discharge. As explained by Benettin & Bertuzzo (2018) soil water content is suitable for this purpose, whereas wet conditions correspond to affinity to young waters and vice versa. The dataset covers a time frame from 7th Sep 2023, 09:00 to 20th Sep 2023, 19:30 and uses 5 min time intervals. The following data and adjustments are used as input for the *tran*-SAS modelling:

Precipitation	Measurements (in mm per 5 min) from the rain gauge at the Hirschgrubenhöhle without any modification.
Evapotranspiration	Evapotranspiration was assumed to be neglectable (discussed in chapter 6.4.2), and values were set to zero for the entire dataset.
Discharge rate (Q)	Cave drip water discharge measurements in 5 min intervals had to be converted by the formula Q [mm] = Q [ml/sec] * 300 [sec] / (1000 * A [m² catchment], whereas A is the catchment size. It was approximately estimated to 60 m² by Rabl (2023) and 120 m² was used for comparison in a second dataset.
Tracer input (C_E)	$\delta^{18}O$ values of precipitation at the Hirschgrubenhöhle from the first to the last sample have been interpolated to 5 min time steps.
Tracer output (C_T)	$\delta^{18}O$ values of cave drip water in the Hirschgrubenhöhle without interpolation or any further modifications.
Wetness index (wi)	Volumetric soil water content (in m³/m³) at the Hirschgrubenhöhle (Port 1, 23 cm depth) was normalized to values from 0 (minimum) to 1 (maximum) over the entire dataset.

The code had to be adjusted for the time step variable “dt_aggr” which by default takes input in the unit of hours and cannot be lower than 1. The modification presented here uses 5 min time steps, meaning that dt_aggr = 1 corresponds to a resolution of 5 min, dt_aggr = 2 respectively to a resolution of 10 min. This ensures that the sampled high-resolution data is not compromised. Furthermore, some minor modifications regarding the layout of the generated plots have been made, that are not explained in detail here since they do not have any effects on the results of the model. Another change of a more descriptive nature was made by using the term fraction of event water (Few) instead of young water fraction (Fyw) for describing the results. This was done because Fyw is defined by Kirchner (2016, S. 288) as the “proportion of the transit time distribution younger than a threshold age”. In the case of the particular rainfall event on the 13th and 14th Sep 2023 and the subsequent hydrological response of discharge rates, water with a TTD younger than ~ 230 h can only be derived from the event itself. This is due to a long dry period beforehand (chapter 6.1). Therefore, for this study Few is defined as $Q_{<230h}$ / Q_T.

A set of variables have to be defined prior to running the model (see above), strongly influencing the results. As the model computes tracer ratios in the discharge and compares them to measured values, these variables can be calibrated using a best-fit approach. The Nash-Sutcliffe efficiency (NSE; Nash & Sutcliffe, 1970) was used as a criterion for a good fit, which is employed to evaluate hydrological models:

$$NSE = 1 - \frac{\sum(o_i - s_i)^2}{\sum(o_i - \mu_O)^2}$$

(Eq. 12)

where s_i represents the simulated values, o_i the modelled values, and μ_O the observed mean of tracer ratios in discharge. In other words the NSE can also be seen as 1- $\left(\frac{root\ mean\ square\ error}{standard\ deviation}\right)^2$ and shows a perfect fit for an NSE close to 1, while values < 0 indicate that μ_O is more suitable than the model itself (Nash & Sutcliffe, 1970; Ritter & Muñoz-Carpena, 2013). Defining a threshold value for satisfactory results depends on the application and is, to some degree, subjective. Nevertheless, Ritter & Muñoz-Carpena (2013) proposed a framework for evaluating model performances using NSE values and suggest that an NSE > 0.65 shows acceptable results in many cases.

6 Results and interpretation

6.1 Meteorological data

Precipitation intensities for the hydrological year 2023 (USGS, 2023) measured at the MS Sonnschienalm are shown in Fig. 22, whereas the rainfall event used for isotope sampling is marked in red. The precipitation on 13th and 14th Sep 2023 was preceded by the longest dry period of the entire hydrological year, which lasted for 9 d and 18 h (at MS Sonnschienalm). Following this event occurred a dry period of 4 d and 6 h. Monthly $\delta^{18}O$ values from precipitation at the ANIP station Weichselboden are also depicted, showing an enrichment of ^{18}O compared to the average hydrological year.

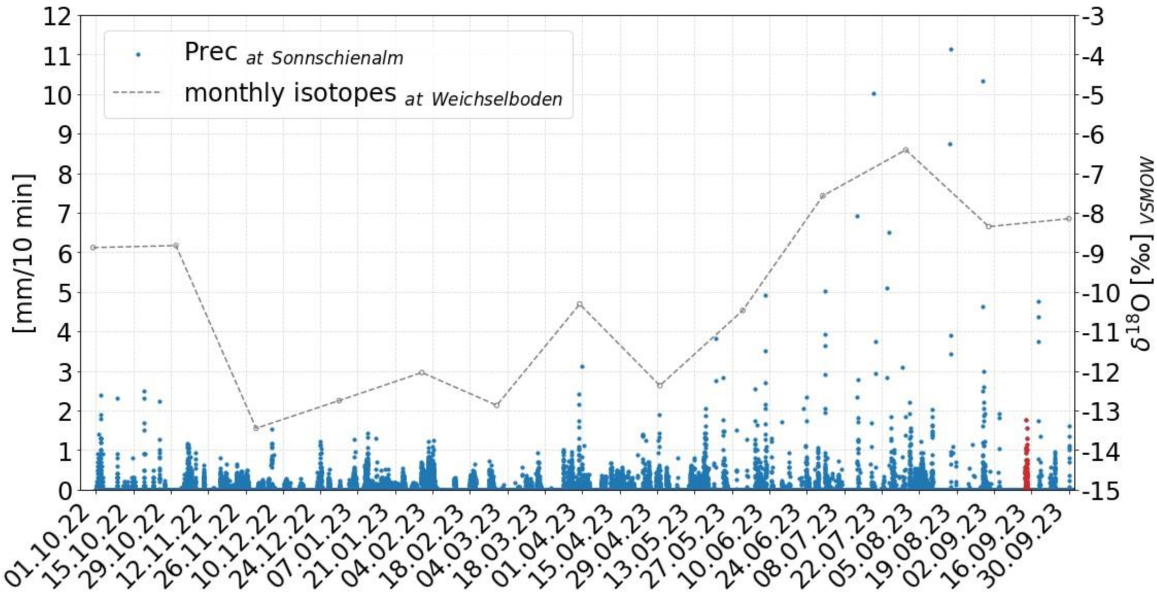

Fig. 22: Precipitation intensities at the MS Sonnschienalm during the hydrological year 2023. The sampled event from the 13th and 14th Sep 2023 is shown in red. Monthly isotope values from the MS Weichselboden are represented in grey.

During the event on 13th and 14th Sep 2023 a sum of 25 (measured at MS Sonnschienalm and MS Graualm) to 33 mm (measured at MS Weichselboden) fell (Fig. 23). The precipitation with the sum of 28 mm at the Hirschgrubenhöhle began at 15:20 with the maximum intensity of 3.5 mm / 10 min and lasted until 10:00 the next day. In general, rainfall amount decreases from NE to SW in the area of the Hochschwab mountain range.

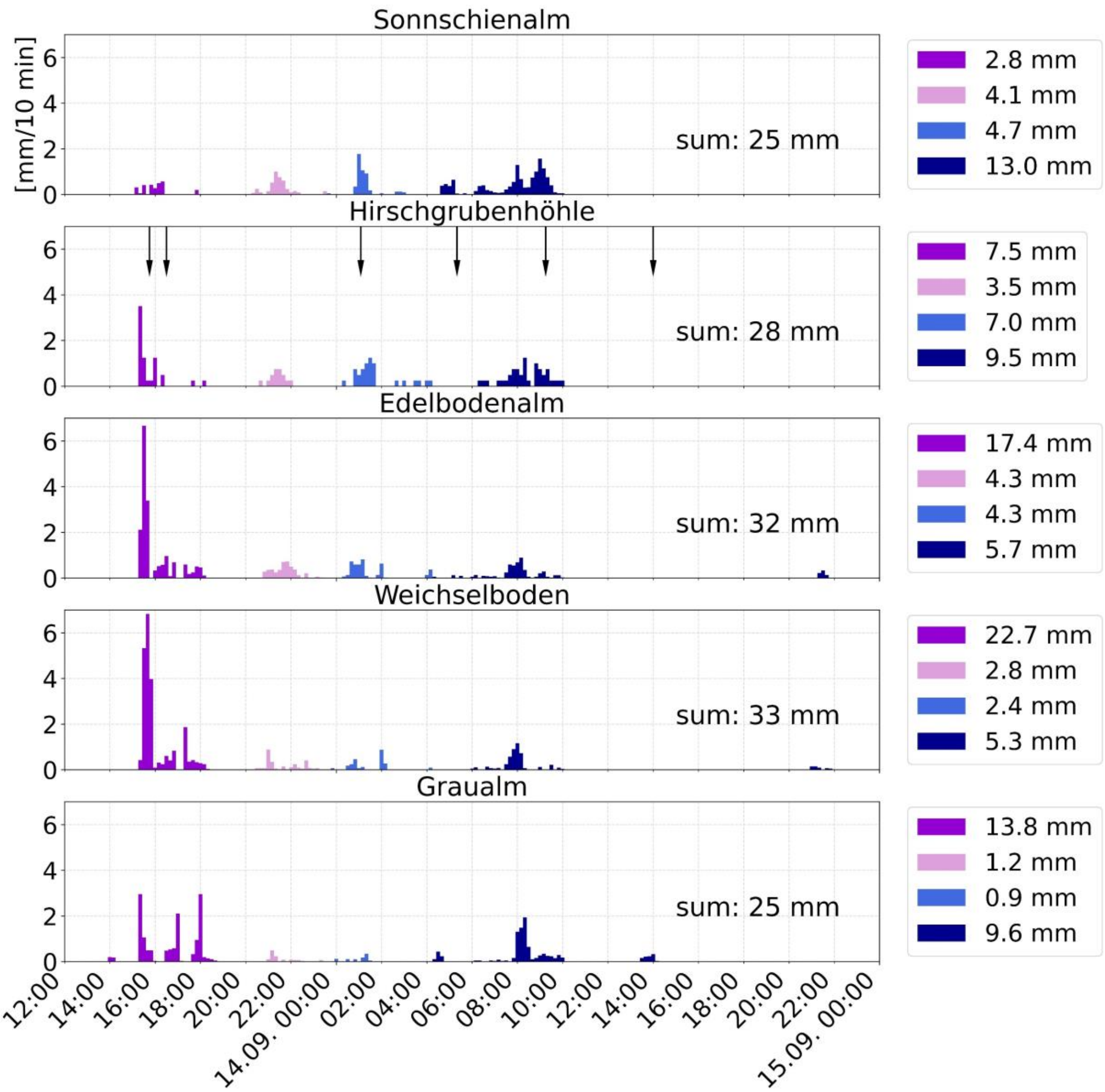

Fig. 23: Detailed plot of precipitation intensities from the 13th and 14th Sep 2023 for all meteorological stations shown from west (Sonnschienalm) to east (Graualm). Arrows at the Hirschgrubenhöhle show times of precipitation isotope sampling.

6.2 Physicochemical parameters of karst water

Physiochemical parameters (discharge rate, electrical conductivity and water temperature) measured for the cave drip water in the Hirschgrubenhöhle and the Kläffer springs are shown in Fig. 24 from 13th Sep to 19th Sep 2023. Additionally, volumetric soil water content, air and soil temperature, as well as rainfall intensity are indicated.

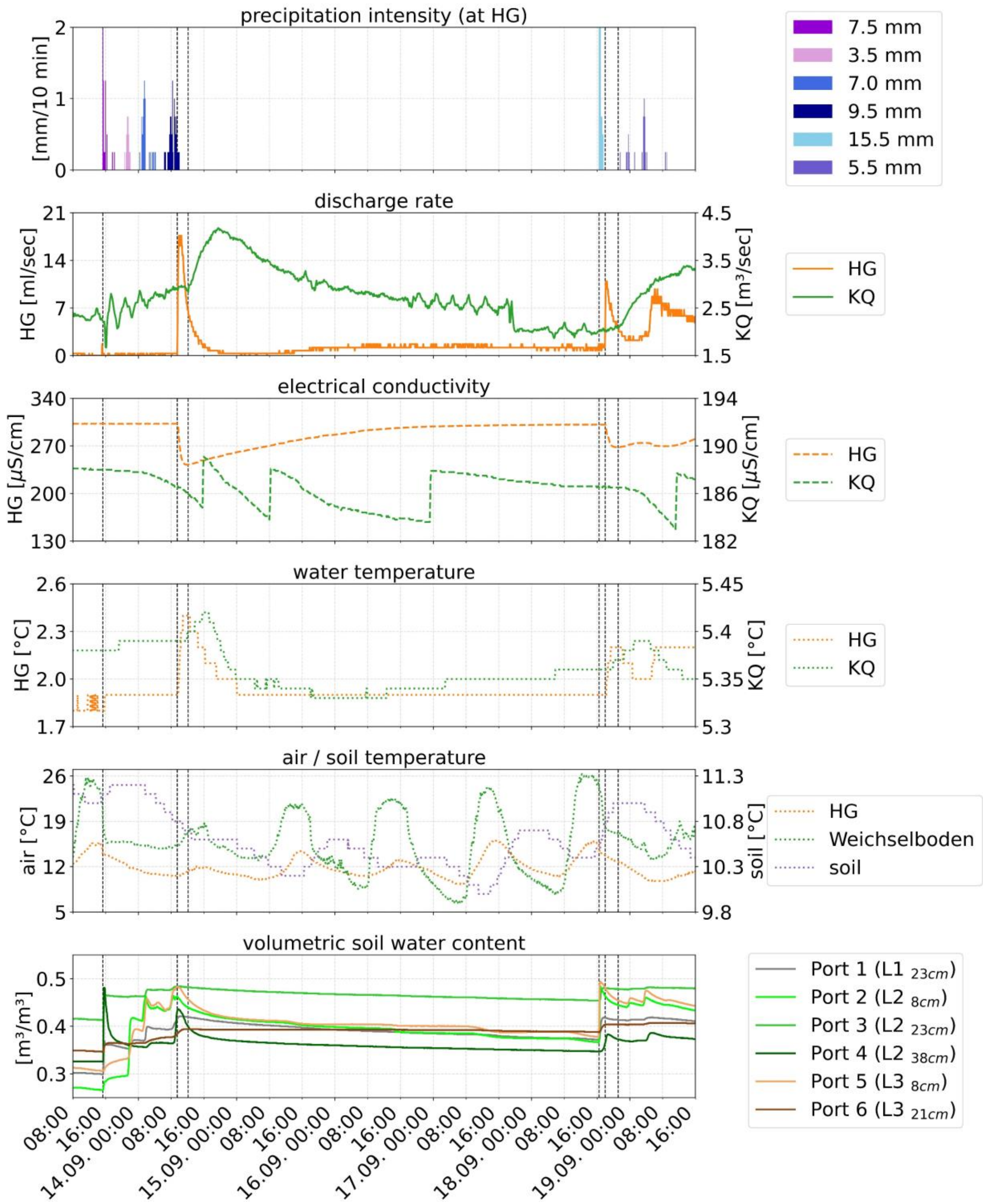

Fig. 24: Physiochemical parameters measured for the cave drip water in the Hirschgrubenhöhle (HG) and the Kläffer springs (KQ) from 13th to 19th Sep 2023 together with precipitation intensity, air and soil temperature, as well as volumetric soil water content at different locations (L1, L2, and L3) and depths.

Discharge

Discharge values for the cave drip water in the Hirschgrubenhöhle were generally low before the rainfall event on 13th and 14th Sep 2023 (Fig. 24), reaching a minimum of < 0.5 ml/sec after the last event. With the exception of a slight increase of 1.7 ml/sec at the time of rainfall onset, a delay in the discharge reaction of 18 h was observed, reaching a peak of 17.7 ml/sec within 25 min. Following a plateau of 45 min between 16.2-17.7 ml/sec, discharge levels drop back below 1.0 ml/sec 24 h after rainfall onset and reach < 0.5 ml/sec on 14th Sep, 19:30, respectively. At the Kläffer springs a minimum in discharge rates of 2.2 m^3/sec before the onset of the rainfall can be observed, continuing to decrease to 1.7 m^3/sec an hour afterwards. From this point onward discharge increases first to 3.0 m^3/sec and further to 4.2 m^3/sec with an accelerated rate, reaching a maximum 28 h after rainfall onset. Decreasing back to pre-event conditions, discharge values of 2.2 m^3/sec are attained on 17th Sep.

Electrical conductivity

Cave drip water in the Hirschgrubenhöhle had a constant electrical conductivity between 302 and 304 µS/cm before 14th Sep 2023, 09:40 (18.5 h after rainfall onset) and subsequently reacts simultaneously with discharge, reaching a minimum of 242 µS/cm 20.5 h after rainfall onset (Fig. 24). From there on a slow increase back to 301 µS/cm on 18th Sep can be observed. For the Kläffer springs a decrease of electrical conductivity to 185 µS/cm within 24.5 h after rainfall onset can be observed, before it jumps back to 188 µS/cm within minutes. This pattern repeats itself in different time intervals.

Temperature

Water temperatures for the cave drip water increase simultaneous to the discharge from 1.9 to 2.4 °C 20 h after rainfall onset, before decreasing back to 1.9 °C on 15th Sep (Fig. 24). For the Kläffer springs a continuous increase from 5.30 °C after the last event to 5.39 °C 21 h after rainfall onset occurs, from where a subsequent jump to 5.42 °C can be observed. From there on water temperatures drop back to 5.33 °C until 15th Sep.

A sudden drop in air temperatures can be observed during the onset of the rainfall from 15.7 to 13.8 °C for the Hirschgrubenhöhle and from 24.1 to 15.7 °C for the MS Weichselboden (Fig. 24). Afterwards temperatures increase only slightly and the first day peak around 15:00 the next day is suppressed, reaching only 12.1 and 18.7 °C respectively.

Similar to air temperatures the first peak of soil temperatures at the end of the rainfall event is strongly suppressed, resulting in a more or less continuous decrease from 11.2 to 10.2 °C within 44 h after rainfall onset (Fig. 24). Temperatures start to rise again on 15th Sep and from this point onwards the typical day-night fluctuation is restored, but continue to show an overall decreasing trend until 17th Sep.

Interpretation

Discharge values of the cave drip water and the Kläffer springs indicate an immediate reaction to the onset of rainfall. For the cave drip water this is visible as a small increase of discharge rate during onset of rainfall that lasts only for a few minutes, whereas the main increase is observed 18 h later. This phenomenon is interpreted as push-out of old water due to increased pressure from the first rainwater penetrating the soil along a certain pathway. From there stored water gets forced towards the cave drip water outlet as piston flow (Fig. 25). This is also visible in the electrical conductivity of the cave drip water showing a typical pattern for concentrated recharge, with less mineralized (and thus younger) water moving through the aquifer. As a change in electrical conductivity cannot be observed at onset of rainfall the theory is strengthened that the small increase in discharge is a result of transfer of water due to a pressure pulse, rather than a transit of water.

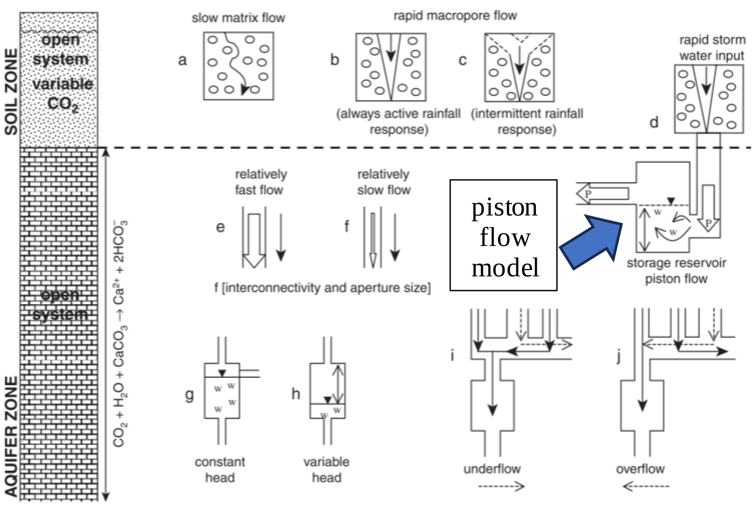

Fig. 25: Potential pathways for water flow in a karst aquifer (modified after Ford & Williams, 2007).

In the case of the Kläffer springs immediate increase of discharge at the onset of rainfall onwards is interpreted as a reaction to rainwater falling in close proximity to the spring, whereas 21 h later water from a further distance leads to the main increase of discharge. The observed course of discharge is therefore a result of the size of the catchment area and various travel times resulting from this. This interpretation is supported by slightly increased water temperatures of 0.01 °C for the spring water. It should be noted here that the fluctuations observed in the discharge values from the Kläffer springs is interpretated as artefacts from the measurement setup. The sudden jumps in electrical conductivity of the Kläffer spring water within seconds or a few minutes can only be explained as a measurement error.

6.3 Volumetric soil water content

Volumetric water contents (Fig. 24) for all sensors decrease from values between 0.38 m^3/m^3 (Port 2) and 0.46 m^3/m^3 (Port 3) at the end of the last event (3rd Sep 2023) to minimum values between 0.27 m^3/m^3 and 0.41 m^3/m^3 respectively at the onset of rainfall (13th Sep 2023, 15:20). While a sudden increase at all sensors can be observed at that time, only Port 4 shows a subsequent rapid release of water. All other sensors experience either a slight further increase (Port 2 and 5), a plateau (Port 3 and 6) or only slight decrease (Port 1) of water content. Values at all sensors continue to rise stepwise with a peak (except Port 4) on 14th Sep between 17-20 h after rainfall onset. A subsequent release of water content at all sensors (except Port 6) with slow but continuous decrease until 18th Sep to between 0.35 m^3/m^3 (Port 4) and 0.45 m^3/m^3 (Port 3) can be observed.

Interpretation

An unusual long dry period preceded the sampled rainfall event on 13th and 14th Sep leading to relatively dry pre-event conditions. The measurements of volumetric water content show that the soil was able to store large proportions of the freshly infiltrating rainwater, whereas some of the event water is also percolating into the underlying epikarst. Since this does not cause an immediate and significant increase in discharge, most of the water is still in storage. This could be an explanation for the relatively long lag between the onset of the first rainfall and increased discharge of the cave drip water. The quick release of fresh water at the base of location 2 (Port 4) indicates fast water flow in this area and reinforces the assumption that the small increase in discharge during that time is caused by push-out of old water (see above). The other possibility, that this pathway connects directly to the outlet of the cave drip water is improbable, due to the isotope data which is shown in the next chapter. Not until 17 h after rainfall onset is the maximum storage capacity of the soil reached and significant amounts of water are released promptly towards the epikarst and the cave, leading to the main increase in discharge of the cave drip water.

6.4 Isotope data

6.4.1 Long-term ^{18}O and ^{2}H in precipitation

From monthly $\delta^{18}O$ and $\delta^{2}H$ data at Wildalpen and Weichselboden (Salza valley) LMWLs were constructed and illustrated together with the GMWL in Fig. 26. While measurements at Wildalpen range from Jan 2007 to Mar 2023 ($n = 193$), they only range from Jan 2015 to Mar 2023 ($n = 95$) in Weichselboden. The data from both sites show an ordinary least square regression (OLSR) trend line of $\delta^2 H = 8.08\, \delta^{18} O + 10.05$, and a precipitation weighted least square regression (PWLSR) trend line of $\delta^2 H = 8.04\, \delta^{18} O + 9.81$.

The mean values weighted by precipitation amount at Wildalpen are -10.35 $\delta^{18}O$ / -73.18 $\delta^{2}H$ for the years 2007 to 2020 and -9.80 $\delta^{18}O$ / -69.91 $\delta^{2}H$ at Weichselboden between 2015 and 2018. Both LMWLs for all data indicate slightly steeper slopes than the GMWL, whereas only the PWLSR approach has a lower intercept. Weichselboden data plots closer to the overall OLSR trend line, while Wildalpen isotope values plot closer to the overall PWLSR trend line. For further comparison the PWLSR of all data was used.

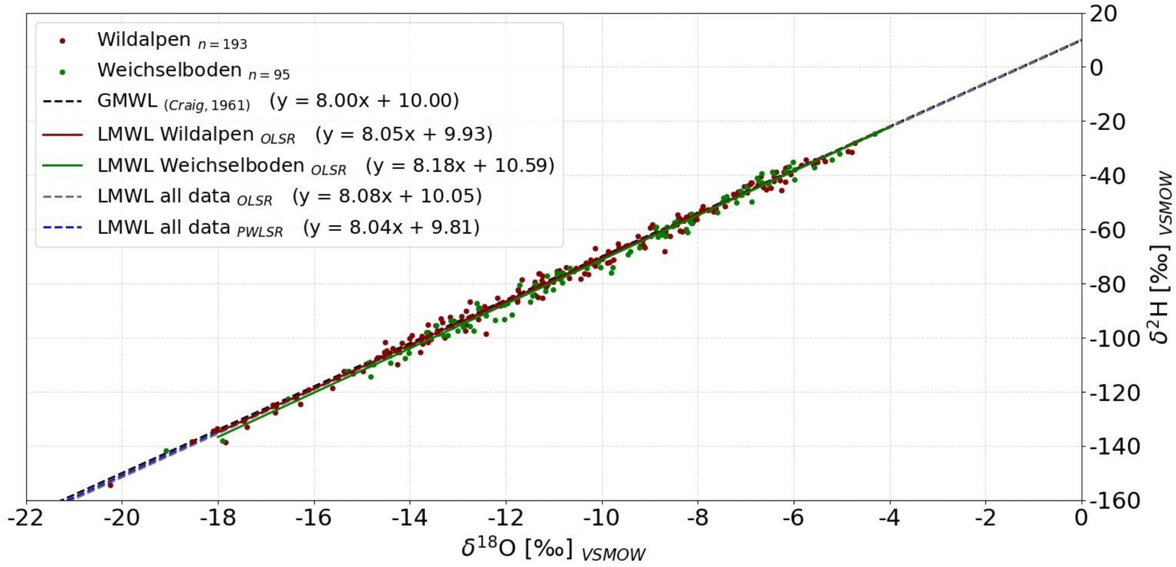

Fig. 26: Global Meteoric Water Line (GMWL) and Local Meteoric Water Lines (LMWLs) for Wildalpen and Weichselboden, as well as LMWLs generated from data from both sites (n = 288) without weighting (OLSR; grey dashed line) and weighted after precipitation (PWLSR; blue dashed line).

6.4.2 Water stable isotopes (^{18}O and ^{2}H) event sampling

Measured values of $\delta^{18}O$ and δ^2H from samples taken between 12th and 19th Sep 2023 in the Hochschwab mountain range are plotted against each other in Fig. 27 together with the GMWL and LMWL. Additionally, one unweighted regression (OLSR) for the six samples representing the precipitation at the cave entrance of the Hirschgrubenhöhle (P-HG) was constructed $\delta^2H = 7.54\ \delta^{18}O + 11.04$, and another one weighted by precipitation amount (PWLSR) $\delta^2H = 6.43\ \delta^{18}O - 1.04$. The sample taken from the MS Sonnschienalm (P-SS), representing a mixture of the entire rain that fell on 13th and 14th Sep 2023, plots with values of -10.19 $\delta^{18}O$ / -68.53 δ^2H between the P-HG trend line and the LMWL (or GMWL respectively). In comparison to this, the mean value for P-HG weighted by precipitation amount at the cave entrance is -10.94 $\delta^{18}O$ / -71.14 δ^2H. It should be noted that the MS Sonnschienalm is situated 371 m below the entrance of the Hirschgrubenhöhle.

Values for the cave drip water (HG) in the Hirschgrubenhöhle plot along the P-HG trend line, whereas they fit both to the PWLSR and OLSR. They range from -10.86 $\delta^{18}O$ / -70.04 δ^2H to -9.12 $\delta^{18}O$ / -58.35 δ^2H. Samples from the Kläffer springs (KQ) plot as cluster in the lower part of the range between the P-HG trend line and the LMWL (or GMWL respectively), ranging from -11.51 $\delta^{18}O$ / -78.34 δ^2H to -10.85 $\delta^{18}O$ / -74.81 δ^2H.

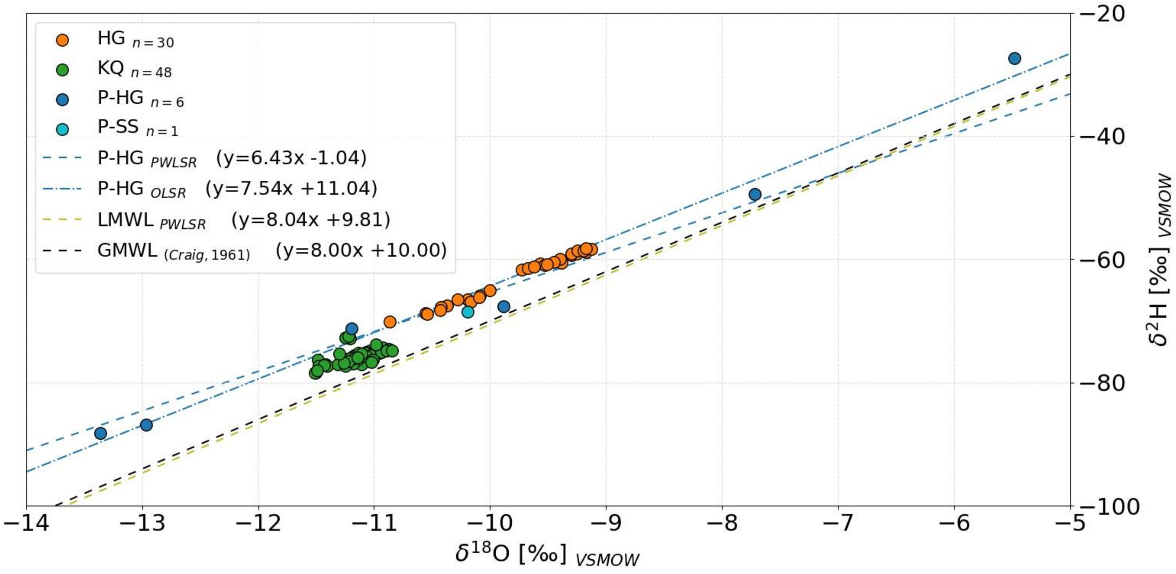

Fig. 27: Dual isotope plot of δ^{18}O and δ^{2}H values for cave drip water in the Hirschgrubenhöhle (HG), the Kläffer springs (KQ), precipitation at the cave entrance (P-HG) and precipitation at the MS Sonnschienalm (P-SS) sampled between 12th and 19th Sep 2023 in comparison to the Global Meteoric Water Line (GMWL) and constructed Local Meteoric Water Line (LMWL).

In Fig. 28 a time series for water stable isotope values in all samples between 12th and 19th Sep 2023 is shown. Both the δ^{18}O and the δ^{2}H values have the same pattern. The isotopic signal in P-HG varies strongly between -13.36 δ^{18}O / -88.22 δ^{2}H and -5.48 δ^{18}O / -27.40 δ^{2}H, following an N-shape. For the values of the cave drip water (HG) a depression of values from onset of rainfall (13th Sep, 15:20) to 17 h afterwards can be observed, before a distinct increase occurs peaking 19 h after rainfall onset. Following this, a short decrease can be observed with a subsequent second peak 2 h after the first one, before decreasing again. At the Kläffer springs (KQ) no clear isotopic signal is visible in the samples, as values only show recurring fluctuations, but without increased amplitude.

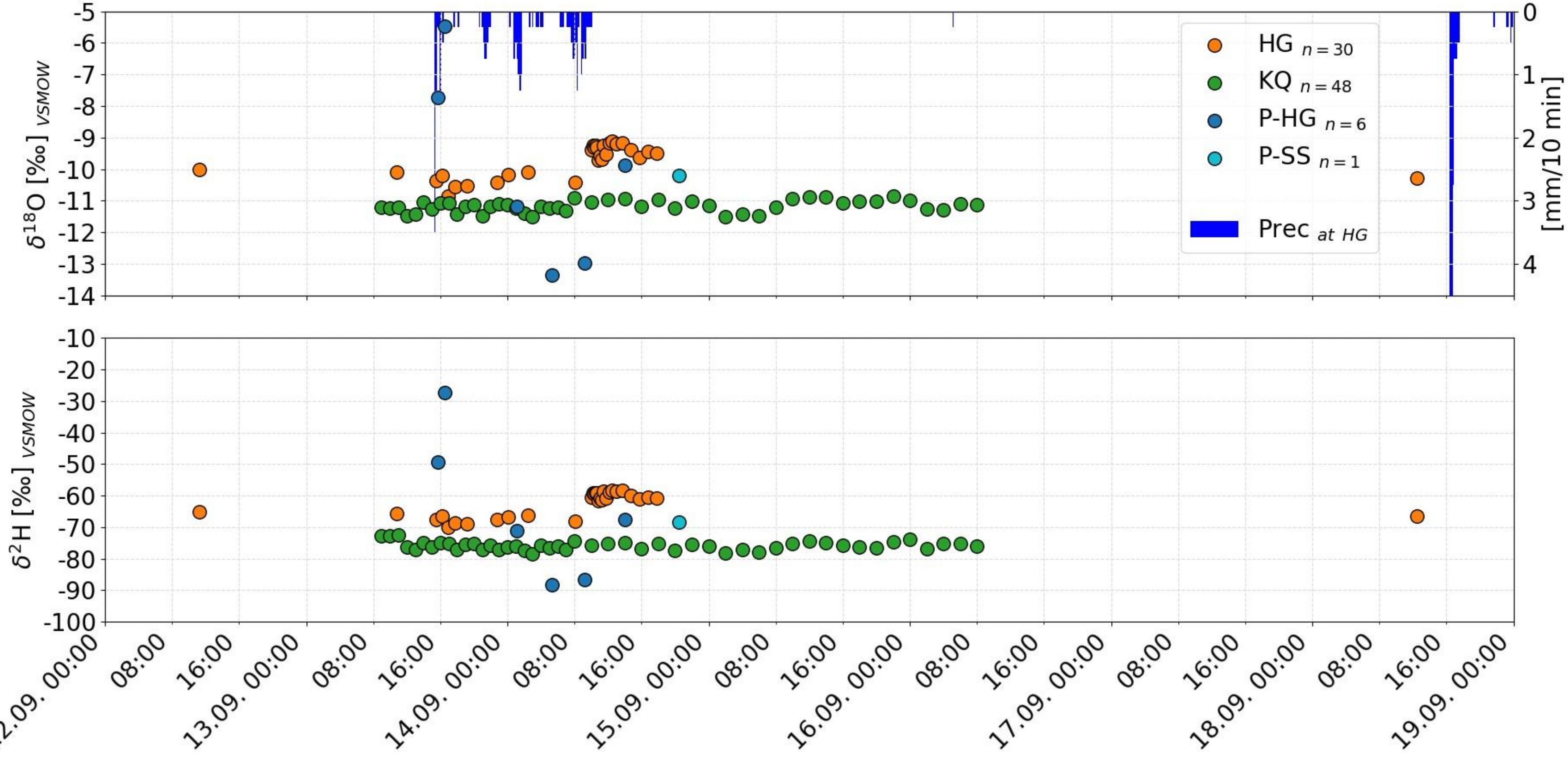

Fig. 28: Time series for ^{18}O (upper) and ^{2}H (lower) values from cave drip water in the Hirschgrubenhöhle (HG), the Kläffer springs (KQ), precipitation at the cave entrance (P-HG) and precipitation at the MS Sonnschienalm (P-SS) sampled between 12th and 19th Sep 2023.

Interpretation

Water stable isotopes for sampled precipitation at the Hirschgrubenhöhle shows a lower slope and d-excess (intersection with y-axis; Fig. 27) compared to the LMWL in the dual isotope plot. This might indicate lower relative humidity and evaporation during rainfall (Clark & Fritz, 1997), resulting in kinetic fractionation of the rainwater (Fig. 29). However, since air temperatures were relatively low, the trend lines still plot close to the LMWL, and altitude and seasonal effects might be sufficient to explain this deviation, evaporation rates are assumed to be neglectable.

Although a seasonal effect, which leads to an enrichment in heavy isotopes in summer can clearly be seen in Fig. 22, precipitation samples from 13th and 14th Sep show similar average $\delta^{18}O$ and $\delta^{2}H$ values as the long-term average from Wildalpen and Weichselboden. It is assumed that a seasonal effect is equalized by an altitude effect. On an intra event basis a pronounced rain-out effect can be observed. During the course of rainfall, surface temperatures decreased and the fractionation factor for the condensing vapor increased, leading to Rayleigh distillation, meaning that rainwater becomes isotopically depleted over time as long as temperatures do not rise (Clark & Fritz, 1997). This effect is clearly visible in Fig. 28.

The isotope values of the cave drip water in the Hirschgrubenhöhle plot along the precipitation trend line, which confirms the rainwater as one of its sources. The dominant isotopic enrichment in Fig. 28, which aligns with increase of discharge shows the timing of rainwater arrival at the cave drip water outlet and further indicates mixture of stored with event water. Depleted values between onset of rainfall and increase of cave drip water discharge are lower than initial baseflow conditions and cannot result from mixture with precipitation either. Therefore, these values are interpreted as push-out of older water, stored from previous rainfall events. However, this process apparently did not lead to an increase in discharge. This idea is supported by physiochemical parameters of the cave drip water and soil water content (see above).

As no clear isotopic signal can be observed in the Kläffer spring water, it is assumed that the amount of precipitation infiltrating into the aquifer was too small compared to the stored water that no effects on the composition of the discharge can be observed. The fact that isotope values do not plot along sampled precipitation values can be explained by the large size of 60-70 km² for the catchment area.

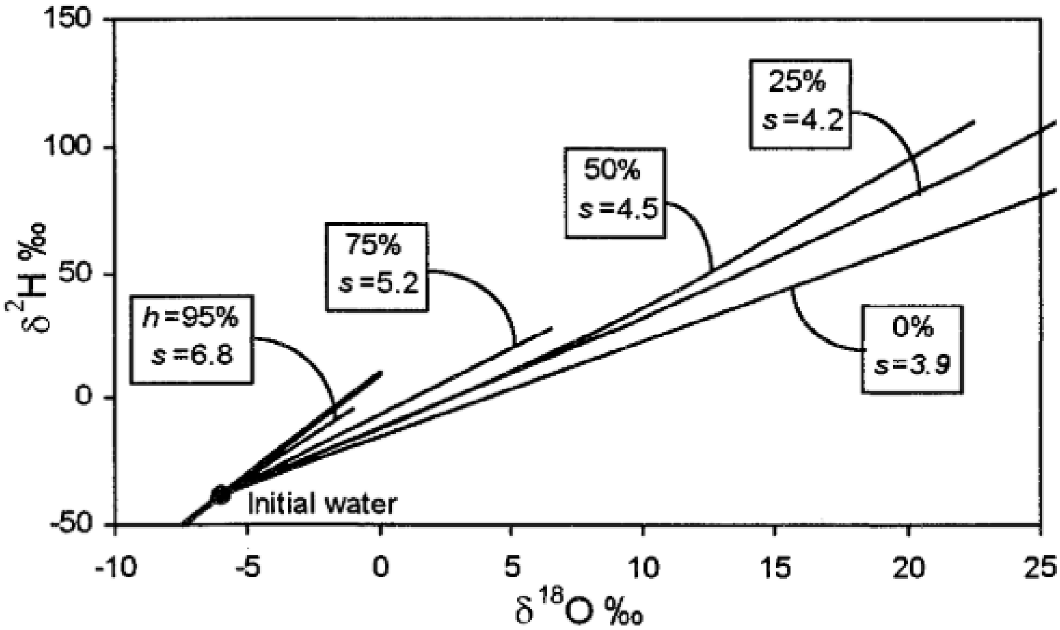

Fig. 29: Relationship of humidity (h) and the slope (s) of meteoric water lines. Slopes are given in reference to a GMWL or LMWL (heavy line) (from Clark & Fritz, 1997).

7 Results and interpretation from mixing models

7.1 End-member mixing

In order to calculate mixing ratios of relatively younger event water and older stored water in the discharge of the cave drip water and the Kläffer springs two different modelling approaches were tested. The end-member mixing approach was applied first due to its lower complexity. As described in chapter 5.6 the choice of end-member values has a strong influence on the results. For the cave drip water $\delta^{18}O$ values of end-members and resulting discharge rates are given in Fig. 30. Q_T represents the total measured discharge and C_T its isotope values respectively, and are marked in black, whereas the chosen pre-event end-member isotopic ratio C_P is given as black dashed line. While the measured isotopic ratio of the rainfall during the event C_E is given as black dotted line, the tested end-members for the event are given in either blue colours if corresponding discharge rates (Q) yield plausible results or grey if this is not the case.

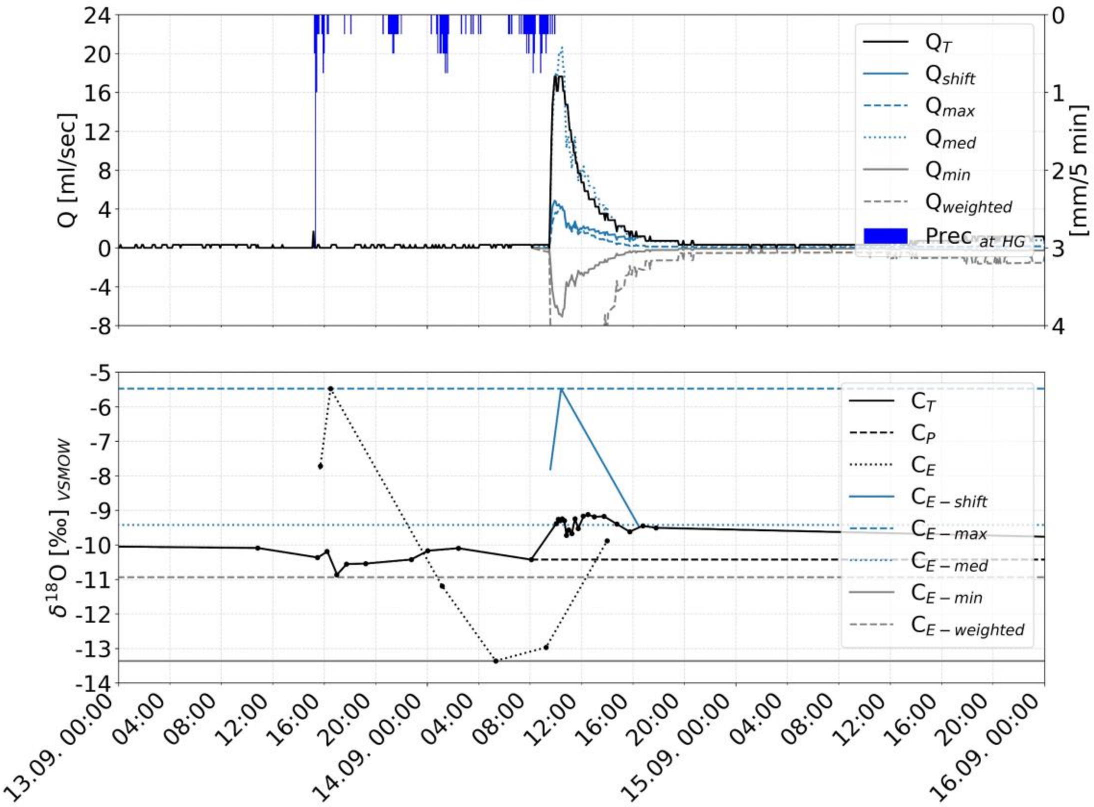

Fig. 30: Hirschgrubenhöhle $\delta^{18}O$ values are shown for total discharge C_T, rainfall C_E, different approaches for event water end-members $C_{E-shift}$, C_{E-max}, C_{E-med}, C_{E-min}, and $C_{E-weighted}$, as well as defined pre-event water end-member C_P. Dots indicate points of sampling. Resulting discharge rates ($Q_{E-shift}$, Q_{E-max}, Q_{E-med}, Q_{E-min}, and $Q_{E-weighted}$) are given in the upper part.

The different approaches for event water end-members show that only $C_{E-shift}$, C_{E-max} and C_{E-med} give reasonable results, as C_{E-min} and $C_{E-weighted}$ do not fulfil the criteria explained in chapter 5.6 and yield event water fractions below 0 %. Using the median value (C_{E-med}) would suggest an event water fraction of ~ 100 %, but this is in strong contrast to the weighted mean ($C_{E-weighted}$) showing an opposite result and therefore not considered to be reliable. Even though showing similar outputs C_{E-max} has one advantage over $C_{E-shift}$ in terms of informative value. Due to the fact that C_{E-max} represents the highest isotopic value for the event end-member and thus is most strongly deviated from C_T, the resulting discharge rates Q_{E-max} can be seen as the lowest possible Few. Therefore, the results of the end-member mixing approach are generated using C_T, C_P, and C_{E-max} as end-members, and are shown for $\delta^{18}O$ ratios in Fig. 31 and for δ^2H ratios in Fig. 32.

These results show that during the increase of cave drip water in the Hirschgrubenhöhle after the rainfall event from 13th to 14th Sep 2023 up to 4.2 ml/sec (using $\delta^{18}O$ as tracer and 4.0 ml/sec for δ^2H, respectively) originate from this particular precipitation. Exactly 2 h later, on 14th Sep at 12:30 the point with the highest relative amount of event water in relation to total discharge is reached with $Q_E/Q_T = 0.26$ based on $\delta^{18}O$. In other words, the maximum Few at a certain time step makes up 26 % of total discharge. Maximum Few is reached 1 h 15 min later at 13:45 based on δ^2H and with a value of 25 % slightly lower. As explained above, the results for Q_E have to be understood as equal to or higher than shown here.

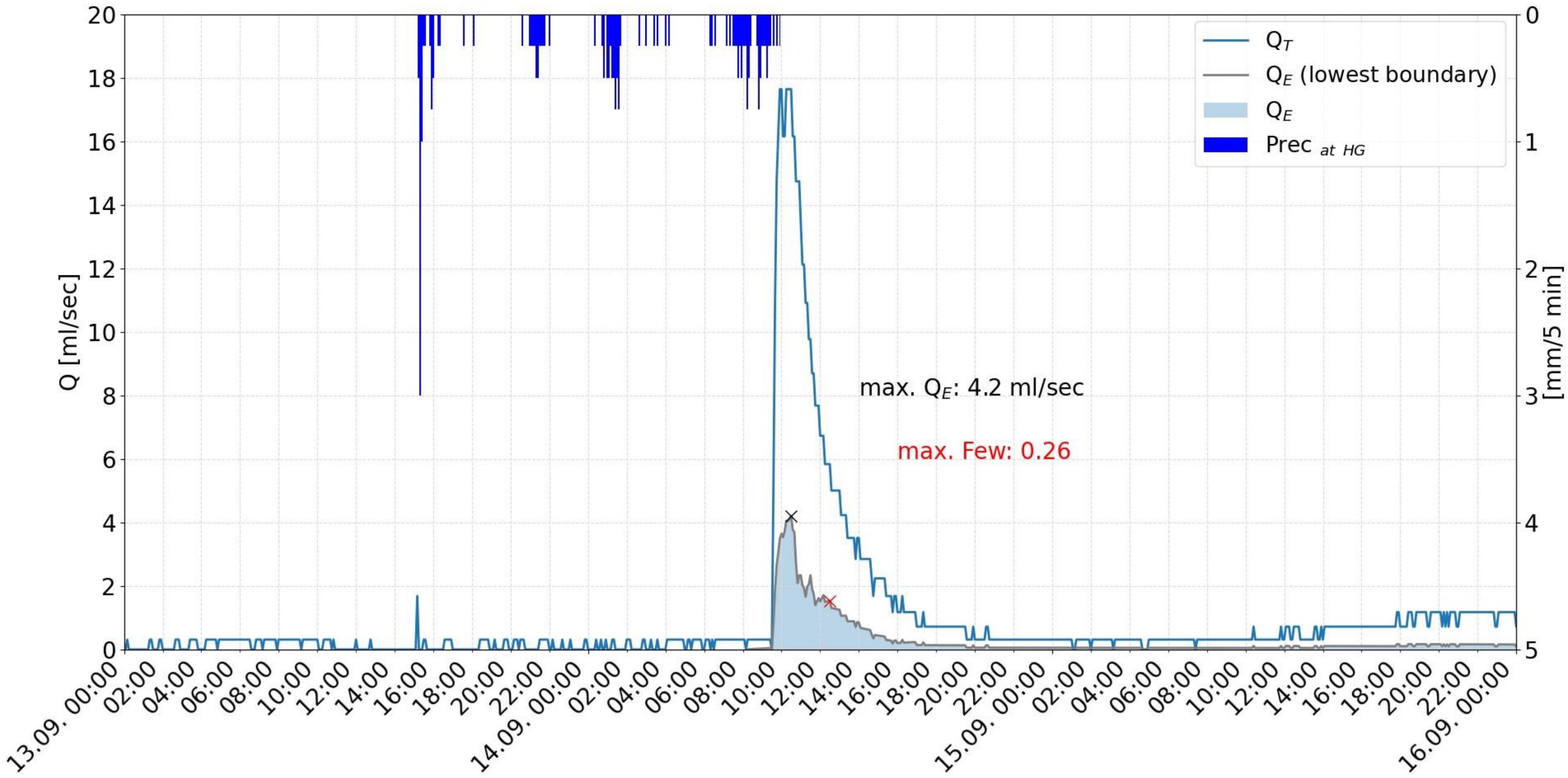

Fig. 31: Event water discharge (Q_E) in the Hirschgrubenhöhle (light blue area) is shown as the lowest possible volume calculated using $\delta^{18}O$ as tracer based on the C_{E-max} approach. The black cross indicates the highest absolute value of Q_E, whereas the red cross indicates the highest relative value of Q_E in relation to total discharge (Q_T), called fraction of event water (Few) here.

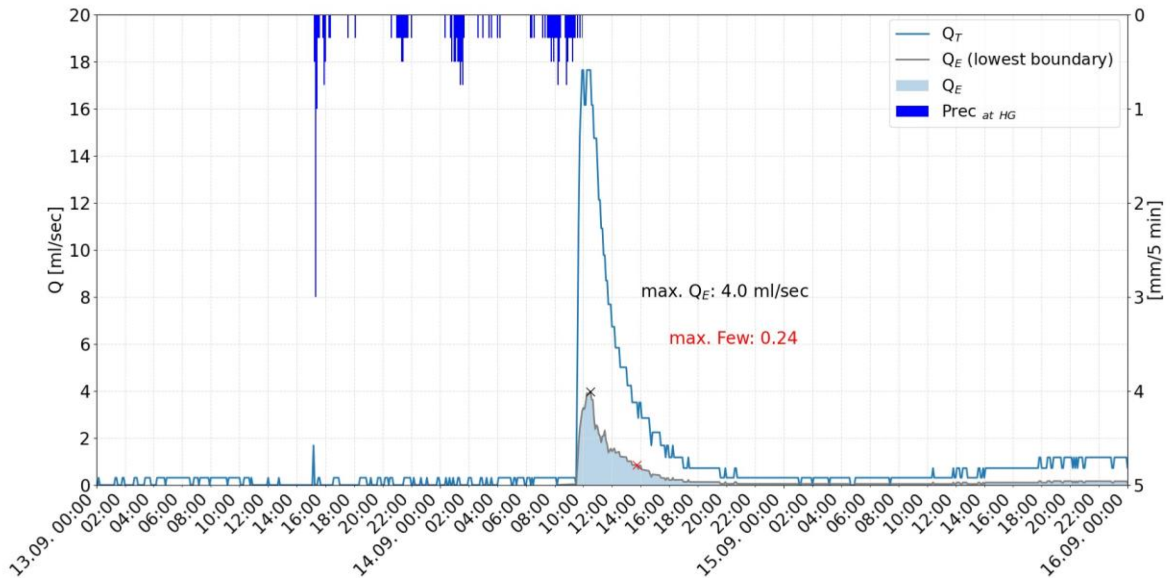

Fig. 32: Event water discharge (Q_E) in the Hirschgrubenhöhle (light blue area) is shown as the lowest possible volume calculated using δ^2H as tracer based on the C_{E-max} approach. The black cross indicates the highest absolute value of Q_E, whereas the red cross indicates the highest relative value of Q_E in relation to total discharge (Q_T), called fraction of event water (Few) here.

The workflow for assigning end-members to the discharge of the Kläffer springs is not described separately here, since it follows the same principle as for the Hirschgrubenhöhle and is shown in Fig. 33 for $\delta^{18}O$ values. Results for mixing ratios of event and pre-event water are shown in Fig. 34 for $\delta^{18}O$ as tracer and in Fig. 35 for δ^2H. The depicted time frame is extended to the 18th Sep 2023, because the Kläffer springs react more inert. As can be observed, the relative amount of event water Q_E is with a maximum Few of 11 % on 15th Sep at 22:00 (and 10 % for δ^2H 2 h later) much lower than for the cave drip water. Furthermore, event water does not follow the same pattern as total discharge and is rather fluctuating in a range of 0.00 to 0.37 m³/sec (0.28 m³/sec respectively).

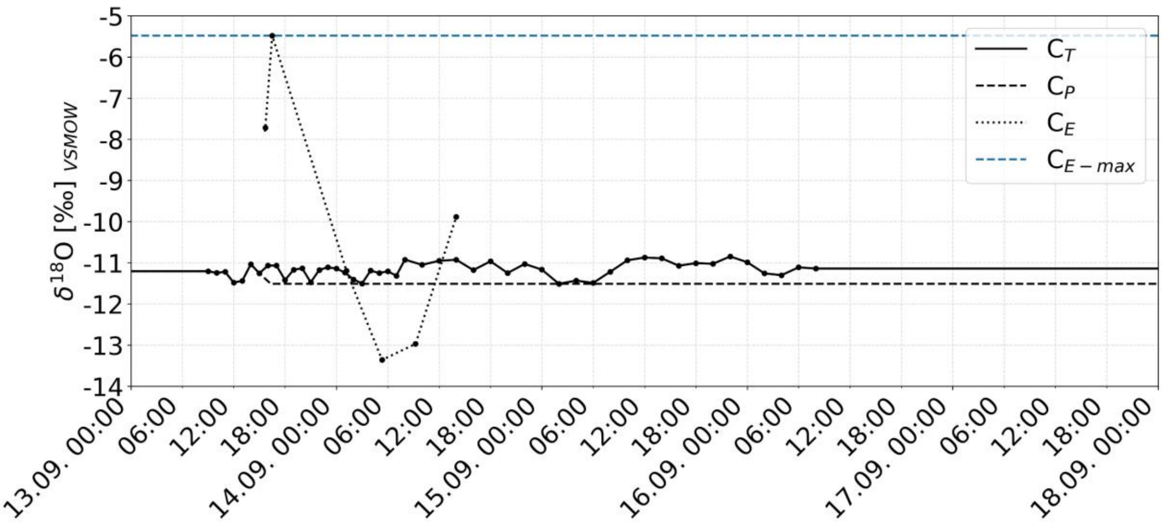

Fig. 33: Kläffer springs $\delta^{18}O$ values are shown for total discharge C_T, rainfall C_E, event water end-member C_{E-max}, as well as defined pre-event water end-member C_P. Dots indicate points of sampling.

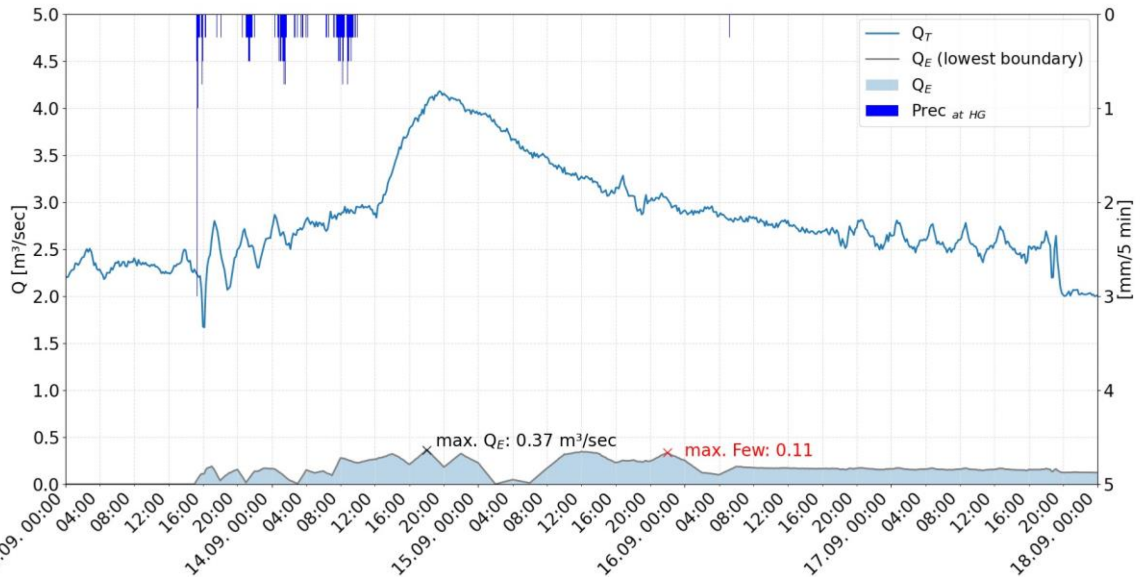

Fig. 34: Event water discharge (Q_E) at the Kläffer springs (light blue area) is shown as the lowest possible volume calculated using $\delta^{18}O$ as tracer based on the C_{E-max} approach. The black cross indicates the highest absolute value of Q_E, whereas the red cross indicates the highest relative value of Q_E in relation to total discharge (Q_T), called fraction of event water (Few) here.

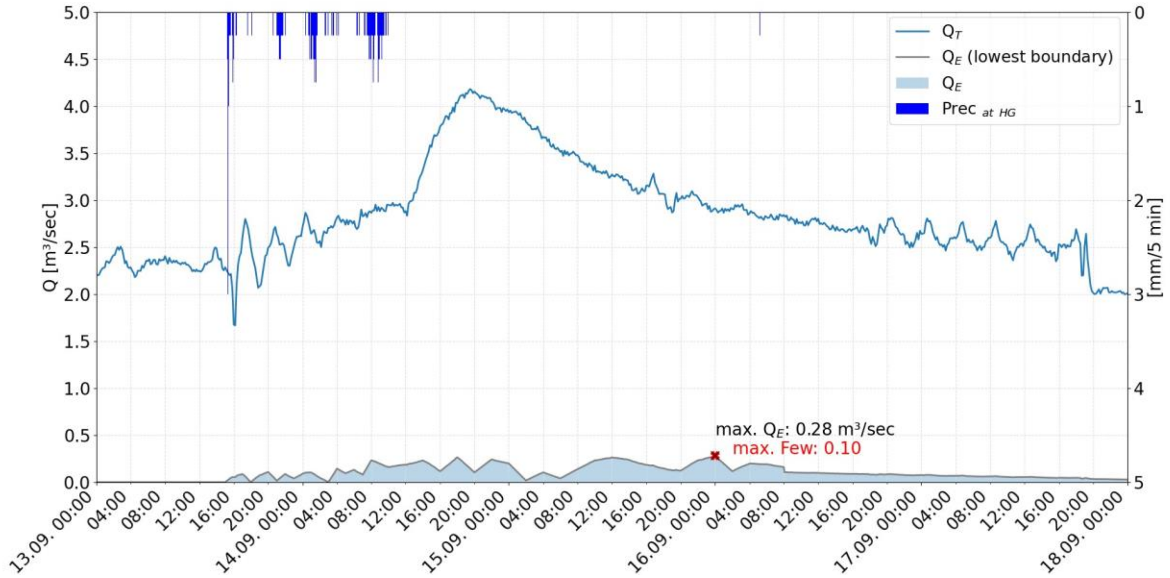

Fig. 35: Event water discharge (Q_E) at the Kläffer springs (light blue area) is shown as the lowest possible volume calculated using δ^2H as tracer based on the C_{E-max} approach. Max. Q_E indicates the highest absolute value of Q_E, whereas the red cross indicates the highest relative value of Q_E in relation to total discharge (Q_T), called fraction of event water (Few) here.

Further interpretation

The presented results for mixing of fresh rainwater (i.e. event water) and stored water are, only useful for conceptual assumptions, as the Few is expected to be much higher. Nevertheless, there is still some insight into water flow and storage behaviour that can be gained from the investigated rainfall event. Firstly, even after a prolonged time without recharge through precipitation a significant amount of water is still stored within the soil and epikarst layer, which gets forced towards the outlet of the cave drip water through a pressure pulse from fresh water entering the aquifer. Secondly, the fact that the maximum Few is reached after the peak of the total discharge, strengthens the applicability of the piston flow model (Fig. 25). The results most likely imply, that imperfect mixing of relatively younger event water with older stored water must have taken place while flowing through the karst, with older water preferably arriving first as discharge in the Hirschgrubenhöhle.

While the sampled precipitation and its measured isotope ratios are a good representation for the event end-member at the Hirschgrubenhöhle this is not the case for the Kläffer springs as the catchment area covers most of the main plateau of the Hochschwab. Lack of isotopic signal in the outflow of the Kläffer springs after the rainfall event (chapter 6.4.2) and results of the end-member mixing model indicate that there are only small amounts of rainfall from this particular event contributing to the subsequently increased discharge of the Kläffer springs. Furthermore, the modelled maximum values for Few do not match the measured water temperatures, which peaked more than 24 h earlier. Therefore and because of the lack of information regarding representative isotope ratios of rainfall, further modelling was limited to the cave drip water of the Hirschgrubenhöhle.

7.2 Numerical modelling

Numerical modelling using SAS functions was accomplished by using a modified version of the *tran*-SAS model by Benettin & Bertuzzo (2018). This approach was only applied on $\delta^{18}O$ data, and only for the cave drip water in the Hirschgrubenhöhle, but not for the Kläffer springs (see above). Many different configurations were used, of which the following gave the best results (Fig. 36) in terms of NSE. A time-variant SAS power function was used for computation of discharge values, as well as kmin_Q and kmax_Q values of 1.1 and 35, respectively. For evapotranspiration the selected function is irrelevant since it is neglected in the dataset already. The initial storage volume (S0) was set to 32 mm with an initial $\delta^{18}O$ ratio of -10 ‰. No spin-up was generated. For more information on the specification the reader is referred to chapter 5.7.

```
% GENERAL SIMULATION SETTINGS
% select the CASE STUDY and the MODEL
datasetName = 'input_tranSAS_60m2.csv';
ModelName = 'SAS_odesolver';  %'SAS_EFs' is a modified euler forward scheme, 'SAS_odesolver' is a
outfilename = 'all_output';     %output filename (both for .mat and .csv outputs)

% select the AGGREGATION timestep and the STORAGE threshold (numerical parameters)
dt_aggr = 1;           %dt for the computations [5 min] (must be integer)
f_thresh = 1;           %fraction of rank storage [-] after which the storage is sampled uniformly
                        %(just leave f_thresh=1 if not interested in this option)

% select the variable 'out' that is returned when calling the model
% 'C_Qsampl': modeled data during time steps with measurements only
% 'C_Qmodel': modeled data over all time steps
data.outputchoice='C_Qsampl';

% some further options
create_spinup = false;        %generate a spinup period
save_output = true;          %save model variables
display_output = true;       %display the output at the end
export_output = false;        %print output to csvfile

% MODEL PARAMETERS
% select the SAS
data.SASQName='fSAS_pltv'; %time-variant power-function SAS
data.SASETName='fSAS_step'; %step SAS

% set parameter names and values
SASQparamnames={'kmin_Q','kmax_Q'}; Param.SAS(1:2)=[1.1, 35]; %[-]
SASETparamnames={'k_ET'};    Param.SAS(3)=1;  %[-]
otherparamnames={'S0'};      Param.SAS(4)=32; %[mm]

data.C_S0 = -10; %concentration of the initial storage
```

Fig. 36: Screenshot from the configuration file of the *tran*-SAS model in an MATALB 2023a environment.

The results were generated in a timeframe from 7th Sep, 09:00 to 20th Sep, 19:30 using two different input files, the first assumes a catchment area of 60 m² and the second 120 m², meaning that discharge values (given in mm) for the latter are only half as large. Assuming that the catchment area of the cave drip water is 60 m², results show a Few up to 47 % in the discharge (Fig. 37) after the precipitation event on 13th and 14th Sep 2023. TTD threshold ages are shown in different colours from 1 h to 36 h, which all have to be classified as event water, since stored water would have to be much older (> 230 h), as the last precipitation event was over a week earlier. Ages above 20 h on the other hand do not change the maximum Few anymore as this value is reached 20 h after onset of rainfall on 14th Sep at 11:15. These TTDs are defined in terms of being counted from the time of entering the system, whereas the Few is the sum of all water from age 0 up to the defined threshold age at a certain time. The Few increases roughly simultaneously as the rise of discharge.

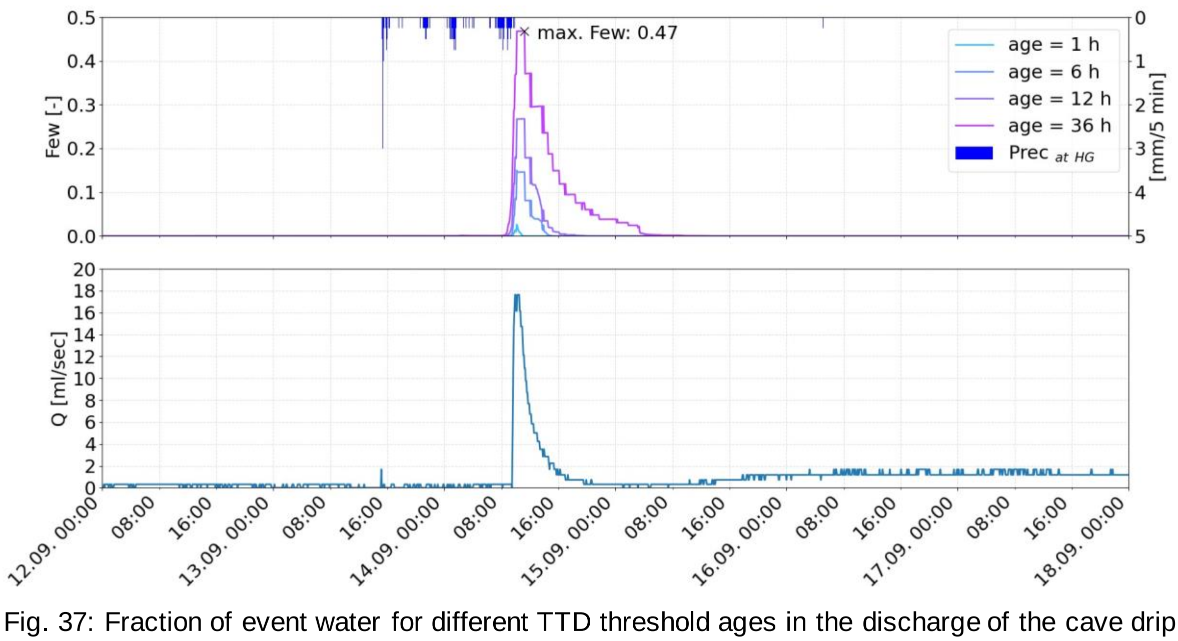

Fig. 37: Fraction of event water for different TTD threshold ages in the discharge of the cave drip water as computed by the *tran*-SAS model for a catchment area of 60 m².

In Fig. 38 probability density functions (pdfs) and cumulative density functions (CDFs) are shown for selected times. CDFs can be understood as the addition of all pdfs at a certain time. On the x-axis the age of water (in terms of time since reaching the surface as rainfall) at a certain time is plotted, while the y-axis shows the frequency of water with a certain age, or cumulative frequency respectively. The overall maximum cumulative frequency of 0.47

is reached on the 14th Sep 2023, 11:15 and correlates to the maximum Few. This point is reached at 20 h, meaning that no event water older than this existed at that particular time (onset of rainfall 13th Sep, 15:20) and all event water together composes 47 % of the total cave drip water on the 14th Sep 2023, 11:15.

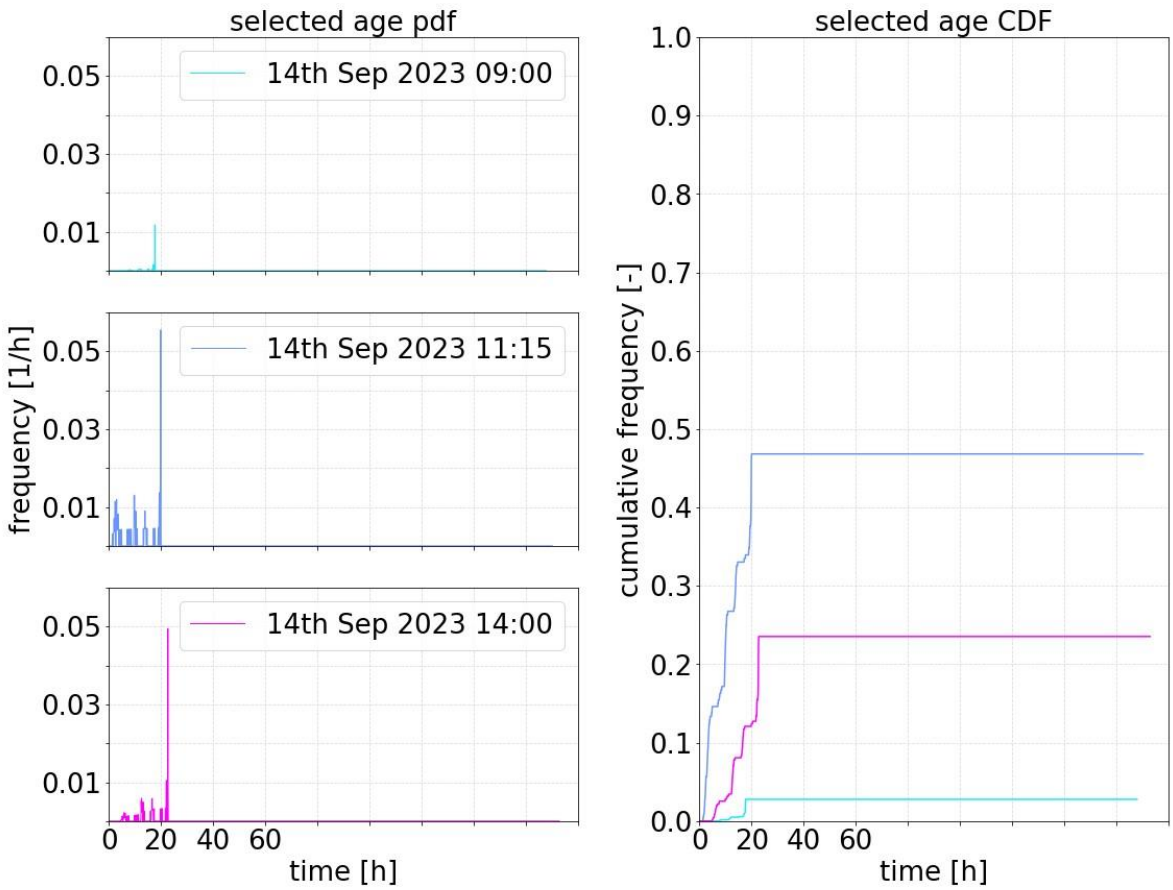

Fig. 38: Probability density functions (pdfs) and cumulative density functions (CDFs) for selected times (shown in different colours) as computed by the *tran*-SAS model for a catchment area of 60 m².

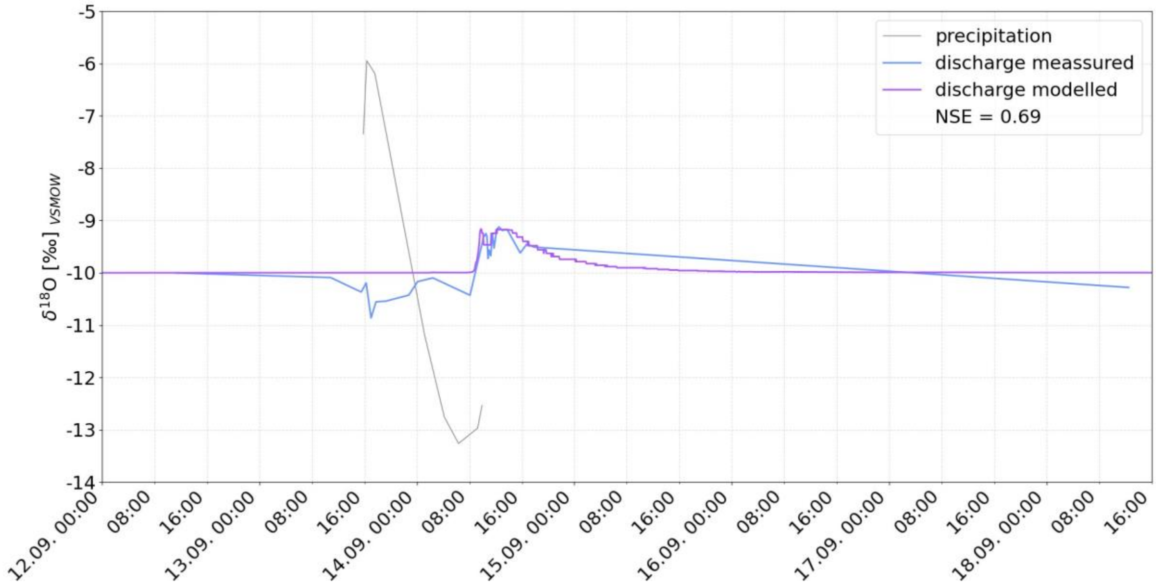

Fig. 39: Modelled tracer ratios of the discharge in comparison to measured ratios and precipitation as computed by the *tran*-SAS model for a catchment area of 60 m².

The performance of the *tran*-SAS model for an assumed catchment area of 60 m² can be observed in Fig. 39. Measured $\delta^{18}O$ ratios for discharge and precipitation were compared to modelled isotope ratios and produce an NSE of 0.69. Even though there is a significant overlap between measured and modelled discharge $\delta^{18}O$ ratios, in some parts the model cannot account fully for the dynamics of the flow. Firstly, the model reacts slower to decreasing tracer ratios after the main increase and secondly a decrease in $\delta^{18}O$ beforehand is neglected by the model.

Results were also generated for an assumed catchment area of 120 m², showing similar values. The maximum Few computed by the model is 45 % (Fig. 40), showing the same pattern and trend as compared to an assumed catchment area only half as large. The fit is slightly better with an NSE of 0.70. However, modelled $\delta^{18}O$ ratios for discharge plot in the same order (Fig. 41).

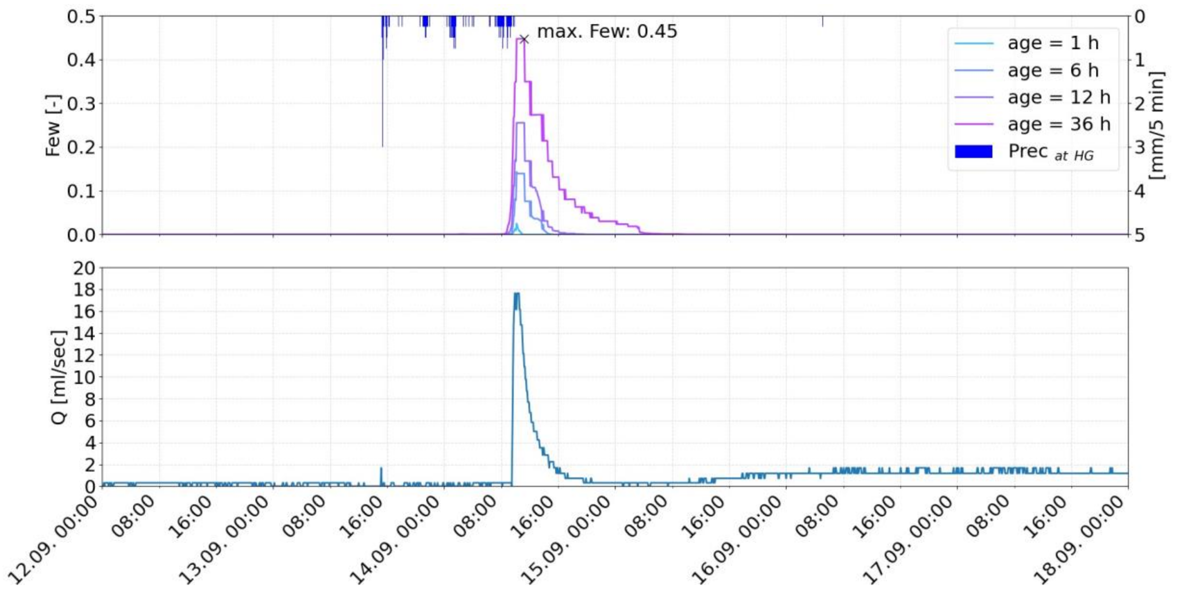

Fig. 40: Fraction of event water for different TTD threshold ages in the discharge of the cave drip water as computed by the *tran*-SAS model for a catchment area of 120 m².

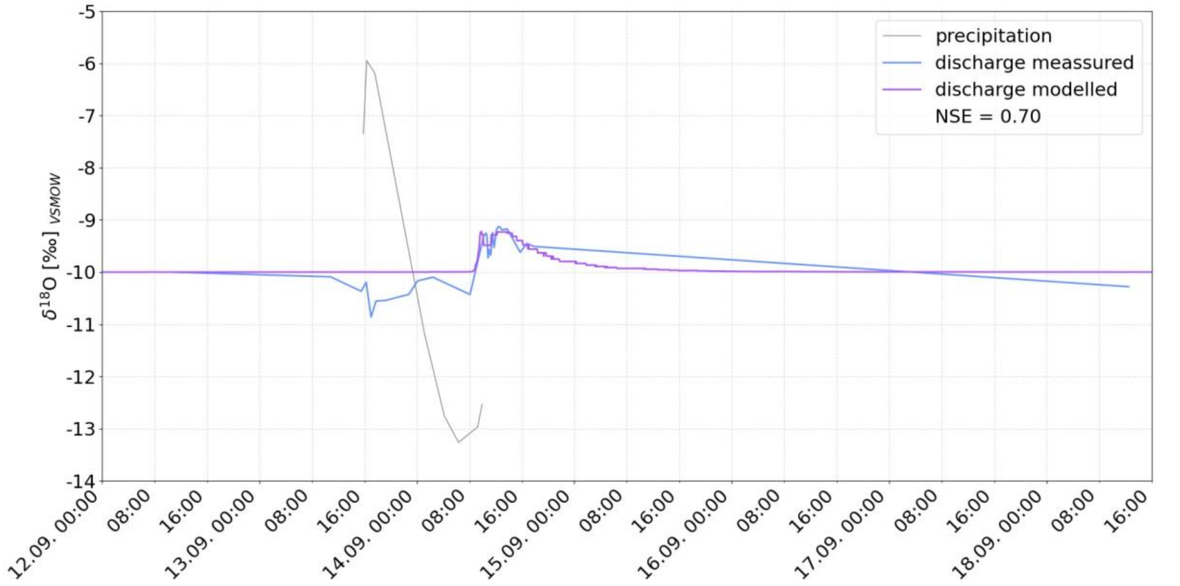

Fig. 41: Modelled tracer ratios of the discharge in comparison to measured ratios in precipitation and discharge as computed by the *tran*-SAS model for a catchment area of 120 m².

Discharge curves for event water reaction after the storm event were plotted using the Few values from the *tran*-SAS model (Fig. 42 and Fig. 43). Total discharge peaks between 09:55 and 10:30 on 14th Sep 2023, while event water reaches its peaks in both cases at 10:30.

Maximum Few values in comparison are reached 45 min later at 11:15 (in both cases). For the smaller assumed catchment maximum discharge values for event water are with 8.3 ml/sec slightly higher than the 7.9 ml/sec for the larger one. However, as with the outputs of the *tran*-SAS model, both diagrams show almost the same results. Event water was furthermore subdivided into different ages, all of which must derive from rainfall on the 13th and 14th Sep 2023, as explained above. While for waters with an age equal to or less than 1 h (Q_{1h}) maximum discharge is reached 20 min earlier at 10:10, no shift in the peak can be observed for water with threshold ages above 6 h.

For an assumed catchment area of 60 m² the measured discharge between 14th Sep, 09:30 and 19:30 yields approximately 3 mm. Based on the calculated Few this can be further separated into 1 mm from event water and 2 mm from pre-event water. In the case of an assumed catchment area of 120 m² it would be 0.5 mm for event water and 1 mm for pre-event water resulting in a total of 1.5 mm.

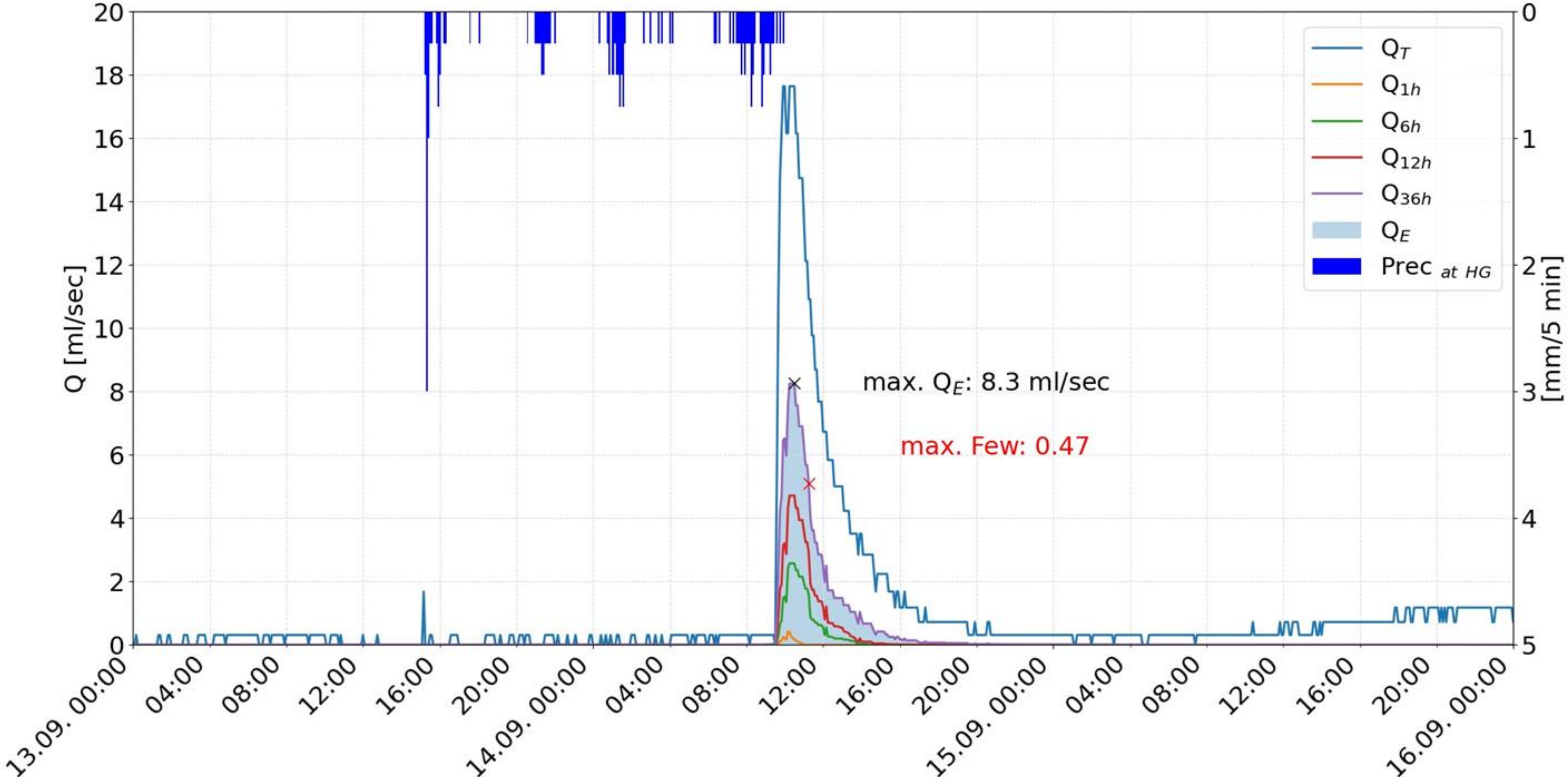

Fig. 42: Overall discharge of cave drip water in the Hirschgrubenhöhle (Q_T) and modelled event water discharge (Q_E) after rainfall on 13th and 14th Sep 2023 for an assumed catchment area of 60 m². Q_{1h} to Q_{36h} indicate water that is equal to or younger in age than 1 h to 36 h, while the maximum event water discharge is shown as a black cross and the maximum event water fraction as a red cross.

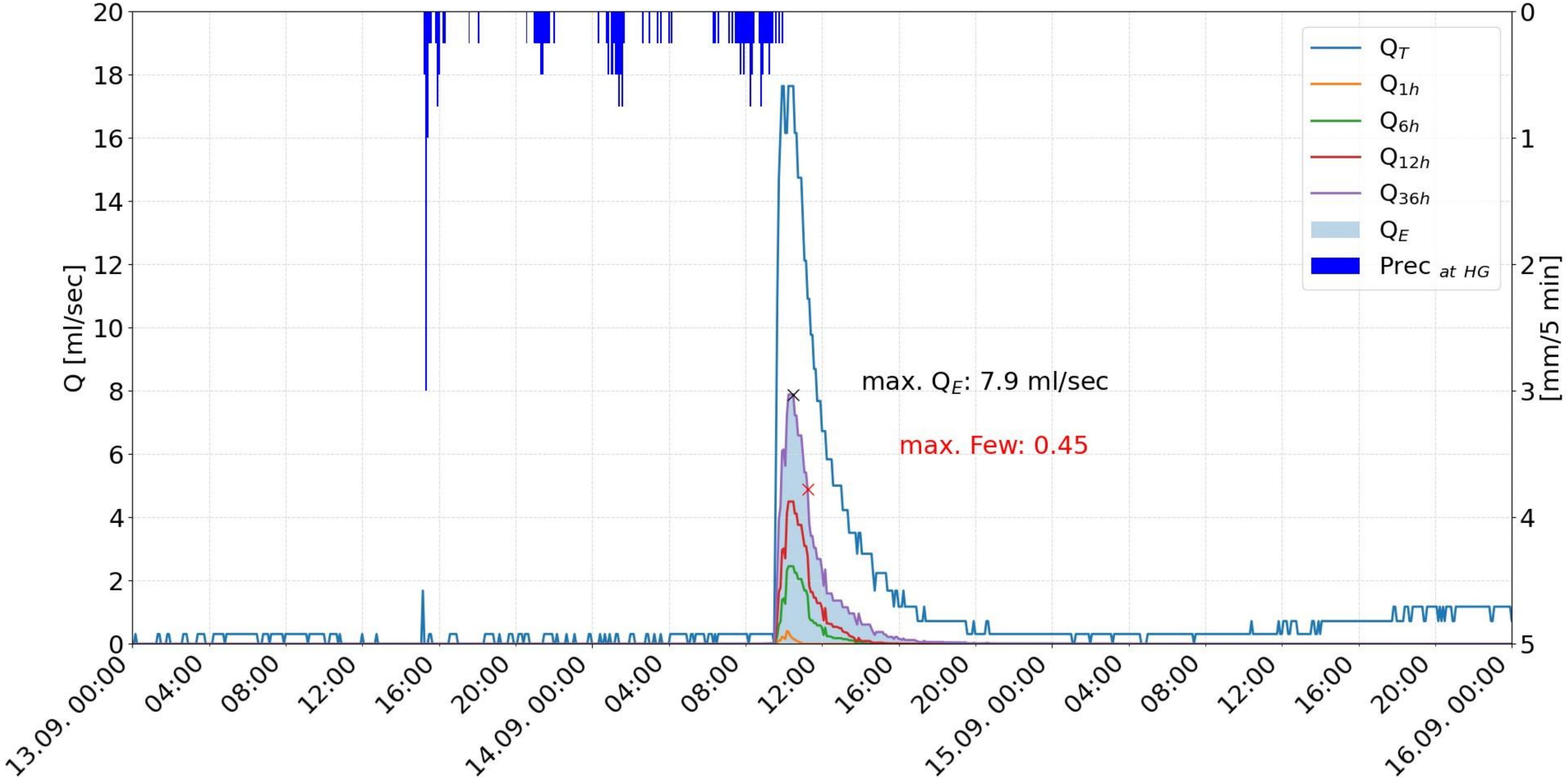

Fig. 43: Overall discharge of cave drip water in the Hirschgrubenhöhle (Q_T) and modelled event water discharge (Q_E) after rainfall on 13th and 14th Sep 2023 for an assumed catchment area of 120 m². Q_{1h} to Q_{36h} indicate water that is equal to or younger in age than 1 h to 36 h, while the maximum event water discharge is shown as a black cross and the maximum event water fraction as a red cross.

Further interpretation

Both, the pdfs and the CDFs in Fig. 38 show a preference for relatively older event water (i.e. from first rainfall during this particular event). In the case of the pdfs this is visible as the large peak for the oldest waters, which is dominant in all datetimes. Smaller, but distinct peaks are also present for very young water, which is assigned to increased rainfall that fell on 14^{th} Sep between 07:00 and 10:00 (chapter 6.1), as well as water with intermediate ages from the rainfall a few hours earlier between 00:00 and 02:00. Consequently, the peak for very young water in the pdfs is most present on the 14^{th} Sep between 10:00 and 13:00, whereas the dominant influence of water from the first rainfall is relatively lower compared to later or earlier datetimes. In other words, most of the water from the last rain during the event (14^{th} Sep, between 07:00-10:00) is arriving approximately 3 h later as cave drip water in the Hirschgrubenhöhle. During that time rain that fell after 13^{th} Sep, 20:00 is generally rather strongly represented in the discharge, while during later times (after 14^{th} Sep, 13:00) discharge consists mainly of rain from 13^{th} Sep, between 15:20 to 20:00. Another feature that can be observed is that later rainfall (i.e. younger water) seems to have lower transit times, which could be explained by higher water content in soil and epikarst from the previous rain. Based on the TTDs at different times it is observed that travel times range between approximately 30 min and 28 h for event water in discharge 14^{th} Sep, between 09:30 to 19:30, and seems to be strongly depended on the volume of water in the aquifer at the given time. However, this is only true for the small portion (< 5 %) of rainwater that reaches the cave drip water outlet in the observed timeframe and is much longer for the portion of event water that is stored (i.e. water with much higher transit times). Based on the evidence from the data and model, it is concluded that even though, the piston flow model is emphasised for discharge generation here, strong mixing of stored water and event water with different ages along the flow path or within a reservoir (Fig. 25) is assumed.

Modelled isotope ratios for discharge (Fig. 39 and Fig. 41) show a good fit but cannot account for depleted conditions within the first hours after onset of rainfall. This is interpreted as a further indication for non-steady-state pre-event conditions and push-out of isotopically depleted water from storage. The model cannot account for this third end-member, as it is unknown and therefore not reflected in the input. Thus, mixing of another end-member (depleted isotope signature) with event water from precipitation cannot be ruled out.

Similar to the results of the end-member model, a max Few is reached only after the total discharge peak (chapter 7.1), which could indicate piston-flow. In any case, it confirms the assumption that the ratio of pre-event water decreases over the course of the discharge curve while event water ratio increases. However, the high proportion of pre-event water (>50 %) in the cave drip water, even after preceding extremely dry conditions and very low baseflow is emphasized here, confirming the high storage capacity of epikarst (e.g. Klimchouk, 2004; Ford & Williams, 2007; De Waele & Gutiérrez, 2022). The maximum Few of 47 % fits well to the results from the end-member model, as these suggested an equal to or higher maximum Few of 25 %.

The assumed catchment size did not affect results strongly, making the *tran*-SAS model unsuitable for predicting catchment sizes. An explanation for this finding could be that the water volumes introduced by precipitation together with stored water volumes are approximately one order of magnitude higher than discharge volumes from the cave drip water. Therefore, the calculated catchment size of approximately 60 m^2 by Rabl (2023) is seen as best estimation.

The here assumed initial storage of 32 mm (on 7th Sep, 09:00), based on a best-fit approached, is not to be confused with a maximum storage capacity. However, simple calculations (Tab. 3) show that 27.5 mm were added via precipitation during the event, whereas only 7.5 mm were subtracted as discharge*, before baseflow conditions were obtained, yielding a remaining storage of approximately 52 mm. Around half of this post-event storage is filled with pre-event water and the other half with event water. Furthermore, it is concluded that, based on the data and the *tran*-SAS model, a storage capacity above 0.052 m^3/m^2 (52 mm) is expected.

Tab. 3: Mass balance based on fractions of event water calculated by the *tran*-SAS model.

Event water **Pre-event water**	7th Sep, 09:00	7th Sep, 09:00 -14th Sep, 09:30	14th Sep, 09:30 -14th Sep, 19:30	14th Sep, 19:30
Recharge	/	**26.5 mm**	**1 mm**	/
Storage	**32 mm**	/	/	**26.5 mm** **25.5 mm**
Q_{SUM} drip water*	/	**4.5 mm**	**1 mm** **2 mm**	/

*(with a catchment area of 60 m²)

8 Discussion

The goal of this study was to characterize water mixing processes in the upper vadose zone of the Hirschgrubenhöhle, as well as at the Kläffer springs by using water stable isotopes and conducting high-frequency sampling during one particular rainfall event with a focus on the special role of newly infiltrated and stored water in the epikarst. In the following a critical evaluation of the applied methods is given.

Volumetric soil water content

Sensors for measurement of volumetric water content in the soil were not calibrated in respect of soil properties, which is why absolute values (Fig. 24) should be viewed with caution. In addition, it is possible that the texture of the soil has been altered by the insertion of the sensors and is therefore not representative. However, this is unlikely, as efforts were made to restore the soil texture afterwards. The accuracy for measuring the volumetric water content with the generic calibration provided by the manufacturer is ± 0.03 m^3/m^3 for typical mineral soils (METER Group Inc., 2024). Therefore, at least relative changes in soil water content are considered reliable.

Isotope data

High-frequency event sampling of water stable isotopes in caves pose a logistical and physical challenge for the individuals conducting the sampling. Therefore, long time series in high resolution are hard to obtain in a high-Alpine environment lacking infrastructure (e.g. electricity) but are essential for accurate quantification of flow and storage patterns within karst aquifers, as demonstrated here. Furthermore, more data and longer time series within the Hochschwab karst aquifer (i.e. caves) are necessary to establish comprehensive models, since findings from one particular event and location are not applicable to other areas. Naturally, on the other hand one advantage are the dark and cool conditions for storage of isotope samples.

End-member mixing

This approach is based on four assumptions (Buttle, 1994; chapter 5.6), which should be treated critically in relation to the results presented here. In particular assumption 2 cannot be fulfilled: The event and pre-event water maintains a constant isotopic signature in space and time, or any variations can be accounted for. It is demonstrated that integrating tempo-spatial variations of isotopic ratios in precipitation (event water) into the mixing model is rather difficult and requires a certain degree of interpretation regarding the influence on discharge generation, even with consistent measurements, but is possible if high-frequency data is available as is the case here (Fig. 27). Pre-event water could be measured, but isotopic variations of pre-event water were not taken into account, e.g. differences between waters stored in different compartments of the epikarst originating from different events. However, since water cannot be sampled from the storage directly this problem has been rarely investigated in general and still poses a great challenge to quantify (Klaus & McDonnell, 2013). This supports the criticism of some authors of the method (e.g. Kirchner, 2019) and shows that it cannot fully capture the strong intra-event variations in small catchment karst aquifers, as in this study. Therefore, the more elaborate *tran*-SAS model was applied.

Numerical modelling

The modelled TTDs (Fig. 37 and Fig. 38) are strongly related to the functioning and the selected parameters of the model (Fig. 36), as it prefers younger water (k_Q ↓) at higher soil water content (wi ↑) and vice versa. It should be pointed out, that since only Port 1 from the soil water content sensors was used to calculate wi, minor deviations are possible compared to other sensors. As the values are normalized and all sensors show similar trends these differences are regarded negligible. In summary, absolute calculated values (Fig. 42) should be treated with caution, as they are based on assumptions about the aquifer properties. Nevertheless, as high-frequency sampling and several meteorological and physiochemical parameters of the discharge are provided, it is assumed that the results described here are reliable for the flow and storage behaviour of the karst aquifer of the cave drip water in the Hirschgrubenhöhle. This is further supported by the correlation with values of electrical conductivity and water temperature (Fig. 24). The maximum cave drip water temperature is reached at the same time as the calculated maximum Few, whereas the minimum for electrical conductivity is reached only 30 min later.

This work represents a first attempt to sample high-frequency water stable isotopes in an alpine cave and precipitation simultaneously to quantify flow and storage within the uppermost vadose zone during a rainfall event using different mixing models. Furthermore, this new approach has the potential to provide new insights for other study areas or questions related to karst aquifers. Thus, the research questions defined at the beginning were answered, and these results are compared with the results of other authors investigating the Hochschwab karst aquifer (Exel, 2014; Kaminsky, 2020; Rabl, 2023) and event-based storage behaviour in other karst catchments (Perrin et al., 2003).

Exel (2014) was the first to conduct event sampling of water stable isotopes in the Hirschgrubenhöhle and installed the weir to capture the cave drip water. His work already implied the mixture of event and pre-event water in the soil and epikarst, but a quantification of these processes was not provided. In addition, indications of possible push-out of older water during these events was given, which confirms the dynamics observed in the here presented study.

Rabl (2023) calculated an average delay between onset of precipitation and increase in discharge for the cave drip water in the Hirschgrubenhöhle of 84 min, based on a dataset from 17 month of discharge measurements between 2021 and 2022. This confirms the unusual conditions prevailing during the event on 13th and 14th Sep 2023. A recession analysis was conducted for two rainfall and two snowfall events, whereas a storage capacity of 0.034 m^3/m^2 (i.e. 34 mm) was calculated based on the event with highest baseflow volume, which showed discharge rates over 600 ml/sec for the cave drip water. Interestingly, only a slightly lower baseflow volume was calculated for another rainfall event with a little more than 200 ml/sec of discharge and only half of it for the two snowfall events. In terms of precipitation amount this is not comparable with the study presented here, as observed time intervals for recession analysis are much longer.

Kaminsky (2020) determined a storage capacity of 0.5 to 10 mm for a cave stream in the Furtowischacht, west of the Hirschgrubenhöhle on the Hochschwab karst massif. In contrast to the Hirschgrubenhöhle, the catchment of the Furtowischacht was strongly modified by glacial processes. The author interpreted the lack of an epikarst layer as the reason for the low storage capacity. In view of the results by Kaminsky, it can be concluded that the storage capacity in the paleo landscape lacking glacial erosion is at least one order of magnitude higher due to the presence of epikarst and soil. From this, conclusions could be drawn about different types of morphology across the Hochschwab.

Perrin et al. (2003) conducted event sampling of water stable isotopes in a cave 40-50 m below surface within the catchment area of the Saivu spring. Located in the Swiss tabular Jura the catchment is estimated to 13 km^2 and contains a soil cover of mainly silty loam in variable thickness up to a few meters. During three flood events a cave stream and cave drip water was sampled. Mixing ratios of freshly infiltrated and stored water were calculated and up to 30 % contribution from newly infiltrated water in the cave stream and 10 % for cave drip water estimated. Furthermore, a numerical model was applied, suggesting most of the overall storage of the karst catchment is in the soil and epikarst layer, whereas the soil functions as a mixing reservoir, while epikarst contributes to dynamic storage. These results fit well to the ones presented in this study and indicate that even higher storage capacities are possible in the vadose zone of karst catchments.

9 Conclusion

The goal of this study was to characterize water mixing processes and storage behaviour in the uppermost vadose zone of the Hochschwab karst aquifer using water stable isotopes. In the first stage of the work, continuous data series of the physiochemical parameters of the karst water, meteorological data of the precipitation, its long-term isotope values and soil water content were acquired. On 13th and 14th Sep 2023, event sampling of water stable isotopes was successfully carried out in the Hirschgrubenhöhle and at the Kläffer springs. The results were used to model the mixing ratios of event and pre-event water. This was originally attempted with the end-member mixing model. To improve the results, a numerical model was employed in addition. The most important conclusions of this study are summarized below.

- The rainfall on 13th and 14th Sep 2023 was preceded by the longest dry period of the entire hydrological year, which lasted for approximately 9.7 d. This precipitation event was followed by a dry period of approximately 4.2 d. The event itself started 13th Sep, 15:20 at the Hirschgrubenhöhle and ended at 10:00 the next day. The detected sum at this location in the given time period is 28 mm.
- Discharge of the cave drip water in the Hirschgrubenhöhle, as well as water temperatures and electrical conductivity reacted with a delay of 18 h to the onset of rainfall, which is unusually long (Rabl, 2023) and most likely related to the extremely dry conditions.
- Different approaches for the end-member mixing model were tested. During high flow conditions the influence of freshly infiltrated event water on the isotope ratios of the cave drip water was distinct, which is in accordance with the increase in soil water content. A clear isotopic signal could not be observed for the Kläffer springs, and it is concluded, that dilution of the recharge was too strong. Therefore, the numerical *tran*-SAS model (Benettin & Bertuzzo, 2018) was only applied at the Hirschgrubenhöhle. It was possible to reproduce the measured isotope values in the cave drip water with a best-fit NSE of 0.69, making the *tran*-SAS model a promising tool for investigation of karst water flow and storage behaviour.

- Stable isotope values from sampled precipitation during the event show a slightly lower slope and d-excess ($\delta^2H = 6.43\ \delta^{18}O - 1.04$) and a higher isotopic enrichment compared to the LMWL. In addition, a depletion of heavy isotopes over time can be observed. This indicates (1) a slight kinetic fractionation of the rainwater compared to the LMWL, (2) a seasonal effect being equalized by an altitude effect, and (3) Rayleigh distillation during the event leading to a rain-out effect. The latter in particular is one of the reasons why it is emphasised in this study that simple end-member mixing models are not suitable for capturing intra-event processes in alpine environments.

- Results from the *tran*-SAS model show that freshwater from precipitation infiltrating into the aquifer was mostly stored in the soil and epikarst. Less than 5 % of newly introduced water reached the outlet of the drip water in the Hirschgrubenhöhle during high flow conditions. This indicates that the intermediate storage in the uppermost vadose zone of the Hochschwab is of even greater magnitude than in the phreatic zone during dry periods and if soil cover and epikarst are present.

- The influence of freshly infiltrated rainwater accounted in average for 34 % of the increased cave drip water discharge during high flow conditions. The Few temporarily increased to a maximum of 47 %. These results are consistent in magnitude with the study by Perrin et al. (2003), which was carried out in a cave system in the Swiss tabular Jura and showed a Few of up to 10 % for cave drip water.

- Both push out of old water and its mixing with freshly infiltrated water can be observed. It is therefore concluded that even under very dry conditions the piston flow model (Ford & Williams, 2007) seems to be valid to describe flow in the karst aquifer of the cave drip water.

- Transit times ranged between 0.5 and 28 h for event water reaching the cave drip water outlet within the observed time period, depending on the water volume in the aquifer at a given time. It can therefore be concluded that high soil water contents lead to shorter travel times and vice versa and influence discharge reaction strongly. Furthermore, the variability of transit times within periods of high recharge might be higher than previously assumed for the Hochschwab karst aquifer.

- After baseflow conditions were obtained 52 mm stored water was left in the epikarst and soil layer of the catchment area, whereas around half of this amount was contributed by the newly introduced event water from the rainfall. This confirms the high storage capacity of the epikarst and soil. It is therefore concluded that their presence in paleo landscapes increases the storage capacity by at least one order of magnitude compared to glacially eroded landscapes on the Hochschwab (e.g. Furtowischacht).

10 Further work

Further investigations of the upper vadose zone, methods for determining its rock properties (porosity, permeability, etc.) are desirable. Geophysical methods in particular, such as geoelectric surveys, could provide important information on water saturation under different conditions. The delineation of the catchment area of the cave drip water in the Hirschgrubenhöhle with salt or dye tracers would be necessary to reduce assumptions in the modelling process and is an important parameter for the flow regime. In combination with knowledge about the degree of saturation of the reservoir and the size of the catchment area, the *tran*-SAS model could be used with increased accuracy. In addition, results would be easier comparable with other models.

Above all, however, further high-frequency event sampling of water stable isotopes should be carried out. Additional sampling in the Hirschgrubenhöhle would allow to investigate flow and storage rates under different conditions, whereas sampling in other caves on the Hochschwab karst plateau (e.g. Furtowischacht) would provide more information about the role of presence/absence of epikarst and soil layer. Thus, a broader model of flow and storage behaviour of the Hochschwab karst aquifer could be developed, for which further sampling of the Kläffer springs is needed.

A long-term spatial resolution campaign for isotope sampling of precipitation and discharge on the Hochschwab could provide important data on the long-term behaviour (e.g. seasonal differences) of water storage and its quantification, which is a valuable information for the management of the water supply. Furthermore, isotope sampling in caves throughout the year could become a new approach to determine recharge processes into the phreatic zone.

11 List of figures

"I have made every effort to contact all owners of the image rights and have obtained their consent to use the images in this work. However, should you become aware of any copyright violations, please contact me."

Fig. 1: Factors controlling the formation of karst systems (from De Waele & Gutiérrez, 2022). 5

Fig. 2: Figure showing calcite dissolution through the described reactions (from Palmer, 2007). 6

Fig. 3: Schematic profile of the first meters below surface in a typical karst setting with a highly porous zone at the top and prominent sub-vertical conduits (from Williams, 1983). 7

Fig. 4: Figure showing the different hydrogeological zones and features in a typical karst aquifer. Infiltrating water enters the karst aquifer preferentially through surface structures such as dolines or ponors. After percolating through the soil, the epikarst, and the vadose zone the water reaches the (epi)phreatic zone, from where it leaves the system through permanent or episodic springs (from Plan, L.). 8

Fig. 5: Hydrologic functioning of the epikarst layer in relation to the underlying vadose zone. The figure shows the development of a temporal aquifer at the base of the epikarst due to increased recharge and preferential flow along larger shafts in the vadose zone (SF = shaft flow), that is accompanied by little flow along smaller fissures (WF = vadose flow) and even smaller rates through the matrix (WS = vadose seepage). From Klimchouk (2004). 9

Fig. 6: Light element isotopes and the abundances of stable isotopes (black), as well as half-lives of radioisotopes (white). Number of protons (Z) is shown vertically and number of neutrons (N) horizontally. From Clark & Fritz (1997) 10

Fig. 7: The study area, the Hochschwab massif, with its characteristic karstic plateau in the Northen Calcareous Alps, south of the Salza river in northern Styria. The locations of the meteorological stations used in this study are indicated with crosses and the cave entrance of the Furtowischacht with a white star, whereas the Kläffer springs and cave entrance of the Hirschgrubenhöhle where water samples are taken are shown as red stars. Background: coloured digital terrain model, resolution 10 m, UTM 33N (data and layers from https://www.landesentwicklung.steiermark.at/cms/) 16

Fig. 8: Entrance of the cave Hirschgrubenhöhle at 1896 m_{ASL} (lower) on a SW dipping slope on the Hochschwab plateau. Direction of view is North. A rain sampler with a total height of ~ 0.5 m can be seen in front of the entrance.. 17
Fig. 9: The Kläffer springs draining into the Salza river during high flow conditions of ~ 14 m^3/sec (photograph taken on 9th May 2017 during snowmelt conditions). Direction of view is South (picture from Plan, L.). 18
Fig. 10: Geological map of the Hochschwab massif after Mandl (2002). Cave entrances are courtesy of Plan, L. (Natural History Museum Vienna) and faults of Decker, K. (University of Vienna). Background: digital terrain model, resolution 10 m, UTM 33N (data and layers from https://www.landesentwicklung.steiermark.at/cms/). L: limestone; D: dolomite; Fm.: formation. 21
Fig. 11: Timetable for maintenance/installation of measurement devices and logistics as well as in-field preparation regarding the event sampling on 12-14th Sep 2023, as well as preparation of water samples in the laboratory facilities. SWCS: soil water content sensors; HG: Hirschgrubenhöhle; KQ: Kläffer springs.. 22
Fig. 12: Meteorological station Sonnschienalm. 24
Fig. 13: (a) Cross section of the uppermost parts of the Hirschgrubenhöhle with height of the entrance and source of the cave drip water, as well as locations of volumetric soil water content (VSWC) sensors and rain gauge indicated (modified from Exel, 2014). (b) Setup to measure discharge (Q), temperature (T) and electrical conductivity (EC) consisting of tarps channelling the water into an acrylic glass weir with an overflow and a pressure rod. 25
Fig. 14: Acrylic glass weir with overflow and a sketch of the minimum water level. 26
Fig. 15: Rating curve based on 28 discharge measurements conducted with a simple measuring vessel for very low flow conditions. 26
Fig. 16: Left: *ZL6* data logger with an integrated solar charging panel, stabilized with rocks; Right: *Teros 12* sensor for measuring volumetric water content.. 27
Fig. 17: Overview of the setup for measuring volumetric soil water content in the supposed catchment area of the cave drip water. Yellow arrows indicate locations of sensors, differentiated with associated values of depth below the surface. The *ZL6* logger (red) is located at approximately 1915 m_{ASL} and 50 m from the cave entrance. Direction of view is roughly South. 28
Fig. 18: Rain sampler at the entrance of the Hirschgrubenhöhle. 30
Fig. 19: Precipitation samples from the rainfall event on 13th and 14th Sep 2023............... 31

Fig. 20: Timing of precipitation sampling at the entrance of the Hirschgrubenhöhle in relation to rainfall intensity........ 31
Fig. 21: *Picarro™ L2140-i* isotopic water analyzer with CRDS technology........ 33
Fig. 22: Precipitation intensities at the MS Sonnschienalm during the hydrological year 2023. The sampled event from the 13th and 14th Sep 2023 is shown in red. Monthly isotope values from the MS Weichselboden are represented in grey. 40
Fig. 23: Detailed plot of precipitation intensities from the 13th and 14th Sep 2023 for all meteorological stations shown from west (Sonnschienalm) to east (Graualm). Arrows at the Hirschgrubenhöhle show times of precipitation isotope sampling........ 41
Fig. 24: Physiochemical parameters measured for the cave drip water in the Hirschgrubenhöhle (HG) and the Kläffer springs (KQ) from 13th to 19th Sep 2023 together with precipitation intensity, air and soil temperature, as well as volumetric soil water content at different locations (L1, L2, and L3) and depths. 42
Fig. 25: Potential pathways for water flow in a karst aquifer (modified after Ford & Williams, 2007)........ 44
Fig. 26: Global Meteoric Water Line (GMWL) and Local Meteoric Water Lines (LMWLs) for Wildalpen and Weichselboden, as well as LMWLs generated from data from both sites (n = 288) without weighting (OLSR; grey dashed line) and weighted after precipitation (PWLSR; blue dashed line). 47
Fig. 27: Dual isotope plot of $\delta^{18}O$ and $\delta^{2}H$ values for cave drip water in the Hirschgrubenhöhle (HG), the Kläffer springs (KQ), precipitation at the cave entrance (P-HG) and precipitation at the MS Sonnschienalm (P-SS) sampled between 12th and 19th Sep 2023 in comparison to the Global Meteoric Water Line (GMWL) and constructed Local Meteoric Water Line (LMWL)........ 48
Fig. 28: Time series for ^{18}O (upper) and ^{2}H (lower) values from cave drip water in the Hirschgrubenhöhle (HG), the Kläffer springs (KQ), precipitation at the cave entrance (P-HG) and precipitation at the MS Sonnschienalm (P-SS) sampled between 12th and 19th Sep 2023. 49
Fig. 29: Relationship of humidity (h) and the slope (s) of meteoric water lines. Slopes are given in reference to a GMWL or LMWL (heavy line) (from Clark & Fritz, 1997). 51
Fig. 30: Hirschgrubenhöhle $\delta^{18}O$ values are shown for total discharge C_T, rainfall C_E, different approaches for event water end-members $C_{E-shift}$, C_{E-max}, C_{E-med}, C_{E-min}, and $C_{E-weighted}$, as well as defined pre-event water end-member C_P. Dots indicate points of sampling.

Resulting discharge rates ($Q_{E-shift}$, Q_{E-max}, Q_{E-med}, Q_{E-min}, and $Q_{E-weighted}$) are given in the upper part........ 52

Fig. 31: Event water discharge (Q_E) in the Hirschgrubenhöhle (light blue area) is shown as the lowest possible volume calculated using $\delta^{18}O$ as tracer based on the C_{E-max} approach. The black cross indicates the highest absolute value of Q_E, whereas the red cross indicates the highest relative value of Q_E in relation to total discharge (Q_T), called fraction of event water (Few) here........ 54

Fig. 32: Event water discharge (Q_E) in the Hirschgrubenhöhle (light blue area) is shown as the lowest possible volume calculated using δ^2H as tracer based on the C_{E-max} approach. The black cross indicates the highest absolute value of Q_E, whereas the red cross indicates the highest relative value of Q_E in relation to total discharge (Q_T), called fraction of event water (Few) here........ 55

Fig. 33: Kläffer springs $\delta^{18}O$ values are shown for total discharge C_T, rainfall C_E, event water end-member C_{E-max}, as well as defined pre-event water end-member C_P. Dots indicate points of sampling........ 56

Fig. 34: Event water discharge (Q_E) at the Kläffer springs (light blue area) is shown as the lowest possible volume calculated using $\delta^{18}O$ as tracer based on the C_{E-max} approach. The black cross indicates the highest absolute value of Q_E, whereas the red cross indicates the highest relative value of Q_E in relation to total discharge (Q_T), called fraction of event water (Few) here........ 56

Fig. 35: Event water discharge (Q_E) at the Kläffer springs (light blue area) is shown as the lowest possible volume calculated using δ^2H as tracer based on the C_{E-max} approach. Max. Q_E indicates the highest absolute value of Q_E, whereas the red cross indicates the highest relative value of Q_E in relation to total discharge (Q_T), called fraction of event water (Few) here........ 57

Fig. 36: Screenshot from the configuration file of the *tran*-SAS model in an MATALB 2023a environment........ 58

Fig. 37: Fraction of event water for different TTD threshold ages in the discharge of the cave drip water as computed by the *tran*-SAS model for a catchment area of 60 m²........ 59

Fig. 38: Probability density functions (pdfs) and cumulative density functions (CDFs) for selected times (shown in different colours) as computed by the *tran*-SAS model for a catchment area of 60 m²........ 60

Fig. 39: Modelled tracer ratios of the discharge in comparison to measured ratios and precipitation as computed by the *tran*-SAS model for a catchment area of 60 m²............. 61

Fig. 40: Fraction of event water for different TTD threshold ages in the discharge of the cave drip water as computed by the *tran*-SAS model for a catchment area of 120 m². 62

Fig. 41: Modelled tracer ratios of the discharge in comparison to measured ratios in precipitation and discharge as computed by the *tran*-SAS model for a catchment area of 120 m².. 62

Fig. 42: Overall discharge of cave drip water in the Hirschgrubenhöhle (Q_T) and modelled event water discharge (Q_E) after rainfall on 13th and 14th Sep 2023 for an assumed catchment area of 60 m². Q_{1h} to Q_{36h} indicate water that is equal to or younger in age than 1 h to 36 h, while the maximum event water discharge is shown as a black cross and the maximum event water fraction as a red cross.. 64

Fig. 43: Overall discharge of cave drip water in the Hirschgrubenhöhle (Q_T) and modelled event water discharge (Q_E) after rainfall on 13th and 14th Sep 2023 for an assumed catchment area of 120 m². Q_{1h} to Q_{36h} indicate water that is equal to or younger in age than 1 h to 36 h, while the maximum event water discharge is shown as a black cross and the maximum event water fraction as a red cross.. 65

Fig. 44: Pictures of soil from three different locations at various depth within the catchment of the cave drip water. Associated ports for measurement of volumetric water content are indicated. The base of soil for profile 1 and 2 is at 40 cm and at 50 cm for profile 2..... 14-A

12 List of tables

Tab. 1: Overview of different measurement stations and their locations. MS: meteorological station; VSWC: volumetric soil water content; Q: discharge rate; T: temperature; EC: electrical conductivity; HG: Hirschgrubenhöhle; KQ: Kläffer springs. 23

Tab. 2: Amount of water samples taken from different locations. 30

Tab. 3: Mass balance based on fractions of event water calculated by the *tran*-SAS model. 68

Tab. 4: Isotope data of all samples taken of the cave drip water (HG), precipitation at the cave entrance (P), precipitation at the MS Sonnschienalm (P-SS), and the Kläffer springs (KQ). 14-B

13 References

“I have made every effort to cite all sources and references and to refer to them correctly in the text. However, should you become aware of any missing or inadequately cited references, please contact me. “

Bauer, H. (2010). *Deformationsprozesse und hydrogeologische Eigenschaften von Störungszonen in Karbonatgesteinen*. University of Vienna.

Benettin, P., & Bertuzzo, E. (2018). Tran-SAS v1.0: A numerical model to compute catchment-scale hydrologic transport using StorAge Selection functions. *Geoscientific Model Development*, *11*, 1627–1639. https://doi.org/10.5194/gmd-11-1627-2018

Benettin, P., Rodriguez, N. B., Sprenger, M., Kim, M., Klaus, J., Harman, C. J., van der Velde, Y., Hrachowitz, M., Botter, G., McGuire, K. J., Kirchner, J. W., Rinaldo, A., & McDonnell, J. J. (2022). Transit Time Estimation in Catchments: Recent Developments and Future Directions. *Water Resources Research*, *58*(11). https://doi.org/10.1029/2022WR033096

Botter, G., Bertuzzo, E., & Rinaldo, A. (2011). Catchment residence and travel time distributions: The master equation. *Geophysical Research Letters, 38*. https://doi.org/10.1029/2011GL047666

Bryda, G., Van Husen, D., Kreuss, O., Koukal, V., Moser, M., Pavlik, W., Peter Schönlaub, H., Wagreich, M., Ahl, A., Heinrich, M., Lenhardt, W. A., Moshammer, B., Pfleiderer, S., Plan, L., Schedl, A., & Slapansky, P. (2013). *Geologische Karte der Republik Österreich 1:50000 - Erläuterungen zu Blatt 101 Eisenerz*. Geologische Bundesanstalt, Vienna.

Buttle, J. M. (1994). Isotope hydrograph separations and rapid delivery of pre-event water from drainage basins. *Progress in Physical Geography: Earth and Environment*, *18*(1), 16–41. https://doi.org/10.1177/030913339401800102

City of Vienna. *Der Weg des Wiener Wassers von den Alpen in die Stadt*. Retrieved 25 April 2024, from https://www.wien.gv.at/wienwasser/versorgung/weg/

Clark, I. D., & Fritz, P. (1997). *Environmental Isotopes in Hydrogeology* (2nd ed.). CRC Press LLC, Boca Raton.

Craig, H. (1961). Isotopic Variations in Meteoric Waters. *Science*, *133*(3465), 1702–1703. https://doi.org/10.1126/science.133.3465.1702

De Waele, J., & Gutiérrez, F. (2022). *Karst Hydrogeology, Geomorphology and Caves*. John Wiley & Sons Ltd, West Sussex.

Diamond, R. E. (2022). *Stable Isotope Hydrology*. The Groundwater Project, Guelph, Ontario.

Exel, T. (2014). *Abschätzung des Wasserspeichervermögens der Bodenzone und des Epikarsts am Hochschwabplateau*. University of Vienna.

Exel, T., Stadler, H., Ottner, F., Wriessnig, K., & Plan, L. (2016). Untersuchungen zum oberflächennahen Wasserspeichervermögen am Hochschwab-Karstplateau. *Die Höhle*, *67*, 77–87.

Federal Ministry of Agriculture Forestry Regions and Water Management. *WISA Datenabfrage*. Retrieved 1 April 2023, from https://wasser.umweltbundesamt.at/wisa-datenabfrage/#/

Ford, D., & Williams, P. (2007). *Karst Hydrogeology and Geomorphology* (2nd ed.). John Wiley & Sons Ltd, West Sussex.

Freeze, R. A., & Cherry, J. A. (1979). *Groundwater*. Prentice-Hall Inc, Englewood Cliffs.

Fritz, P., Cherry, J. A., Sklash, M., & Weyer, K. U. (1975). Storm runoff analysis using environmental isotopes and major ions. *Advisory Group Meeting on Interpretation of Environmental Isotope and Hydrochemical Data in Groundwater Hydrology*, 111–130.

Goldscheider, N., & Drew, D. (Eds.). (2007). *Methods In Karst Hydrogeology*. Taylor & Francis Group, London.

Harman, C. J. (2015). Time-variable transit time distributions and transport: Theory and application to storage-dependent transport of chloride in a watershed. *Water Resources Research*, *51*(1), 1–30. https://doi.org/10.1002/2014WR015707

Hrachowitz, M., Benettin, P., van Breukelen, B. M., Fovet, O., Howden, N. J. K., Ruiz, L., van der Velde, Y., & Wade, A. J. (2016). Transit times - the link between hydrology and water quality at the catchment scale. *WIREs Water*, *3*, 629–657. https://doi.org/10.1002/wat2.1155

Hughes, C. E., & Crawford, J. (2012). A new precipitation weighted method for determining the meteoric water line for hydrological applications demonstrated using Australian and global GNIP data. *Journal of Hydrology*, *464–465*, 344–351. https://doi.org/10.1016/j.jhydrol.2012.07.029

IPCC (2023). *Climate Change 2023: Synthesis Report. Contribution of Working Groups I, II and III to the Sixth Assessment Report of the Intergovernmental Panel on Climate Change* (Core Writing Team, H. Lee, & J. Romero, Eds.). https://doi.org/10.59327/IPCC/AR6-9789291691647

Kaandorp, V. P., de Louw, P. G. B., van der Velde, Y., & Broers, H. P. (2018). Transient Groundwater Travel Time Distributions and Age-Ranked Storage-Discharge Relationships of Three Lowland Catchments. *Water Resources Research*, *54*(7), 4519–4536. https://doi.org/10.1029/2017WR022461

Kačaroğlu, F. (1999). Review of Groundwater Pollution and Protection in Karst Areas. *Water, Air, and Soil Pollution*, *113*(1/4), 337–356. https://doi.org/10.1023/A:1005014532330

Kaminsky, E. (2020). *Characterisation of the Water Flow Regime in the Upper Vadose Zone, Furtowischacht (Hochschwab, Austria)*. University of Vienna.

Kaminsky, E., Plan, L., Wagner, T., Funk, B., & Oberender, P. (2021). Flow dynamics in a vadose shaft – a case study from the Hochschwab karst massif (Northern Calcareous Alps, Austria). *International Journal of Speleology*, *50*(2), 157–172. https://doi.org/10.5038/1827-806X.50.2.2375

Kirchner, J. W. (2016). Aggregation in environmental systems-Part 1: Seasonal tracer cycles quantify young water fractions, but not mean transit times, in spatially heterogeneous catchments. *Hydrology and Earth System Sciences*, *20*(1), 279–297. https://doi.org/10.5194/hess-20-279-2016

Kirchner, J. W. (2019). Quantifying new water fractions and transit time distributions using ensemble hydrograph separation: Theory and benchmark tests. *Hydrology and Earth System Sciences*, *23*(1), 303–349. https://doi.org/10.5194/hess-23-303-2019

Kirchner, J. W., Feng, X., & Neal, C. (2000). Fractal stream chemistry and its implications for contaminant transport in catchments. *Nature*, *403*, 524–527.

Klaus, J., & McDonnell, J. J. (2013). Hydrograph separation using stable isotopes: Review and evaluation. *Journal of Hydrology*, *505*, 47–64. https://doi.org/10.1016/j.jhydrol.2013.09.006

Klimchouk, A. (2004). Towards defining, delimiting and classifying epikarst: Its origin, processes and variants of geomorphic evolution. *Speleogenesis and Evolution of Karst Aquifers*, *2*(1).

Kralik, M. (2001). *Strategie zum Schutz der Karstwassergebiete in Österreich*. Umweltbundesamt, Vienna.

Lakey, B., & Krothe, N. C. (1996). Stable isotopic variation of storm discharge from a perennial karst spring, Indiana. *Water Resources Research*, *32*(3), 721–731. https://doi.org/10.1029/95WR01951

Liu, F., Williams, M. W., & Caine, N. (2004). Source waters and flow paths in an alpine catchment, Colorado Front Range, United States. *Water Resources Research*, *40*(9). https://doi.org/10.1029/2004WR003076

Mandl, G. W. (2002). *Erstellung moderner geologischer Karten als Grundlage für karsthydrogeologische Spezialuntersuchungen im Hochschwabgebiet*. Geologische Bundesanstalt, Vienna.

McDonnell, J. J., & Beven, K. (2014). Debates - The future of hydrological sciences: A (common) path forward? A call to action aimed at understanding velocities, celerities and residence time distributions of the headwater hydrograph. *Water Resources Research*, *50*(6), 5342–5350. https://doi.org/10.1002/2013WR015141

METER Group Inc. *Environment Products - Soil Moisture*. Retrieved 1 March 2024, from https://metergroup.com/meter-environment/products/soil-moisture/

Mook, W. G., Groeneveld, D. J., Brouwn, A. E., & Ganswijk, A. J. van. (1974). Analysis of a run-off hydrograph by means of natural 18O. *Symposium on Isotope Techniques in Groundwater Hydrology*, 0–520.

Nash, J. E., & Sutcliffe, J. V. (1970). River flow forecasting through conceptual models part I — A discussion of principles. *Journal of Hydrology*, *10*, 282–290. https://doi.org/10.1016/0022-1694(70)90255-6

Palmer, A. N. (1984). Geomorphic interpretation of karst features. In R. G. LaFleur (Ed.), *Groundwater as a Geomorphic Agent* (pp. 0–408). Allen & Unwin, Inc.

Palmer, A. N. (2007). *Cave Geology*. Cave Books, Dayton.

Perrin, J. (2003). *A conceptual model of flow and transport in a karst aquifer based on spatial and temporal variations of natural tracers*. University of Neuchâtel.

Perrin, J., Jeannin, P. Y., & Zwahlen, F. (2003). Epikarst storage in a karst aquifer: A conceptual model based on isotopic data, Milandre test site, Switzerland. *Journal of Hydrology*, *279*(1–4), 106–124. https://doi.org/10.1016/S0022-1694(03)00171-9

Plan, L. (2004). Speläologische Charakterisierung und Analyse des Hochschwab-Plateaus, Steiermark. *Die Höhle*, *55*(1–4), 19–33.

Plan, L. (2016). Hochschwab. In C. Spötl, L. Plan, & E. Christian (Eds.), *Höhlen und Karst in Österreich* (pp. 645–660). Oberösterreichisches Landesmuseum, Linz.

Plan, L., & Decker, K. (2006). Quantitative karst morphology of the Hochschwab plateau, Eastern Alps, Austria. *Z. Geomorph. N.F. Suppl*, *147*, 29–54.

Plan, L., Kuschnig, G., & Stadler, H. (2010). Chapter 10.2 - Case Study: Kläffer Spring-the major spring of the Vienna water supply (Austria). In N. Kresic & Z. Stevanovic (Eds.), *Groundwater Hydrology of Springs* (pp. 411–427). Butterworth-Heinemann, Oxford.

Plan, L., Spötl, C., & Bryda, G. (2019). Speläologie und Geologie der Hirschgrubenhöhle am Hochschwab (Steiermark). *Die Höhle*, *70*(1–4), 79–93.

Poulain, A., Watlet, A., Kaufmann, O., Van Camp, M., Jourde, H., Mazzilli, N., Rochez, G., Deleu, R., Quinif, Y., & Hallet, V. (2018). Assessment of groundwater recharge processes through karst vadose zone by cave percolation monitoring. *Hydrological Processes*, *32*(13), 2069–2083. https://doi.org/10.1002/hyp.13138

Prettenthaler, F., Podesser, A., & Pilger, H. (2010). *Klimaatlas Steiermark Periode 1971-2000*. Verlag der ÖAW, Vienna.

Rabl, J. (2023). *Dynamik der Wasserparameter in einem Schlot der Hirschgrubenhöhle (Hochschwab, Steiermark)*. University of Vienna.

Rinaldo, A., & Marani, A. (1987). Basin scale model of solute transport. *Water Resources Research*, *23*(11), 2107–2118. https://doi.org/10.1029/WR023i011p02107

Ritter, A., & Muñoz-Carpena, R. (2013). Performance evaluation of hydrological models: Statistical significance for reducing subjectivity in goodness-of-fit assessments. *Journal of Hydrology*, *480*, 33–45. https://doi.org/10.1016/j.jhydrol.2012.12.004

Stadler, H., & Strobl, E. (1997). *Karstwasserdynamik Zeller Staritzen Endbericht*. Joanneum Research, Graz.

Stadler, H., & Strobl, E. (2006). *Hydrogeologie Hochschwab Zusammenfassung*.

Stevanović, Z. (2019). Karst waters in potable water supply: a global scale overview. *Environmental Earth Sciences*, *78*(23), 662. https://doi.org/10.1007/s12665-019-8670-9

Stumpp, C., Klaus, J., & Stichler, W. (2014). Analysis of long-term stable isotopic composition in German precipitation. *Journal of Hydrology*, *517*, 351–361. https://doi.org/10.1016/j.jhydrol.2014.05.034

The MathWorks Inc. *MATLAB*. Retrieved 17 January 2024, from https://mathworks.com/products/matlab.html

USGS. *Explanations for the National Water Conditions*. Retrieved 5 March 2024, from https://water.usgs.gov/nwc/explain_data.html

Van Husen, D. (2000). Geological Processes during the Quaternary. *Mitteilungen Der Österreichischen Geologischen Gesellschaft*, *92*(1999), 135–156.

Weiler, M., McGlynn, B. L., McGuire, K. J., & McDonnell, J. J. (2003). How does rainfall become runoff? A combined tracer and runoff transfer function approach. *Water Resources Research*, *39*(11). https://doi.org/10.1029/2003WR002331

Williams, P. W. (1983). The role of the subcutaneous zone in karst hydrology. *Journal of Hydrology*, *61*(1–3), 45–67. https://doi.org/10.1016/0022-1694(83)90234-2

Williams, P. W. (2008). The role of the epikarst in karst and cave hydrogeology: a review. *International Journal of Speleology*, *37*(1), 1–10. http://dx.doi.org/10.5038/1827-806X.37.1.1

Zhang, Z., Chen, X., Cheng, Q., & Soulsby, C. (2019). Storage dynamics, hydrological connectivity and flux ages in a karst catchment: Conceptual modelling using stable isotopes. *Hydrology and Earth System Sciences*, *23*(1), 51–71. https://doi.org/10.5194/hess-23-51-2019

Zhang, Z., Chen, X., Cheng, Q., & Soulsby, C. (2021). Using StorAge Selection (SAS) functions to understand flow paths and age distributions in contrasting karst groundwater systems. *Journal of Hydrology*, *602*. https://doi.org/10.1016/j.jhydrol.2021.126785

14 Appendix

14.1 Soil profiles

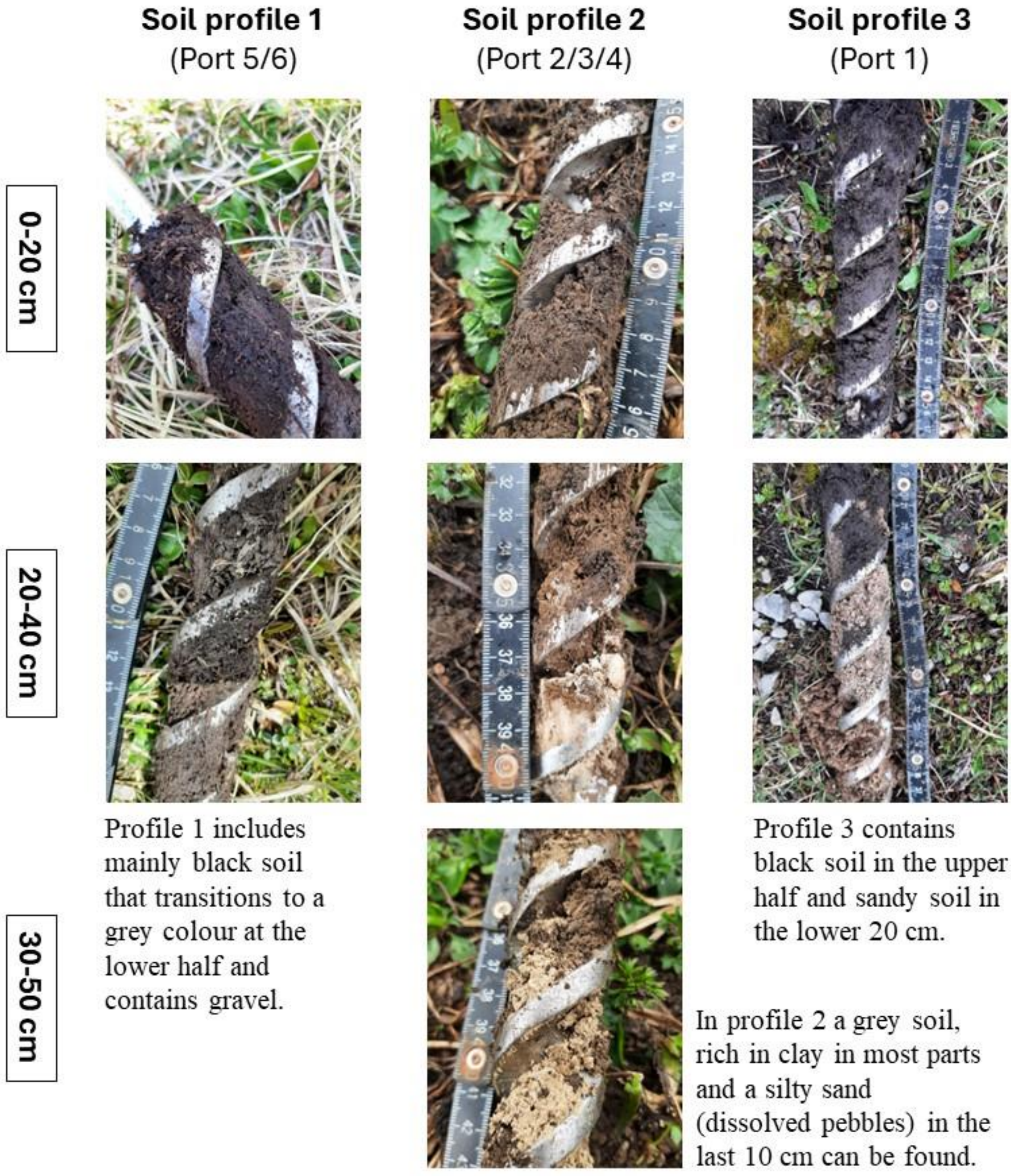

Fig. 44: Pictures of soil from three different locations at various depth within the catchment of the cave drip water. Associated ports for measurement of volumetric water content are indicated. The base of soil for profile 1 and 2 is at 40 cm and at 50 cm for profile 2.

14.2 Water stable isotope samples

Tab. 4: Isotope data of all samples taken of the cave drip water (HG), precipitation at the cave entrance (P), precipitation at the MS Sonnschienalm (P-SS), and the Kläffer springs (KQ).

name	date_MEZ_winter	d¹⁸O	d²H	StdAbw_d¹⁸O	StdAbw_d²H	d-Excess
HG-01	12.09. 11:15	-10.0019142	-65.0649932	0.03	0.06	15.0
HG-02	13.09. 10:50	-10.0906691	-65.8332236	0.00	0.20	14.9
HG-03	13.09. 15:28	-10.3673859	-67.4814884	0.10	0.59	15.5
HG-04	13.09. 16:13	-10.1931315	-66.527155	0.07	0.42	15.0
HG-05	13.09. 16:58	-10.862392	-70.0384052	0.01	0.04	16.9
HG-06	13.09. 17:43	-10.5553478	-68.6828927	0.07	0.50	15.8
HG-07	13.09. 19:13	-10.5416404	-68.8425111	0.04	0.64	15.5
HG-08	13.09. 22:46	-10.4259848	-67.7298035	0.05	0.26	15.7
HG-09	14.09. 00:03	-10.1694863	-66.8531463	0.01	0.49	14.5
HG-10	14.09. 02:26	-10.0971801	-66.1720128	0.02	0.19	14.6
HG-11	14.09. 08:06	-10.4279578	-68.2606508	0.04	0.27	15.2
HG-12	14.09. 10:02	-9.38172974	-60.5175205	0.09	0.81	14.5
HG-13	14.09. 10:12	-9.25943897	-59.1348818	0.04	0.09	14.9
HG-14	14.09. 10:20	-9.29693697	-59.3187621	0.02	0.11	15.1
HG-15	14.09. 10:30	-9.24930437	-59.0521356	0.04	0.48	14.9
HG-16	14.09. 10:40	-9.29558569	-59.0903262	0.01	0.18	15.3
HG-17	14.09. 10:50	-9.72563033	-61.671016	0.05	0.37	16.1
HG-18	14.09. 11:00	-9.56482809	-60.7229714	0.08	0.40	15.8
HG-19	14.09. 11:15	-9.67529518	-61.4524813	0.08	0.41	15.9
HG-20	14.09. 11:30	-9.24457489	-58.5386851	0.05	0.11	15.4
HG-21	14.09. 11:45	-9.52799285	-60.9177656	0.03	0.14	15.3
HG-22	14.09. 12:08	-9.17059455	-58.8448718	0.01	0.69	14.5
HG-23	14.09. 12:30	-9.12317389	-58.3448718	0.02	0.16	14.6
HG-24	14.09. 13:00	-9.1901207	-58.5679487	0.03	0.24	15.0
HG-25	14.09. 13:45	-9.173384	-58.246337	0.02	0.01	15.1
HG-26	14.09. 14:45	-9.39758605	-59.8884615	0.04	0.24	15.3
HG-27	14.09. 15:45	-9.62109075	-61.1811355	0.02	0.08	15.8
HG-28	14.09. 16:47	-9.45093429	-60.4782051	0.01	0.11	15.1
HG-29	14.09. 17:48	-9.5084667	-60.8562271	0.01	0.14	15.2
HG-30	18.09. 12:30	-10.2797497	-66.4910256	0.03	0.43	15.7
P-01	13.09. 15:42	-7.71942637	-49.3945554	0.01	0.29	12.4
P-02	13.09. 16:30	-5.47948894	-27.4028367	0.09	0.51	16.4
P-03	14.09. 01:10	-11.1914351	-71.1561176	0.04	0.33	18.4
P-04	14.09. 05:20	-13.3615728	-88.2189559	0.09	0.22	18.7
P-05	14.09. 09:15	-12.9678035	-86.7733078	0.02	0.10	17.0
P-06	14.09. 14:00	-9.88298608	-67.6594933	0.09	0.21	11.4
P-SS	14.09. 20:30	-10.1923821	-68.5269647	0.07	0.53	13.0
KQ-01	13.09. 09:00	-11.2044785	-72.847364	0.01	0.11	16.8
KQ-02	13.09. 10:00	-11.2443137	-72.6738274	0.03	0.21	17.3
KQ-03	13.09. 11:00	-11.2199896	-72.4896286	0.03	0.10	17.3
KQ-04	13.09. 12:00	-11.4812546	-76.3337003	0.03	0.62	15.5
KQ-05	13.09. 13:00	-11.4386451	-77.1076398	0.07	0.47	14.4

KQ-06	13.09. 14:00	-11.0343914	-74.8334195	0.03	0.19	13.4
KQ-07	13.09. 15:00	-11.2549585	-76.3434448	0.08	0.55	13.7
KQ-08	13.09. 16:00	-11.0673332	-75.0556694	0.03	0.27	13.5
KQ-09	13.09. 17:00	-11.0680494	-75.1917179	0.02	0.18	13.4
KQ-10	13.09. 18:00	-11.4196677	-77.0952718	0.09	0.43	14.3
KQ-11	13.09. 19:00	-11.1690233	-75.4964214	0.03	0.14	13.9
KQ-12	13.09. 20:00	-11.1332169	-75.2172035	0.03	0.11	13.8
KQ-13	13.09. 21:00	-11.4751676	-77.2523084	0.04	0.25	14.5
KQ-14	13.09. 22:00	-11.1726093	-75.892172	0.05	0.30	13.5
KQ-15	13.09. 23:00	-11.1098891	-77.0479648	0.02	0.83	11.8
KQ-16	14.09. 00:00	-11.141074	-76.3064228	0.02	0.13	12.8
KQ-17	14.09. 01:00	-11.2377822	-76.1490149	0.01	0.08	13.8
KQ-18	14.09. 02:00	-11.4049193	-77.3290243	0.03	0.22	13.9
KQ-19	14.09. 03:00	-11.501978	-78.4029943	0.02	0.09	13.6
KQ-20	14.09. 04:00	-11.1890777	-75.8063131	0.04	0.55	13.7
KQ-21	14.09. 05:00	-11.250046	-76.6847157	0.02	0.03	13.3
KQ-22	14.09. 06:00	-11.2058965	-75.9974776	0.02	0.14	13.6
KQ-23	14.09. 07:00	-11.3131166	-77.0226475	0.04	0.14	13.5
KQ-24	14.09. 08:00	-10.9228243	-74.2985266	0.00	0.13	13.1
KQ-25	14.09. 10:00	-11.0494797	-75.7034268	0.01	0.09	12.7
KQ-26	14.09. 12:00	-10.9524231	-75.1710022	0.02	0.17	12.4
KQ-27	14.09. 14:00	-10.9259219	-74.9350047	0.03	0.10	12.5
KQ-28	14.09. 16:00	-11.1771675	-76.9470621	0.07	0.35	12.5
KQ-29	14.09. 18:00	-10.9637808	-75.1617053	0.02	0.13	12.5
KQ-30	14.09. 20:00	-11.248067	-77.2706647	0.06	0.35	12.7
KQ-31	14.09. 22:00	-11.0274527	-75.4967502	0.01	0.21	12.7
KQ-32	15.09. 00:00	-11.1654657	-75.9844784	0.08	0.46	13.3
KQ-33	15.09. 02:00	-11.5110145	-78.3440958	0.01	0.03	13.7
KQ-34	15.09. 04:00	-11.4327512	-77.1437979	0.06	0.51	14.3
KQ-35	15.09. 06:00	-11.4891884	-78.0340665	0.04	0.21	13.9
KQ-36	15.09. 08:00	-11.216879	-76.595543	0.05	0.23	13.1
KQ-37	15.09. 10:00	-10.9392785	-75.0946675	0.04	0.22	12.4
KQ-38	15.09. 12:00	-10.8722594	-74.5382957	0.01	0.07	12.4
KQ-39	15.09. 14:00	-10.8916597	-74.8581726	0.01	0.07	12.3
KQ-40	15.09. 16:00	-11.0708477	-75.6853513	0.05	0.50	12.9
KQ-41	15.09. 18:00	-11.0084141	-76.2730835	0.03	0.56	11.8
KQ-42	15.09. 20:00	-11.0235816	-76.6516229	0.03	0.18	11.5
KQ-43	15.09. 22:00	-10.8465099	-74.813899	0.02	0.78	12.0
KQ-44	16.09. 00:00	-10.9856195	-73.7941328	0.07	0.19	14.1
KQ-45	16.09. 02:00	-11.2574251	-76.7317281	0.05	0.42	13.3
KQ-46	16.09. 04:00	-11.3009276	-75.2499982	0.04	0.19	15.2
KQ-47	16.09. 06:00	-11.1098405	-75.3235458	0.01	0.17	13.6
KQ-48	16.09. 08:00	-11.1404153	-75.9265282	0.03	0.05	13.2